STUDIES OF PHASE TRANSITION IN POLYMERIC SYSTEM IN THE PRESENCE OF HETERO-SPECIES BY DYNAMIC MONTE CARLO SIMULATION

Submitted in Partial Fulfillment of the Requirements for the Degree of

DOCTOR OF PHILOSOPHY

in

CHEMICAL ENGINEERING

by

ASHOK KUMAR DAS MAHAPATRA

(Roll Number: 03402709)

Supervisor:

Prof. H. Nanavati

Dr. K. Guruswamy (NCL, Pune)

DEPARTMENT OF CHEMICAL ENGINEERING

INDIAN INSTITUTE OF TECHNOLOGY BOMBAY

(2009)

Thesis Approval Sheet

Thesis entitled '**Studies of Phase Transition in Polymeric System in the Presence of Hetero-Species by Dynamic Monte Carlo Simulation**' by Ashok Kumar Das Mahapatra (03402709) is approved for the degree of Doctor of Philosophy.

Examiners

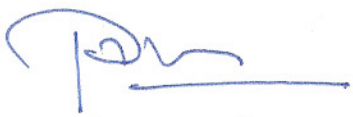

[Prof. P. B. Sunil Kumar]

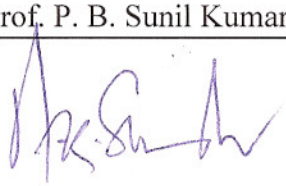

[Prof. A. K. Suresh]

Supervisors

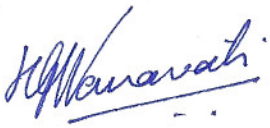

[Prof. Hemant Nanavati]

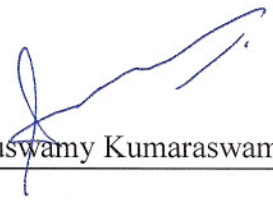

[Dr. Guruswamy Kumaraswamy]

Chairman

[Prof. B. L. Tembe]

Date: July 13, 2009

Place: IIT Bombay, Mumbai

Declaration

I declare that this written submission represents my ideas in my own words and where others' ideas or words have been included, I have adequately cited and referenced the original sources. I also declare that I have adhered to all principles of academic honesty and integrity and have not misrepresented or fabricated or falsified any idea/data/fact/source in my submission. I understand that any violation of the above will be cause for disciplinary action by the Institute and can also evoke penal action from the sources which have thus not been properly cited or from whom proper permission has not been taken when needed.

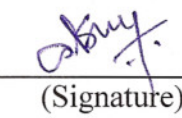

(Signature)

Ashok Kumar Das Mahapatra

(Name of the student)

03402709

(Roll No.)

Date: July 13, 2009

Abstract

We report in this dissertation, our investigations on the phase transition in polymeric systems, in the presence of hetero-species. We report two types of phase transitions: single chain coil to globule collapse transition of copolymer and melt crystallization in the presence of sticky additive. In our analyses, we have employed the lattice based dynamic Monte Carlo (DMC) simulation algorithm, coupled with the bond fluctuation algorithm and periodic boundary condition in a cubic lattice. We use Metropolis scheme for conformational sampling during simulation. In addition, we have initiated analysis of the nucleation phenomenon, by first considering crystallization of unadditivated homopolymer, and have explored the applicability of Weighted Histogram Analysis Method (WHAM) for the same.

We have examined the coil to globule collapse of single chains of a copolymer comprising monomer units, *m* and comonomer units, *c*, wherein there is a net attractive interaction between *c*-units. As the copolymer is cooled, the solvent quality becomes poorer, and the size of the chain decreases, driven by the net *m*-*m* and *c*-*c* attractions. The strong *c*-*c* attraction increases the overall solvophobicity of the chain relative to a homopolymer and therefore, copolymers collapse more abruptly and at a higher effective temperature relative to homopolymers. We compare copolymers with homopolymers by rescaling collapse data to the same theta values to account for the effect of overall solvophobicity. This comparison shows that the behavior of copolymers and of the corresponding homopolymers, are identical as the chain size reduces from high temperatures to the theta value. Beyond theta, copolymers with *c* content < ~50%, collapse more abruptly than the corresponding homopolymer, even after accounting for the difference in overall solvophobicity. Collapse of copolymers containing higher *c* content is dominated entirely by the *c*-*c* attractions and these

chains behave qualitatively like homopolymers with a higher effective solvophobicity. Analysis of the chain structure during collapse provides a structural reason for the qualitative change in copolymer collapse at low *c* content. When such copolymers are cooled below theta, the *c* units rapidly aggregate to form an isotropic, compact core surrounded by an anisotropic solvated shell of *m* units. The shell densifies as the copolymer is further cooled, but remains anisotropic for the finite chain sizes investigated.

In order to understand microstructure effects, we have also studied the effect of sequence distribution on the single chain collapse transition of a copolymer. Our simulations show that copolymers with uniformly (or periodically) distributed sticky comonomers, collapse "cooperatively", abruptly forming a compact intermediate, comprising a monomer shell surrounding a core of the aggregated solvophobic comonomers. In comparison, random copolymers collapse through a relatively less-compact intermediate comprising a comonomer core surrounded by a fluffy monomer shell, that densifies over a wide temperature range. This difference between the collapse pathways for random and uniform copolymers persists to higher chain lengths, where uniform copolymers tend to form multiple comonomer cores. In this chapter, we describe the formation of such an intermediate state, and the subsequent collapse, by recognizing that these arise from the expected balance between comonomer aggregation enthalpy and monomer loop formation entropy, dictated by the chain microstructure.

The DMC algorithm has then been implemented to investigate polymer melt crystallization. The trends of crystallinity and specific heat with temperature, indicate that the transition is of the first order type. Crystallization and melting shows a hysteresis, which is a characteristic feature of a first order transition in bulk polymers. Structural analysis shows the formation of lamellar type crystals. We have investigated the effect of "sticky" additives (viz. those that have attractive interactions with the polymer) on polymer

crystallization. Additive-polymer attractive interactions, result in a slowing down of the polymer chain diffusivity in the melt state. Our results show that, with increasing additive stickiness, polymer crystallinity decreases monotonically, and thinner crystallites form, viz. crystallization is inhibited by the presence of sticky additives. Unusually, the specific heat peak at the phase transition shows non-monotonic behavior with additive stickiness and exhibits a maximum for intermediate values of additive stickiness. While the origins of this unexpected behavior are not clear, we show that it correlates with a large interchange between crystalline and amorphous states of the monomers in the vicinity of the additives. At this intermediate additive stickiness, we also find that crystallization follows a qualitatively different route – crystallinity shows a non-Avrami-like evolution, unlike the case at low or high additive stickiness.

Finally, we have initiated exploratory analyses to understand nucleation, and have considered nucleation of crystallization of unadditivated homopolymer, as the first case. We have employed WHAM to study the nucleation in polymer crystallization. The method is based on the combining several energy histograms to obtain the density of states (DOS) and from the DOS, to estimate the free energy as a function of energy states. We have combined 96 energy histograms generated from our DMC simulation. The energy states sampled, span over temperatures ranging from the melt to the crystalline state. We have implemented WHAM by splitting the energies into sub zones, since the range of energies are too high to apply WHAM equation. The combined histogram does not look like a flat histogram. The sampling of energy states near the transition zone is not adequate, and we see an abrupt transition in the energy states from melt to crystal. As a result, we have not been able to estimate the energy barrier for polymer nucleation. Introduction of a restraining potential might allow better sampling in the transition zone enabling implementation of WHAM.

Contents

List of Figures

Nomenclature

B	Monomer-solvent interaction
B_{mc}	Monomer-comonomer interaction
B_{cs}	Comonomer-solvent interaction
B_{θ}^{h}	Theta *B*-value for homopolymer
B_{θ}^{c}	Theta *B*-value for copolymer
B^{*}	Scaled value of *B*
CC	Number of *c*-*c* contacts
C_v	Specific heat at constant volume
C_v^{*}	Peak value of specific heat
$C(\tau)$	Auto correlation function
c	Comonomer
d_{cm}^{2}	Mean square displacement of the center of mass of polymer chain
d_{m}^{2}	Mean square displacement of monomers at the vicinity of additive
ΔE	Energy of energy
F_r	Feed mole ratio
$F(\beta)$	Helmholtz free energy
f_m	Parameter equal to the free energy at β_m
ΔG	Change of free energy
ΔG^{*}	Critical Gibbs free energy
G_t	Mean square fluctuation of the occupation density around additive
G_{ac}	Mean square fluctuation of $g(1)_{ac}$

G_{ac}^{*}	Peak value of G_{ac}
g(1)	Pair distribution function at a radial distance 1
$g(1)_{ac}$	Pair distribution function of additive-crystalline monomer at r = 1
$g(1)_{anc}$	Pair distribution function of additive-noncrystalline monomer at r = 1
g_m	Statistical inefficiency for *m*-th simulation
ΔH_m	Change of enthalpy
$H(E)$	Energy histogram
ΔS_m	Change in entropy
K	Rate constant in Avrami equation
k	Boltzman constant
$k(T)$	Cooling or heating function
L_i^2	Shape factor
L_X	Lattice dimension
$\langle L \rangle$	Average crystallite thickness
M_i	Loop length
$\langle M \rangle$	Average loop length
m	Monomer
N	Length of the chain
$N_{cc}(n)$	Number of *c*-*c* contacts in a cluster of size *n*
N_m	Number of conformations sampled at the *m*-th simulation
n	Avrami exponent
n	Cluster size
$64n_a$	No. of additive molecules

$P(E,\beta)$	Probability of finding a system at the energy state E and β
p	Random number
pb	Block length in a block copolymer
$P(n)$	Probability of the formation of n-mer cluster
R	Random copolymer
$\left\langle R_N^2 \right\rangle$	Square average end-to-end distance of chain length N
R_g	Radius of gyration
R^*	Critical nucleus size
r_m	Reactivity ratio of monomer
r_c	Reactivity ratio of comonomer
S^2	Shape tensor
s	Solvent
T	Temperature, K
T_g	Glass transition temperature
T_c	Crystallization temperature
T_m	Melting temperature
U	Uniform copolymer
U_p	Parallel bond interaction energy
U_c	Collinear bond interaction energy
U_{ma}	Monomer-additive interaction energy
U_p^q	Quench depth
W_i	Loop forming probability
w(n)	Frequency of the n-mer cluster
X_c	Fractional crystallinity

X_c^{sat}	Saturation crystallinity
X_c^0	Crystallinity at the beginning of the isothermal annealing run
X_c^∞	Crystallinity at the end of isothermal annealing
x	Additive concentration
x	Comonomer mole %
Z	Partition function

α	Co-efficient of thermal expansion
β	$1/kT$
δ	Randomness Index
χ	Flory's χ parameter
ν	Universal exponent in scaling law
λ	Stickiness parameter
γ	Surface free energy
$\Delta\mu$	Difference in chemical potential between two phases (liquid and solid)
ν	Universal Scaling Exponent
ρ_c	Density of crystal
ρ_l	Density of liquid (melt)
θ	Theta point
τ_m	Correlation time for m-th simulation
$\Omega(E)$	Density of states at energy state E

CBMC	Configuration Biased Monte Carlo
CMA	Cooperative Motion Algorithm
DOS	Density of States
DP	Degree of polymerization
FWHM	Full Width at Half Maximum
MCS	Number of Monte Carlo Steps
PERM	Pruned Enriched Rosenbluth Method
PNIPAM	poly(N-isopropylacrylamide)
PS	Polystyrene
PSSA	Polystyrene Sulphonic Acid
RES-CBMC	Random End Switch CBMC
SAW	Self Avoiding Walk
WHAM	Weighted Histogram Analysis Method

Chapter 1

Introduction and Background

1.1 Introduction and Objective

Polymeric materials, viz. materials consisting of covalently connected monomeric units, are ubiquitous in nature. We encounter polymers in biology – DNA, RNA and proteins are polymeric; as natural plastics such as starch, cellulose, etc., and in synthetic, man-made polymeric materials that are now manufactured, in volumes of several hundred million tonnes per annum. Synthetic polymers now touch every aspect of our existence, and find applications in day-to-day household commodity items to highly demanding medical implants and devices.

In addition to being useful materials, polymers represent interesting objects for fundamental studies. Covalent connectivity results in a large spatial extent (typically on the order of tens of nanometers) for each polymer chain, and in slow dynamics. As each polymer molecule comprises a large number of connected monomers, each molecule can be considered to be a statistical object, rendering it amenable for analysis. Polymers also exhibit a wide variety of phase transitions – di Marzio[1] has identified ten distinct phase transitions exhibited by polymers, five of which have no analogy in non-polymeric systems. These phase transitions are grouped into phase transitions that can be experienced by a single chain,

such as the coil-globule transition, and into transitions that result from collective interactions of polymers (such as the transition from the liquid to the crystalline state). Thus, polymer phase transitions present us with a rich variety of phenomena, two of which – the coil globule transition and polymer crystallization, we explore in this work, using simulation techniques.

We begin this chapter with a brief description of coil-globule transition in section 1.2 and polymer crystallization in section 1.3, followed by the organization of the thesis in section 1.4.

1.2. Coil to Globule Collapse Transition

Behavior of polymer in dilute solution

The behavior of a polymer molecule in a solution, depends on its interaction with the solvent. When a polymer readily dissolves in a solvent, the solvent is called a "good solvent". On the other hand, if the polymer is insoluble, the solvent is called a "poor solvent". Polymer-solvent interactions (and therefore, solvent quality), can be varied by varying temperature, pH of the solution, addition of salt, by adding a second solvent or by changing the solvent chemistry. Experimentally, solvent quality is frequently varied by changing temperature. Polymers can either be miscible at elevated temperatures and less miscible at low temperature[2-4] (viz. they exhibit upper critical solution temperature) or the polymer chain can become less miscible at higher temperatures[5-8] (viz. they can exhibit a lower critical solution temperature; poly(N-isopropylacrylamide) (PNIPAM) in water).

The thermodynamics of polymer solutions, was considered independently by Huggins[9] and Flory[10], who described the free energy of mixing as the sum of an entropic mixing term and an enthalpic term, that combined polymer-solvent, monomer-monomer and solvent-solvent interactions. In their lattice model, they modeled the enthalpic interaction by a pairwise interaction potential, expressing the net polymer-solvent enthalpic interactions in

terms of a χ-parameter. For the dissolution of a polymer, the contribution to the free energy of the monomeric χ-parameter, is scaled with the molecular weight of the polymer – thus, polymers typically dissolve in solvents only if driven by favorable enthalpic interactions, viz. a favorable χ-parameter.

In a "good" solvent, there is a net repulsive interaction between monomers leading to swelling of the polymer chain in solution – a situation that can also be rationalized as arising from effective monomer excluded volume interactions. In this expanded coil state, the coil size, given by the radius of gyration, scales with the length of the chain approximately as: $\left\langle R_g^2 \right\rangle \sim N^{1.2}$. In contrast, in a poor solvent, the polymer chain collapses driven by net effective monomer-monomer attraction. Thus, the collapsed polymer chain forms a compact globule with a size given by $\left\langle R_g^2 \right\rangle \sim N^{2/3}$. But this 1/3 scaling ($R_g \sim N^{1/3}$), is difficult to achieve, due to the lack of the desired compactness in the globule state. Rissanou and co-workers[11] have recently simulated chain lengths ranging from 20 to 10,000, by configuration biased Monte Carlo. They have demonstrated that chains never really densify to achieve this $N^{1/3}$ scaling. Shorter chains never form a constant density core, whereas longer chains also deviate from the expected dense core, and fail to yield this scaling. Only at extraordinary long chain (molecular weight of $O(10^9)$) lengths, this scaling is achievable.

As the solvent quality changes from good to poor, there is an intermediate state, where the net excluded volume is zero, there is no net penalty for monomer-monomer interaction,[12] and the chain attains an ideal* state. This is called the theta condition, and the coil size scales with N as: $\left\langle R_g^2 \right\rangle \sim N$. Although the phase behaviors in these three states are understood, transitions between these states remain poorly understood.[13]

* Chains are not really ideal due to the logarithmic corrections at the theta condition.[12]

Interest in understanding the collapse of copolymers, viz. polymers comprising more than one kind of monomer unit, is motivated by the relevance of the collapse transition to protein folding. Recent experiments[14] show that when a protein is transformed from a denatured to the native state, the size of the molecule decreases, reaching a size only about 10% larger than the native folded state. Thus, the collapsed globule state, appears to be an intermediate state on the way to the folded native state for, at least some proteins.

As proteins typically comprise covalently connected amino acids, they can be considered as copolymers. Proteins are typically constituted by both hydrophilic and hydrophobic building blocks – in the collapsed globular state, hydrophobic residues are segregated to the core and surface hydrophilic groups, hydrogen-bond with water, to stabilize the globule against aggregation. Despite their simplicity, minimal "toy models" such as the two-letter HP (H: Hydrophobic, P: Polar) model by Dill,[15,16] already provide useful insights into the protein folding problem. The HP model poses certain limitations as described by Shakhnovich[17]: it is unable to exhibit the cooperative folding transition observed in real protein molecules. The sequence (random or designed) cannot have unique native folded state; hence, there are multiple global minimum energy states, which is described as ground state degeneracy.

In copolymers, the collapse transition is first order in nature, unlike the second order collapse observed in homopolymers. In copolymers, particularly of the HP type, hydrophobic groups from aggregates as the solution is cooled, and these drive the collapse to yield a core-shell globule structure. The pathway followed from the coil to the globule state, is expected to be a strong function of the comonomer distribution along the chain – for example, it seems intuitive that the collapse of a diblock copolymer will yield different structures and follow kinetics different from that of a random copolymer with comparable comonomer content. Again, a multiblock copolymer will exhibit different collapse behavior

compared to a diblock copolymer with identical comonomer content. The effect of hetero-species (viz. co-units) in a polymer chain, would influence the collapse transition by their content, as well as by their sequence distribution along the chain.

In the present work, we will elaborate the collapse transition of a single copolymer chain and also describe the effect of the composition and the sequence distribution of co-units on the collapse transition.

We discuss next, crystallization, a liquid-to-solid phase transition that typically involves collective densification or compaction of several polymer chains in the bulk, similar to the single-chain, coil-globule transition.

1.3. Polymer Crystallization

1.3.1. Background

Crystallization in polymers has several significant differences with respect to crystallization of small molecules, and we will highlight these features in this section. While polymer crystallization has been of great interest for several decades, understanding of crystallization out of a polymer melt or solution, continues to pose significant research challenges.[18]

Polymers that have a high degree of structural regularity (viz., chemical and stereochemical regularity) can crystallize, viz., they can organize into a three dimensional periodic lattice that diffracts X-rays.[19] The chemical structure of the polymer, plays an important role in governing crystallization – for example, crystallization of homopolymers, results in higher crystallinity relative to their copolymers. Thus, linear polyethylene (high density polyethylene) obtained using a Ziegler-Natta catalyst, typically contains very few side chains,[19] and can attain crystallinities as high as 90%. In comparison, copolymerizing ethylene with higher α-olefins such as butene or hexane, gives rise to a lower crystallinity

linear low density polyethylene wherein the degree of crystallinity can be controlled via the extent of comonomer inclusion.

Crystallization of polymers results in the formation of a non-equilibrium structure, where crystalline regions coexist with amorphous domains. Thus, polymer crystallization is kinetically controlled – kinetic factors control the rate of crystallization and the resulting morphology. In this section, we present a general overview of crystallization and melting phase transition in polymers.

1.3.2 The Crystallization Transition

Crystallization of polymers is a first order phase transition in the Ehrenfest sense[20-22]. Thus, there is a discontinuity in the first derivative of the free energy of the polymer as it crystallizes. Thus, the specific volume, specific entropy, etc., of the polymer, change abruptly as the polymer crystallizes or melts. The equilibrium melting point of a polymer is defined as:

$$T_m^{\infty} = \Delta H_m / \Delta S_m \quad \text{.....(1)}$$

where ΔH_m is the heat of fusion and ΔS_m is the entropy change on fusion. The kinetics of polymer crystallization become vanishingly slow at T_m^{∞}; thus, the equilibrium melting temperature can be obtained only by extrapolation from experimentally accessible conditions. As the temperature is reduced, polymer chain mobility decreases, and at the glass transition temperature, T_g, cooperative motions of the chain are frozen. Since crystallization involves a change in density that can be achieved only via center of mass diffusion of polymer chains, polymers cannot crystallize as the temperature approaches the glass transition. Thus, the rate of crystallization drops to zero as temperatures increase to near the equilibrium melting point where the driving force for crystallization decreases, and as temperatures decrease to near the glass transition, where the polymer chain mobility decreases (schematically represented in

Figure 1.1). The rate of crystallization is maximum, at a temperature between the equilibrium melting point and the glass transition.

1.3.3. Nucleation

Crystallization of polymers involves two steps. The first step is the formation of a nucleus, via a process called nucleation. The second step is the growth of the crystal, a procedure that involves diffusion of material to the phase boundary.

When a crystalline polymeric phase is created from a solution or melt, the bulk free energy is reduced. At the same time, creation of a new phase in a matrix of the old, also involves the creation of interphases between the crystal and solution/melt, increasing the free energy. Thus, as the size of the nucleus increases, the overall free energy passes through a maximum called the critical point. The nucleus at this point is called the critical nucleus. Nuclei larger than the critical size can grow, while those smaller than the critical size, are unstable, and dissolve back into the solution/melt. Nucleation may be homogeneous or heterogeneous in nature.

Homogeneous nucleation is the process by which crystalline nuclei are formed via thermal fluctuations in the pure supercooled melt. Thus, homogeneous nucleation happens in the absence of external surfaces.

In heterogeneous nucleation, an epitaxial match of lattice parameters between the polymer crystal and an external nucleating surface, results in enhanced rates of nucleation on or near the external surface. The external surface, reduces the free energy barrier for nucleation, and makes it more rapid. The reduction in free energy leads to the formation of a nucleus of critical size, smaller than that obtained via homogeneous nucleation.[23]

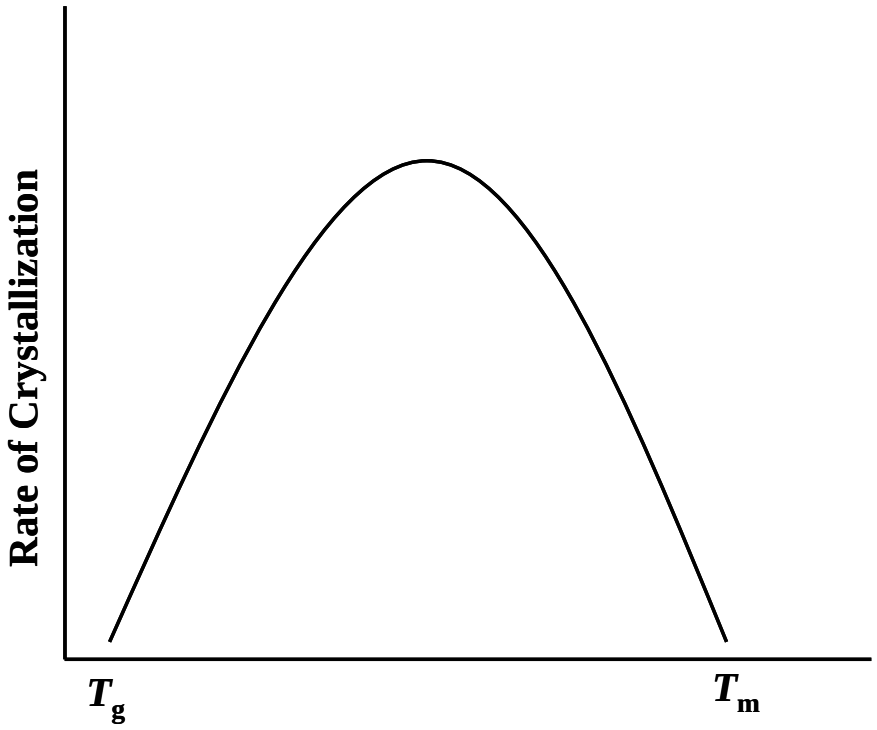

Figure 1.1: Rate of crystallization as a function of temperature[24]

1.3.4. Crystal Growth

Thermodynamic considerations alone are insufficient to understand the growth of polymer crystals, and kinetic theories are typically used to model growth. Growth happens via secondary nucleation onto the growing surface of crystals.

Morphology of Semicrystalline Polymers

During polymer crystallization, chain folding takes place to yield thin, folded-chain crystals, called lamellae. Chains pack parallel to each other, and are approximately normal to the basal surface of the lamellae. As the lamellar thickness is significantly smaller than the contour length of the polymer chain, the chain folds. The reason for the chain folding is attributed to the minimization of surface free energy[25] and to yield a compact crystal structure. The lamellar thickness is a function of temperature and, decreases with decrease in crystallization temperature. A single polymer chain can thread through multiple lamellae and be part of multiple unit cells. Such behavior is unique to polymers, and there is no analogous behavior in small molecules.

The formation of spherulites takes place when lamellae are organized into higher order structures[26,27] on a micron length scale. For quiescent crystallization, these structures develop isotropically and produce spherulite structures. Fig. 1.2 illustrates the formation of a spherulite from lamella. The size of the spherulites depends on the magnitude of the supercooling, and spherulites can grow to 100μm. Spherulite structures are also observed in a thin film of polyethylene, crystallized from the melt studied under the optical microscope.[26]

1.3.5. Phenomenological Models for Polymer Crystallization

Isothermal crystallization is carried out by rapidly cooling a polymer liquid from above its melting temperature to the crystallization temperature, T_c, and holding it at that

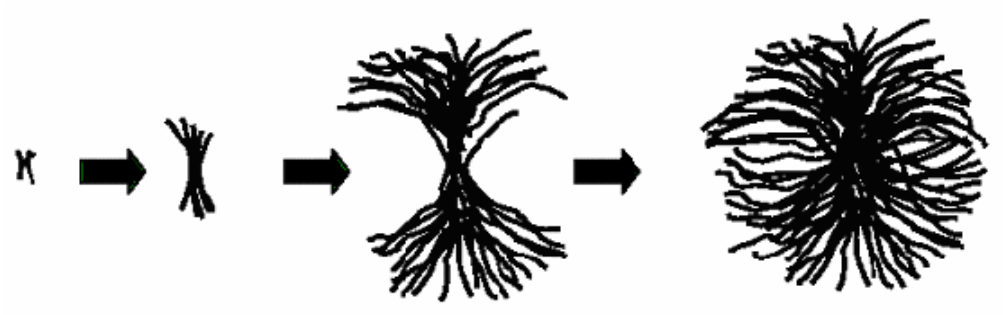

Figure 1.2: Stages of spherulites growth[28]

temperature until crystallization is completed. Since the crystallinity, X_c, is a function of time and temperature, the rate of change of crystallinity can be expressed by the so-called Avrami equation, described below.

Avrami Equation

Avrami[29] formulated an empirical relation, to model the isothermal solidification behavior of crystallizable polymers, expressed as:

$$X_c = 1 - \exp[-Kt^n] \quad \text{,.....(2)}$$

where K is the rate constant containing the temperature dependence of the growth rate, and **n** is the Avrami exponent. The Avrami exponent, **n,** is given by the sum of $d_1 + d_2$. d_1 is zero or unity, depending on whether nucleation is predetermined (heterogeneous) or sporadic (homogeneous), and d_2 is the dimensionality of crystal growth. Thus, in homogeneous nucleation, **n** is equal to 3 for the growth of disk-like crystals and is equal to 2 for heterogeneous nucleation.

Defining X_c^∞ as the mass fraction crystallized at the end of crystallization, equation 2 can be written as:

$$1 - \frac{X_c}{X_c^\infty} = \exp\left[-\frac{K}{X_c^\infty}t^n\right] \quad \text{.....(3)}$$

or

$$\ln\left[1 - \frac{X_c}{X_c^\infty}\right] = -K't^n \quad \text{.....(4)}$$

where $K' = \frac{K}{X_c^\infty}$.

The Avrami exponent, **n**, assumes integer values if the value of ρ_c/ρ_l is constant during the crystallization process, and the growth morphology of the crystallizing particles is consistent.[30] Since these conditions are typically not met in experiments, the Avrami exponent is frequently observed to be non-integer.

Non-isothermal Crystallization

During processing, polymer crystallization never occurs at a fixed, constant temperature. Instead, the polymer is cooled from the molten state to the solid state at some rate, determined by the processing conditions. Assuming that the ratio of rate of nucleation to the overall growth is constant and temperature independent (isokinetic process), Nakamura and coworkers[31,32] have modified the Avrami equation to the following form[24]:

$$\ln\left[1-\frac{X_c}{X_c^{\infty}}\right]=\left[\int_0^t K''\{T(\tau)\}d\tau\right]^n \quad \text{.....(5)}$$

where $K''(T)=K'(T)^{1/n}$

and **n** is the Avrami exponent determined from data on isothermal crystallization. For polyethylene, the modified Avrami equation, represents the crystallization very well.

Processing conditions such as the temperature or flow history imposed on a polymer, the chemistry of the polymer molecule and additives, control the kinetics and morphology of semicrystalline polymers, and therefore, control their properties. The widespread usage of synthetic polymers, largely results from the ability to tune their properties to suit applications. While chemical modifications of the polymer structure, such as copolymerization, can be used to vary properties, it is often more economical to vary properties by varying processing conditions, or by using additives. Additives that are commonly used to control polymer crystallization, include nucleating agents that heterogeneously nucleate polymer crystallization. Nucleating agents result in accelerated crystallization kinetics, and therefore, reduce cycle time in processing operations, and can also enhance the degree of crystallization.

While additives are widely used, the mechanisms through which they function, have not received significant attention in the scientific literature. Design of additives is still

largely done intuitively, using empirical rules-of-thumb, rather than through rational design. In our work, we explore the influence of additive stickiness on polymer crystallization. We systematically vary the additive-polymer interactions and additive loading, to map out the influence on the morphology and kinetics of polymer crystallization. In Chapter 5, we describe polymer crystallization from a melt containing additives and suggest possible experimental realizations of our scheme.

1.4. Organization of Thesis

In this chapter, we have presented a brief introduction to polymer phase transitions in general, and particular to (i) the dilute solution coil-globule transition and (ii) melt crystallization. In Chapter 2 we will describe the simulation methodology (dynamic Monte Carlo) employed in this work. Chapter 3 will describe our simulations of the collapse transition of a random copolymer and introduce the concept of "copolymer-ness". Chapter 4 will describe the effect of sequence distribution on single chain collapse. We will present the analysis of the collapse transition of a random and uniform distribution copolymer, and show that uniform copolymers show a cooperative collapse, transitioning to the globule state in a manner that is different compared to random copolymers. In Chapter 5, we describe the effect of sticky additives on homopolymer crystallization. We demonstrate that changing the stickiness of the additives has an unanticipated, nontrivial effect on the crystallization behavior. In Chapter 6, as a first step towards understanding the nucleation process, we initiate an exploratory analysis of nucleation in unadditivated homopolymer crystallization using DMC simulations in conjunction with a histogram reweighting technique, WHAM (Weighted Histogram Analysis Method) applied to our DMC data. We find that at this time, framework refinement is necessary, to make WHAM suitable to study nucleation in polymer

crystallization. Finally, we present a summary of our work, and outline the possible research work for future directions in Chapter 7.

References

(1) Di Marzio, E. A. *Prog. Polym. Sci.* **1999**, *24*, 329-377.

(2) Baysal, B. M.; Karasz, F. E. *Macromol. Theory Simul.* **2003**, *12*, 627-645.

(3) Baysal, B. M.; Kayaman, N. *J. Chem. Phys.* **1998**, *109*, 8701-8707.

(4) Kayaman, N.; Gürel, E. E.; Baysal, B. M.; Karasz, F. E. *Polymer* **2000**, *41*, 1461-1468.

(5) Wu, C.; Zhou, S. *Macromolecules* **1995**, *28*, 5388-5390.

(6) Wu, C.; Zhou, S. *Macromolecules* **1995**, *28*, 8381-8387.

(7) Wu, C.; Wang, X. *Phys. Rev. Lett.* **1998**, *80*, 4092-4094.

(8) Wu, C.; Qiu, X. *Phys. Rev. Lett.* **1998**, *80*, 620-622.

(9) Huggins, M. L. *J. Chem. Phys.* **1941**, *9*, 440.

(10) Flory, P. J. *J. Chem. Phys.* **1941**, *9*, 660-661.

(11) Rissanou, A. N.; Anastasiadis, S. H.; Bitsanis, I. A. *J. Polym. Sci. Part B: Polym. Phys.* **2006**, *44*, 3651-3666.

(12) Rubinstein, M.; Colby, R. H. *Polymer Physics*; Oxford University Press: New York, 2004.

(13) Binder, K.; Baschnagel, J.; Müller, M.; Paul, W.; Rampf, F. *Macromol. Symp.* **2006**, *237*, 128-138.

(14) Sherman, E.; Haran, G. *Proc. Natl. Acad. Sci. USA* **2006**, *103*, 11539-11543.

(15) Dill, K. A.; Bromberg, S.; Yue, K.; Fiebig, K. M.; Yee, D. P.; Thomas, P. D.; Chan, H. S. *Protein Sci.* **1995**, *4*, 561-602.

(16) Dill, K. A. *Biochemistry* **1985**, *24*, 1501-1509.

(17) Shakhnovich, E. I. *Curr. Opin. Struct. Biol.* **1997**, *7*, 29-40.

(18) Di Lorenzo, M. L.; Silvestre, C. *Prog. Polym. Sci.* **1989**, *24*, 917-950.

(19) Vaughan, A. S.; Basset D.C., "Crystallization and melting" in *Comprehensive Polymer Science*, Booth, C. and Price, C. (Eds.) Pergamon Press, UK, **1989**, 415-425

(20) "Ehrenfest sense" refers to a classification scheme of various phase transitions, proposed by Paul Ehrenfest. According to this scheme, in a first order phase transition, the first derivative of the chemical potential (e.g., enthalpy, entropy, volume) is discontinuous. In a second order phase transition, the first derivative of the chemical potential is continuous, but the second derivative is discontinuous.

(21) *http://www. answers. com/topic/ehrenfest-classification* **2009**.

(22) Ambrosone, L.; Fontana, F. *Eur. Phys. J. B* **2005**, *48*, 537-545.

(23) Wunderlich, B. *Macromolecular physics*; Academic Press: New York, 1976, [2] .

(24) Kumar, A.; Gupta, R. K. *Fundamentals of Polymers*; McGraw-Hill: Singapore, 1998.

(25) Hu, W.; Mathot, V. B. F.; Frenkel, D. *Macromolecules* **2003**, *36*, 2165-2175.

(26) Dosière, M. Cheremisinoff, N. P. *Handbook of Polymer Science and Technology*; Marcel Drekker: New York, 1989, [2] .

(27) Bower, D. I. *Introduction to polymer physics*; Cambridge University Press: UK, 2002.

(28) Frank, C. *www. stanford. edu* **2001**.

(29) Avrami, M. *J. Chem. Phys.* **1939**, ***7***, 1103-1112.

(30) Long, Y.; Shanks, R. A.; Stachurski, Z. H. *Prog. Polym. Sci.* **1995**, *20*, 651-701.

(31) Nakamura, K.; Watanabe, T.; Katayama, K.; Amano, T. *J. Appl. Polym. Sci.* **1972**, *16*, 1077-1091.

(32) Nakamura, K.; Katayama, K.; Amano, T. *J. Appl. Polym. Sci.* **1973**, *17*, 1031-1041.

Chapter 2

Simulation Methodology

2.1. Introduction

Computer simulations have emerged as a powerful tool to study polymer behavior, and in particular, polymer phase transitions. Various simulation techniques are used to simulate chain molecules. Some of them are used on the lattice and rests are off-lattice. Lattice based simulations are more coarse grained, and all the molecular details cannot be achieved. On the other hand, off lattice simulations such as molecular dynamic (MD), provide a superior platform to gain atomistic details. While MD is an off-lattice simulation tool, Monte Carlo (MC) on the other hand, can be employed with or without a lattice framework. MD simulations have been used for single chain[1,2] as well as melt simulation[3,4]. However, MD simulation need significantly more computational time (i.e. more expensive) compared to MC. We have used lattice-based dynamic Monte Carlo (DMC) simulation as a tool to study phase transitions in polymers. Although DMC is a coarse grained simulation technique, difficult to map to real systems – it can give insights at relatively small computational expense. In this chapter, we describe the DMC technique, and the specific implementation that we use in our work.

2.2. Dynamic Monte Carlo (DMC) Algorithm

The DMC algorithm was first developed by Verdier and Stockmeyer[5] in 1962. The original formulation was developed to study the dynamic behavior of macromolecules using a simple model. Polymer molecules are represented by bead-spring models, and the molecule is "constructed" on a square lattice by joining successive lattice sites. Dynamic properties are represented by the change in the configuration with simulation steps, which leads to the change in other measurable properties with time. Time in Monte Carlo simulations is expressed as the number of simulation steps. In DMC, configurational changes in a chain molecule are achieved by rule-based random displacements of chain units. There are three different types of motion prescribed –kink jump motion (Figure 2.1), crankshaft motion (Figure 2.2) and end bond rotation (Figure 2.3). In the schematics, the bonds that undergo motion are colored in red. Subsequent development of DMC has led to the introduction of other movements such as the pivot algorithm (Figure 2.4) and slithering diffusion[6] (also called reptation, Figure 2.5) that enable long range displacements and speed up equilibration. For a better presentation of the chemical structure and dynamic behavior of chain molecules, Carmesin and Kremer[7] introduced the bond fluctuation model (Figure 2.6). In this model a bond is simply the connecting link between any two successive lattice sites. The length of that link can vary up to a certain maximum length (up to $\sqrt{2}$ and $\sqrt{3}$ on a 2D and 3D lattice, respectively), mimicking the fluctuation of a bond in the presence of a stochastic force. In our work, the implementation of the DMC algorithm, includes three different types of moves –single site bond fluctuation, slithering diffusion and end bond rotation. These are selected as they are physically realistic moves, and since this combination results in faster structural relaxation during simulations[8].

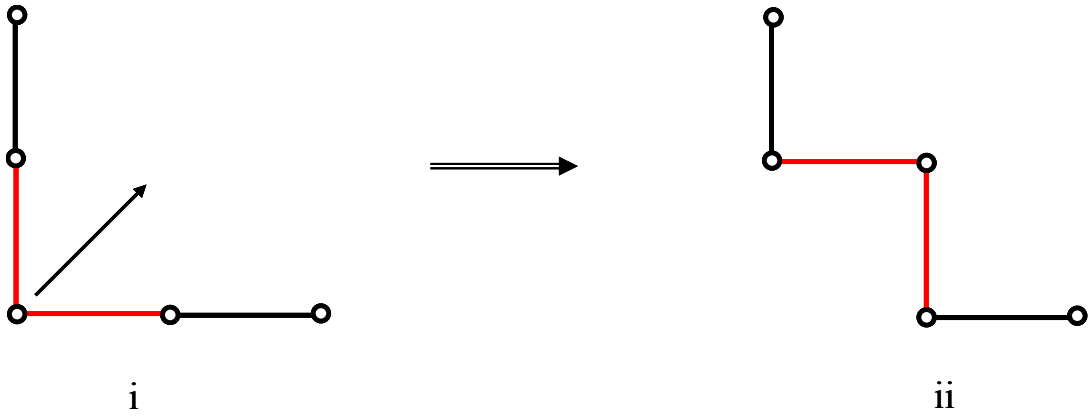

Figure 2.1. Schematic of Kink Jump Motion, i and ii represent conformation before and after move respectively.

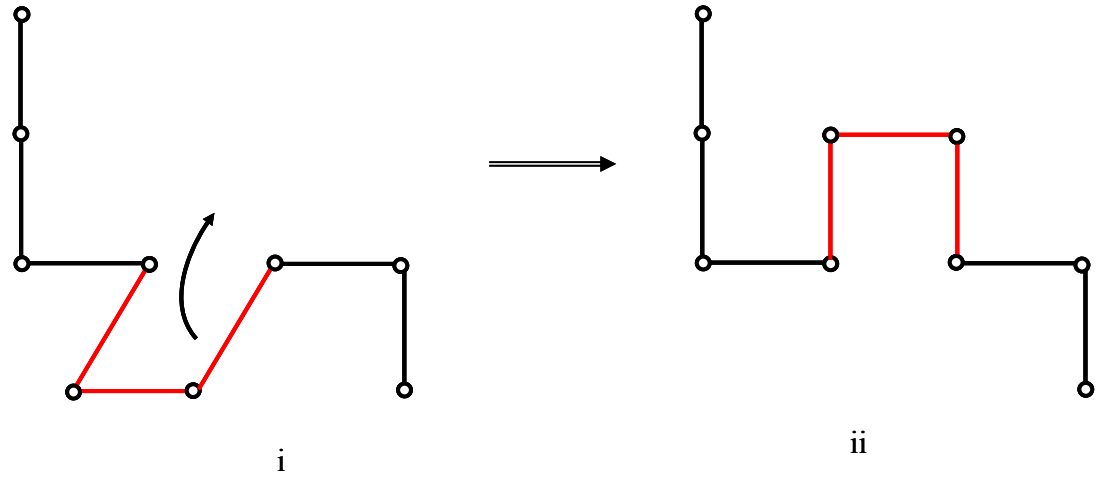

Figure 2.2. Schematic of Crank Shaft Motion, i and ii represents arrangement before and after move respectively.

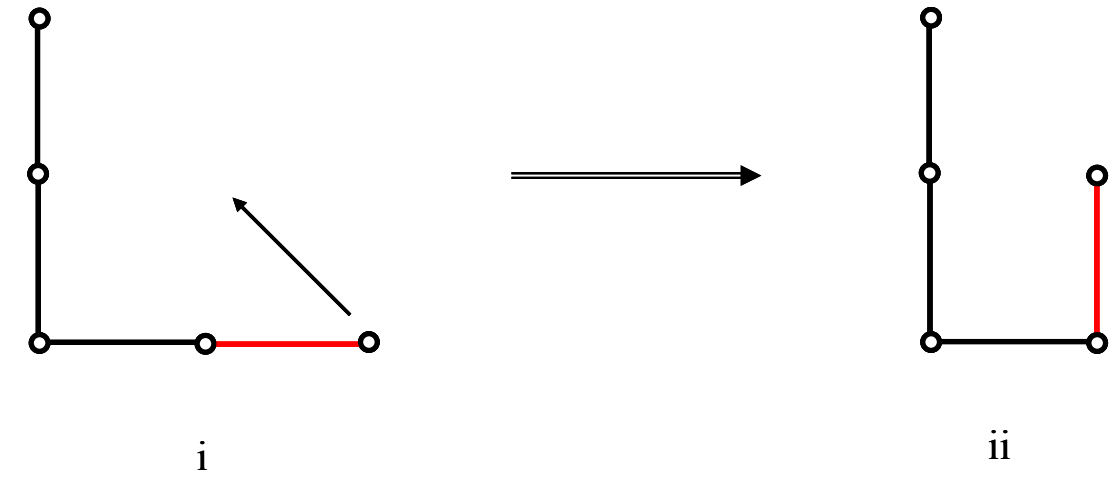

Figure 2.3. Schematic of End Bond Rotation, i and ii represent the conformation before and after move respectively.

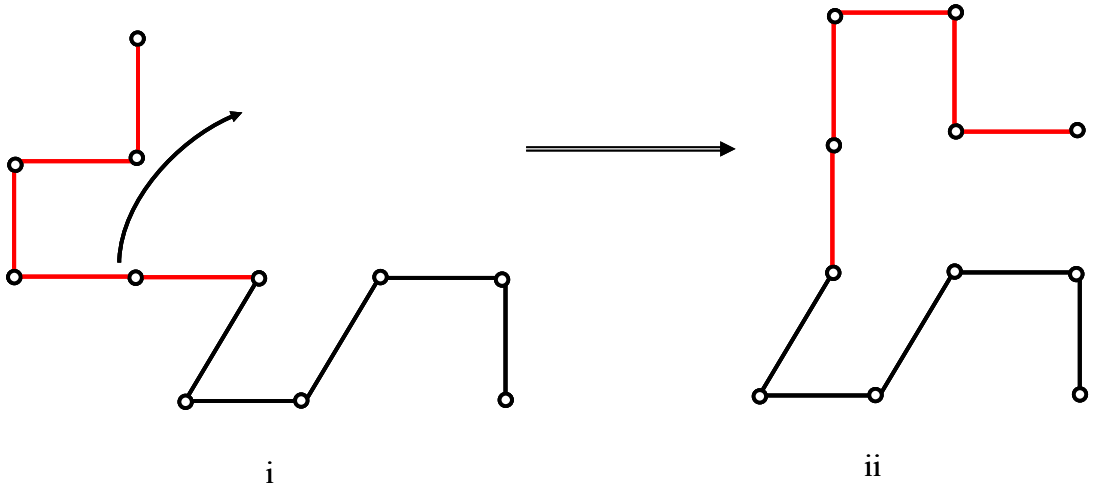

Figure 2.4. Schematics of Pivot Algorithm, i and ii represent conformation before and after move respectively.

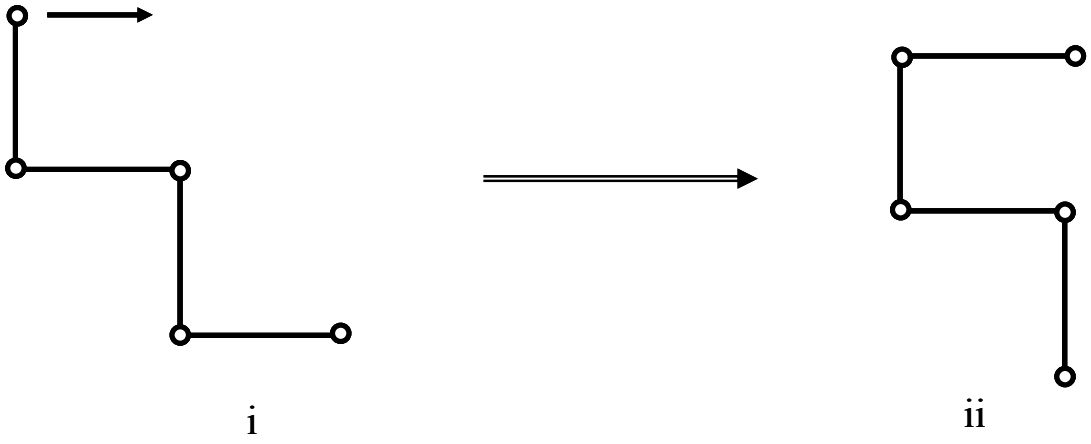

Figure 2.5. Schematics of Slithering Diffusion (Reptation), i and ii represent the conformation before and after move respectively.

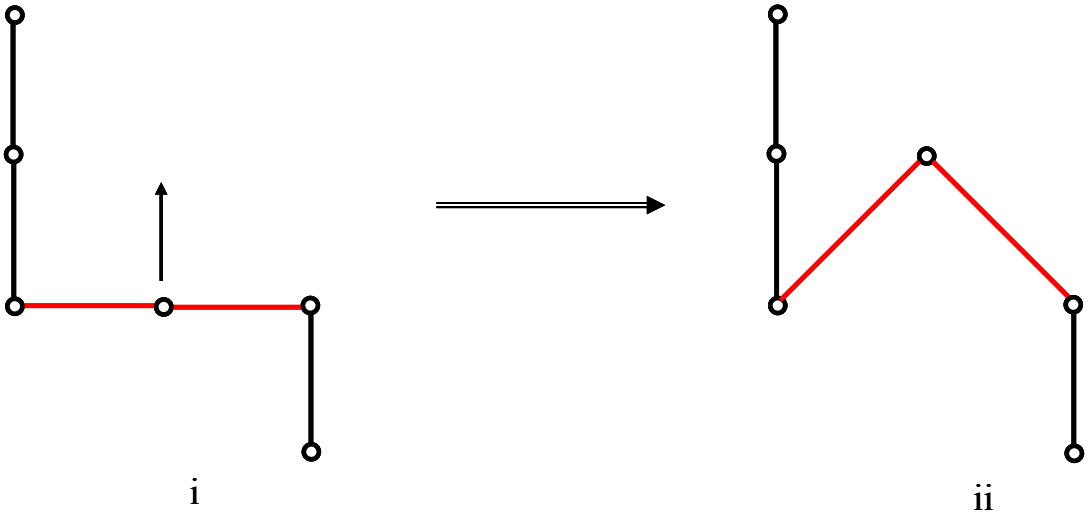

Figure 2.6. Schematic of Bond Fluctuaiton (Single Site), i and ii represent the conformation before and after move respectively.

2.2.1. Why Called Dynamic?

Dynamic Monte Carlo (DMC) is a generic name given to those systems where the transition probability from an initial state to a final state follows a "dynamical hierarchy[9]. Essentially, the transition follows a first order Markov process. The dynamical interpretation of Monte Carlo simulations has been well-illustrated through the application to the simulation of a Poisson process[9], simulation of a Lennard-Jones system[10] as well as the Rouse dynamics of a polymeric system executing "Brownian motion in a heat bath[6]". In our lattice model, random configurational changes are achieved by micro-relaxation models such as bond fluctuation, slithering diffusion and end bond rotation[6]. Thus, though we do not study dynamics of polymeric system in this work, the conformational evolution follows a dynamical hierarchy, and hence, the term "dynamic" is used.

In our simulations, we generate new configurations for the polymer chains using the aforementioned moves, and calculate the change in energy of the system due to the move. In an unbiased sampling, one rejects the conformation for which the change in energy is positive. However, we use Metropolis sampling[11] which is a biased sampling and also satisfies the principle of detail balance[6]. In Metropolis sampling, lower energy configurations are always accepted, and higher energy configurations are accepted by comparing with a random number.

2.2.2. DMC vs. Other Techniques

Other more powerful biased MC methods have been used to simulate single chain collapse transitions. These are configurational biased Monte Carlo (CBMC[12]) and Pruned Enriched Rosenbluth method (PERM[13]). CBMC and PERM are growth algorithms, and involve "growing" or generating the polymer chains at each step – thus, they are not appropriate to follow the dynamic progression of bulk transition. Further, implementing

growth algorithms for copolymers with a variety of comonomer distributions is not straightforward. Instead, the DMC algorithm that we have implemented follows Markovian statistics, i.e., each conformation is generated from its previous conformation. Thus, a dynamic progression of conformational states, traced by the chain undergoing the collapse transition can be followed. Further, the simulation strategy that we implement can easily be adapted to examine high density systems such as polymer melts, where growth algorithms are not applicable.

Other techniques that are efficient in equilibrating simulations such as CBMC[12], RES-CBMC[14], Wormhole moves[15], etc., are also not suitable to simulate dense melts, since they too are variants of growth algorithms. The cooperative motion algorithm (CMA) by Pakula[16,17] efficiently relaxes chain conformations in dense systems - however, this algorithm cannot mimic the dynamical motion needed to represent crystallization, which is a transition from a disordered to an ordered state. The Metropolis-DMC method that we employ, is similar to the method applied by Hu and Frenkel[18] in their copolymer crystallization work, and efficiently simulates polymer crystallization.

2.2.3. Lattice Occupation Density for a Melt

How many chains need to be put on the lattice so that it is representative of a polymer melt? We know from melt thermodynamics and scaling arguments, that chain behaves ideally in melt state, i.e., the scaling exponent in the relation between radius of gyration with chain length is 0.5, and the relation is $R_g \approx N^{0.5}$. To estimate the scaling exponent, we have simulated different chain lengths for a given occupation density. We have repeated the simulation at other occupation densities, and have observed that as the occupation density increases, the value of the exponent approaches 0.5 (Figure 2.7). Many melt simulations in

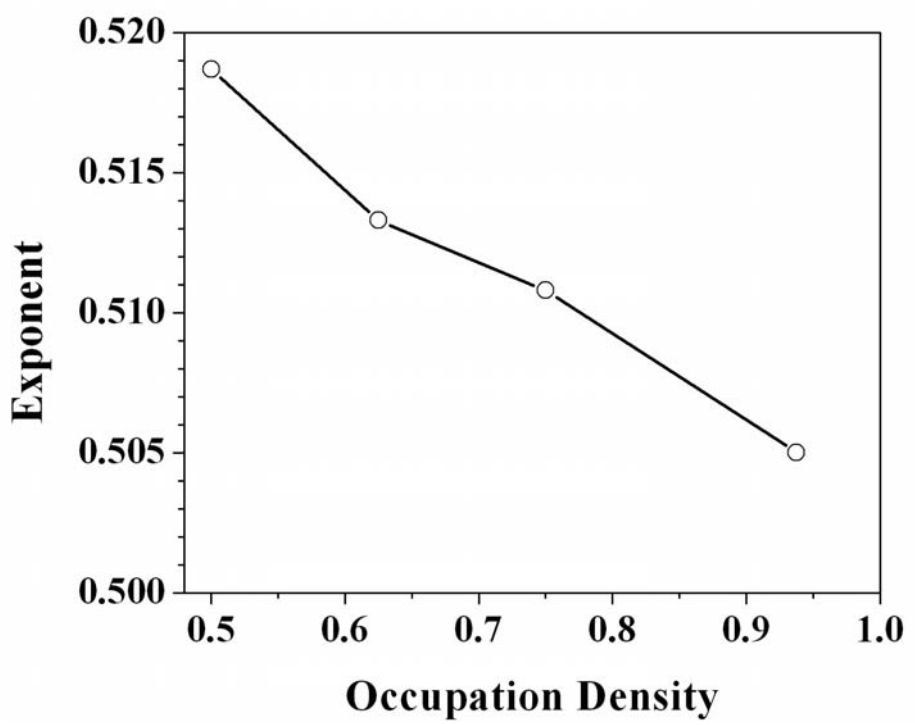

Figure 2.7. Change of scaling exponent with lattice occupation density in a lattice of size of 32^3.

the literature report simulations with the lattice occupation density of 0.5[19]. However, in our simulations on melt crystallization, we use a more densely packed lattice with an occupation density of 0.9375 since we believe that this is a more appropriate representation of melt crystallization. Hu and co-workers have used the same high dense melt density for melt simulation[20] and crystallization[18].

2.2.4. Lattice Size vs. Chain Size

In lattice simulations, the appropriate choice of lattice size for a given size of polymer chain is important: the lattice size should be large enough to avoid aphysical interactions with self replicas[21]. To satisfy this condition, the lattice dimension, L_X must be greater than the diameter of the chain. For example, for a chain comprised of 512 monomer units (N = 512), the average size of the chain, $\left\langle R_g^2 \right\rangle \sim 281$ lattice units (in the coil state). Thus, $2R_g \sim 34$, and therefore, it is acceptable to simulate the behaviour of using a lattice of size 64 × 64 × 64. Another way to estimate the size of the lattice has been described by Di Cacca and Friere[22]: $L_X = 2N^{1/2} + 5l$, where l is the root mean square (rms) bond distance (after equilibration using the bond fluctuation algorithm). For a chain with N = 512 units, l takes a value ~ 1.45. Thus, the value of L_X becomes ~ 53. In our work, we use a lattice of size 64 × 64 × 64, which is appropriately large, according to either of these conditions. For simulations of melt crystallization, we used a lattice of size 32 × 32 × 32 and a smaller chain size, N = 64. Here, $2R_g \sim 9$, and $L_X \sim 24$: thus, the size of the lattice is appropriate for the simulations, so that we avoid the problem of self-interaction of chains with their periodic image.

2.2.5. Implementation of Excluded Volume Criterion

We have enforced excluded volume interaction by restricting each lattice site to be occupied by only one unit and disallowing bond crossing. Positions of all the units are updated at the end of each MC move. During an MC move if the target lattice site is already occupied, then the move is rejected. It is also possible to have a situation, where two or more bonds can cross each other. The bond crossing violates the excluded volume criterion. We have disallowed bond crossing as follows: We track the bond positions during simulation – the position of a bond is given by the mid point of the bond, and this is stored in a secondary lattice[23,24]. Bond positions are updated at the end of each MC move (the bond position changes by only up to one lattice site). During an MC move, we check whether the concerned bond position is vacant or occupied. If vacant, then the move is possible, else the move is rejected due to bond crossing.

2.3. Simulation Strategy

We have adopted a different simulation strategy for collapse transition and melt crystallization (see also Chapter 3, 4 and 5). In collapse transition, we have selected a lattice site occupied by a monomer randomly and searched for a nearest vacant site to move. In contrast, for melt simulation, we have selected a vacant site randomly, and then searched for a nearest lattice site occupied by chain unit and attempted to move. The approach for the melt crystallization yields much faster relaxation. For a system with an occupation density of 0.9375, finding a vacant site next to an occupied site is less probable, but finding an occupied site next to a vacant site is more likely. Figure 2.8 illustrates the simulation strategy for single chain collapse and results will be presented in Chapter 3 and 4. Figure 2.9 illustrate the simulation strategies for melt crystallization and results will be presented in Chapter 5 and 6.

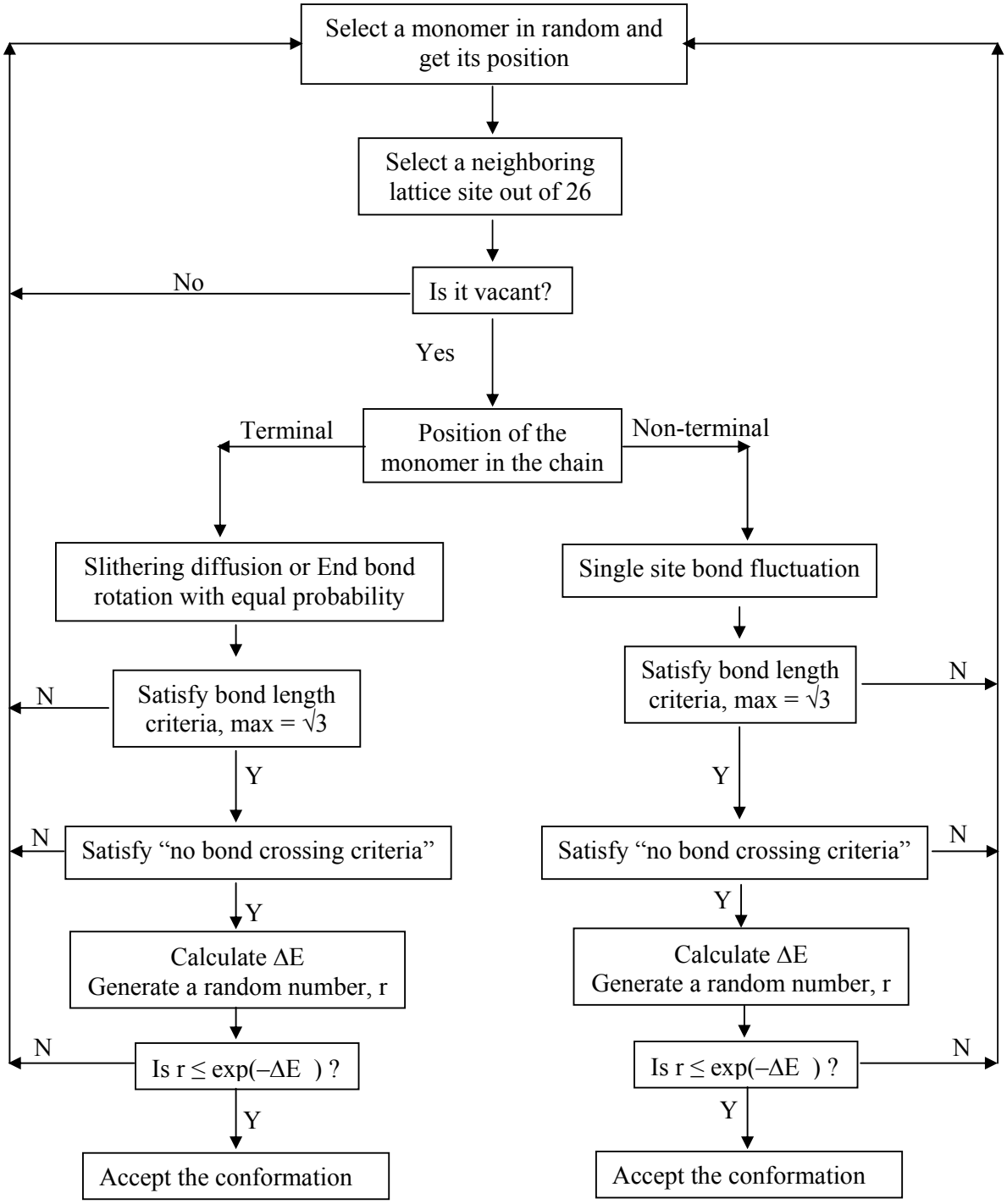

Figure 2.8: Flow diagram for the DMC algorithm applied to single chain

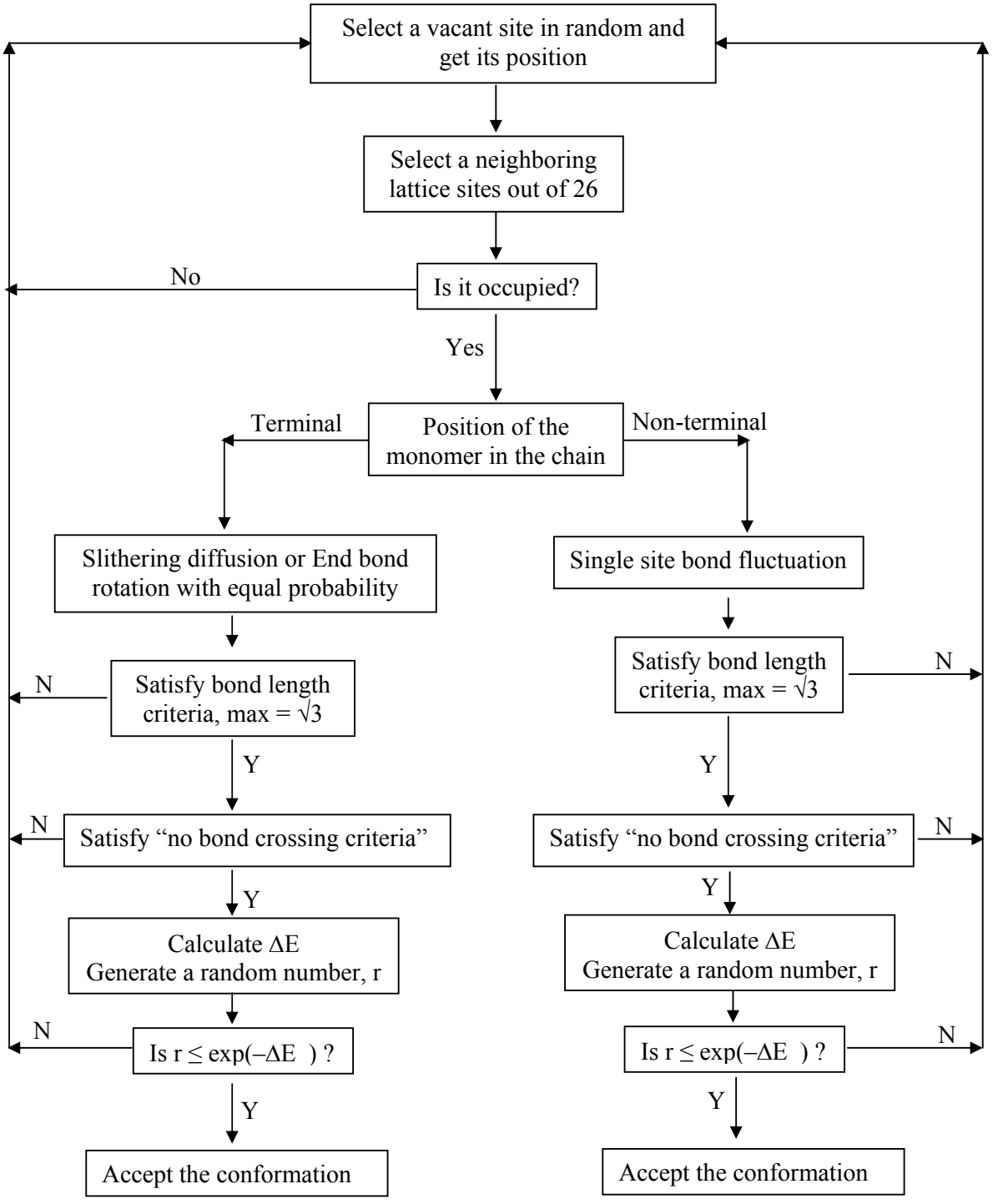

Figure 2.9: Flow diagram for the DMC algorithm applied to melt simulation

References

(1) Michel, A.; Kreitmeier, S. *Comput. & Theo. Polym. Sci.* **1997**, *7*, 113-120.

(2) Vasilevskaya, V. V.; Klochkov, A. A.; Lazutin, A. A.; Khalatur, P. G.; Khokhlov, A. R. *Macromolecules* **2004**, *37*, 5444-5460.

(3) Meyer, H.; Müller-Plathe, F. *J. Chem. Phys.* **2001**, *115*, 7807-7810.

(4) Meyer, H.; Müller-Plathe, F. *Macromolecules* **2002**, *35*, 1241-1252.

(5) Verdier, P. H.; Stockmayer, W. H. *J. Chem. Phys.* **1962**, *36*, 227-235.

(6) Kremer, K.; Binder, K. *Comput. Phys. Rep.* **1988**, *7*, 259-310.

(7) Carmesin, I.; Kremer, K. *Macromolecules* **1988**, *21*, 2819-2823.

(8) Binder, K.; Paul, W. *Macromolecules* **2008**, *41*, 4537-4550.

(9) Fichthorn, K. A.; Weinberg, W. H. *J. Chem. Phys.* **1991**, *95*, 1090-1096.

(10) Huitema, H. E. A.; van der Eerden, J. P. *J. Chem. Phys.* **1999**, *110*, 3267-3274.

(11) Metropolis, N.; Rosenbluth, A. W.; Rosenbluth, M. N.; Teller, A. H.; Teller, E. *J. Chem. Phys.* **1953**, *21*, 1087-1092.

(12) Siepmann, J. I.; Frenkel, D. *Molec. Phys.* **1992**, *75*, 59-70.

(13) Grassberger, P. *Phys. Rev. E* **1997**, *56*, 3682-3693.

(14) Karaiskos, E.; deJoannis, J.; Anastasiadis, S. H.; Bitsanis, I. A. *Macromol. Theory Simul.* **2004**, *13*, 762-770.

(15) Houdayer, J. *J. Chem. Phys.* **2002**, *116*, 1783-1787.

(16) Pakula, T. *Macromolecules* **1987**, *20*, 679-682.

(17) Pakula, T.; Geyler, S. *Macromolecules* **1987**, *20*, 2909-2914.

(18) Hu, W.; Mathot, V. B. F.; Frenkel, D. *Macromolecules* **2003**, *36*, 2165-2175.

(19) Subramanian, G.; Shanbhag, S. *Phys. Rev. E* **2008**, *77*, 011801-1-011801-9.

(20) Hu, W. *J. Chem. Phys.* **2000**, *113*, 3901-3908.

(21) Kremer Kurt. *Macromolecules* **1983**, *16*, 1632-1638.

(22) Di Cecca Antonio; Freire Juan J. *Macromolecules* **2002**, *35*, 2851-2858.

(23) Shaffer, J. S. *J. Chem. Phys.* **1994**, *105*, 4205-4213.

(24) Shaffer, J. S. *J. Chem. Phys.* **1995**, *103*, 761-772.

Chapter 3

Collapse Transition in Random Copolymer Solutions

3.1. Introduction

Understanding how the solution conformation of a random copolymer changes with solvent conditions is of fundamental interest and has implications for the more complex problem of protein folding[1-3]. In a good solvent, a flexible polymer exists in an expanded coil state that, as the solvent quality becomes poorer, shrinks to an ideal theta condition and, finally collapses to a compact globule[4,5]. A comprehensive review of theoretical, simulation and experimental work on the collapse transition of homo and copolymers has been recently published by Baysal and Karasz[6]. We will not summarize the extensive literature on coil-globule transitions here; rather, we briefly discuss investigations that probe the steepness of the collapse transition and the intermediate structures that form during collapse.

The nature of the transition from coil to globule depends on the chemical nature of repeat units. For example, theory[7] and simulations[8-10] demonstrate that homopolymers collapse via a smooth second order transition while, copolymers containing mutually attractive comonomer units collapse abruptly through a first order transition[11,12]. Experimental studies also indicate that copolymers collapse over a narrower temperature range relative to the corresponding homopolymers[13,14].

Several reports[15-26] indicate the formation of intermediate states during the collapse of a coil to its final compact globule state. Hu[10] suggests that prior to the formation of the completely collapsed coil in a homopolymer, “microphase separation” within the chain leads

to the formation of a molten globule comprising a dense core surrounded by a shell of incompletely collapsed chains. These results accord with experiments on aqueous solutions of poly(N-isopropylacrylamide) by Wu and co-workers[17-21] who have observed the formation of a "crumpled coil" state that further compacts to form a "molten globule" before complete collapse and, with the temperature quench experiments of Chu and co-workers[15,16] wherein polystyrene (PS) chains have been observed to collapse via the formation of an intermediate "crumpled globule" when solutions in cyclohexane are quenched from the theta temperature. Molecular dynamics simulations also support the picture of a two-stage collapse for flexible homopolymers[8]. Raos and Allegra[25] have suggested that inter-chain clustering could provide an alternative explanation for the experimental results of Chu and co-workers[15,16] – however, they do not rule out a two-stage collapse.

Intermediate molten or crumpled globule states during collapse of a protein could play an important role in mediating the formation of the final folded "native" globule. Therefore, the intermediate states formed during copolymer collapse have attracted considerable attention[17-21]. The structures formed during copolymer collapse are driven by the interactions between the monomers, comonomers and solvent. Zhang and co-workers[22] report a two-stage collapse for poly(N-isopropylacrylamide-*s*-styrene) in cyclohexane, where the intermediate state is an ordered coil resembling a molten globule. Wu and Qiu[21] have reported the formation of a core-shell structure during collapse of poly(N-isopropylacrylamide) grafted with polyethylene oxide branches. Molecular dynamics simulations of hydrophobic polymers with hydrophilic branches[24] indicate that the chain microstructure results in the formation of stable, shape-persistent globules with a hydrophobic core surrounded by a hydrophilic shell of the branches. Strong comonomer mutual interactions have been shown to lead to the formation of frustrated, incompletely

collapsed structures[11,26] that are strongly influenced by the chain microstructure, viz. the distribution of comonomers in the chain[11].

Copolymer collapse transitions have been investigated using averages over annealed disorder, especially for the protein folding problem. Pande and co-workers[27] have shown that the validity of the annealed approximation is suspect for folding of short proteins modeled using Dill's HP model[1]. Bastolla and Grassberger[28] show that the annealed approximation, though inexact even for large molecules, provides a useful estimate of the thermodynamics governing collapse in both the high and low temperature states. Garel and co-workers[29] have shown that for a statistical hydrophilic-hydrophobic copolymer, annealed and quenched averages predict similar phase behavior, but the former predicts a higher transition temperature than the latter.

Most theories or simulations have addressed the problem of amphiphilic copolymer collapse, wherein like units repel each other while unlike units attract show a theta transition only above a critical value of chain asymmetry[30,31]. However, a theta transition is always observed for copolymers wherein like units attract each other while unlike units repel[30]. We describe in this chapter dynamic Monte Carlo simulations of the collapse of a random copolymer containing solvophilic monomers (*m*-units) and solvophobic comonomers (*c*-units)(e.g., a copolymer containing polar comonomers in an apolar solvent). We show that the behavior that we observe is not "trivial" or "qualitatively similar to a homopolymer case", as suggested by Ganazzoli[12], but that it demonstrates an interesting dependence on the chain microstructure. Briefly, we show that copolymers containing a small percentage of solvophobic *c*-units collapse abruptly after the theta point relative to the corresponding homopolymers, even after accounting for the increase in their solvophobicity. This qualitative change in behavior appears to be linked to the formation of an intermediate core-

shell structure with incompletely collapsed *m*-units surrounding a compact core of the mutually attractive *c*-units.

We organize this chapter as follows: In the next section, we describe the model and our simulation technique. Then, we describe our results and discuss them in the subsequent section, and finally summarize our conclusions.

3.2. Model and Simulation Technique

A polymer chain of N units is represented by joining N successive lattice sites on a simple cubic grid of size 64 × 64 × 64, with periodic boundary conditions. Each lattice site is occupied by only one unit (either an *m*-unit or a *c*-unit or a solvent molecule). Copolymer chains are generated as described by Hu and co-workers[32]. While we are interested in the collapse of copolymer containing polar comonomers, we use reactivity ratios for ethylene copolymerization with 1-octene using a vanadium catalyst (*m*-unit and *c*-unit reactivity ratios, r_m = 24.7 and r_c= 0.017 respectively taken from Ref. 28; $r_m r_c$ = 0.42). To generate a chain with a *c*-unit mole fraction of x, we calculate the appropriate feed mole ratio[33], F (by solving $F^2 r_m x + F(2x-1) + (x-1) r_c = 0$) and use r_m, r_c and F to calculate the propagation probabilities for the chain[34,35]. The *c*-unit sequence in the copolymer is random-to-slightly alternating for these reactivity ratios. For simplicity we will call these copolymers random. We generate a new chain for each simulation and each chain, so generated, represents a particular state of quenched disorder for fixed N and *c*-unit content, x. Thus, the data presented in this paper are averaged over different microstructures, viz., different manifestations of quenched disorder. For example, for N = 128, λ = 20, x = 12.5%, our results represent an average over 20 different chains.

Polymer chains are then equilibrated, via a dynamic Monte Carlo (DMC) algorithm with periodic boundary conditions in a cubic lattice. Our algorithm selects a unit (*m*-unit or

c-unit) randomly**,** and attempts to move to an unoccupied lattice site among the 26 nearest neighbor lattice sites (along the lattice grid, along body diagonals and face diagonals, viz. 6 + 8 + 12 = 26). Each attempted move is termed one Monte Carlo (MC) move. If a vacant site is found, depending on the position of unit along the backbone chain, our algorithm selects the appropriate micro-relaxation move. For example, if the selected unit is terminal, then it will attempt to move either by slithering diffusion[36] or by a single site bond fluctuation[37] (cf. end bond rotation) with equal probability. On the other hand, if the selected unit is a non-terminal one, it will attempt to move by a single site bond fluctuation[37]. If a vacant site is not found, it will be treated as an MC move, and the conformation is counted twice for averaging structural properties. Our algorithm ensures that there is no bond crossing[38] and that no lattice site is occupied by more than one monomer, thus satisfying the excluded volume effect criterion. Violation of volume exclusion criteria leads to the termination of an attempted move and counts as an MC move.

Moves are accepted according to the Metropolis criterion[39]. Thus, the change of energy, ΔE (ΔE is normalized by Boltzmann's constant times absolute temperature, kT), for the MC move is calculated, and the move is accepted if $\exp(-\Delta E) \geq p$, where p is a random number, $0 \leq p \leq 1$, generated by using random number generator, MT19937, developed by Nishimura and Matsumoto[40]. This process is repeated to equilibrate the polymer chain.

Our simulation method is not as efficient as recent sophisticated techniques (such as PERM[41] used for simulating the conformations of an isolated chain; Multicanonical Monte Carlo simulation[42] and Expanded Ensemble Method[43] to study collapse, especially in the low temperature region where the conformational relaxation is very slow; Parallel Tempering[44] to speed up the equilibration process, etc.); however, our algorithm can be readily used for simulations of polymer melts, results for which we will describe in chapter 5 and 6 and for dilute solutions of polymers with complex architecture, such as star and ring polymers.

The change in energy for a single MC move, ΔE, is associated with the net change in nearest neighbor *m*-unit-solvent (*m*-*s*), *c*-unit-solvent (*c*-*s*) and *m*-unit-*c*-unit (*m*-*c*) contacts, ΔN_{ms}, ΔN_{cs} and ΔN_{mc}, respectively. The exchange energy (normalized by *kT*) of one *m*-unit-solvent contact, *B*, represents the net *m*-unit-solvent repulsion, and is directly related to the Flory χ parameter[5]. Therefore, an increase in *B* leads to collapse of a solvated chain to form a compact globule. Similarly, the net *c*-unit-solvent repulsion is given by B_{cs}. In the lattice framework, exchange energies are related to the *m*-unit and *c*-unit interaction energies via the quasichemical approximation, assuming that these interaction energies are pairwise additive[45]. Exchange of *m*-units and *c*-units with solvent during an MC move, leads to a net change in the number of *m*-*c* contacts. The energy change (normalized by *kT*) arising from the change of an *m*-*c* contact is given by B_{mc}. Thus, the total normalized energy change for one MC move, ΔE is given by:

$$\Delta E = \Delta N_{ms} B + \Delta N_{cs} B_{cs} + \Delta N_{mc} B_{mc} \quad \text{.....(1)}$$

Repulsive interactions between *m*-*s*, *c*-*s* and *m*-*c*, lead to a net attractive interaction between *m*-*m* and *c*-*c*. Note that equation (1) reduces to the homopolymer case by setting $B_{cs} = B$ and $B_{mc} = 0$.

Here, since we are simulating the collapse of a model chain representing polar copolymers in non-polar solvents, we assume that the interaction energies of the solvophobic *c*-unit with the relatively solvophilic *m*-unit is similar to that with the solvent. Thus, we set the *c*-unit-solvent interaction parameter equal to the *c*-unit-*m*-unit interaction parameter, viz., $B_{cs} = B_{mc}$. Further, for convenience we assume that $B_{cs} = B_{mc} = \lambda B$, where, $\lambda > 1$, represents the enhancement of the net *c*-unit-solvent repulsion relative to the net *m*-unit-solvent repulsion. Therefore, equation (1) can be simplified to:

$$\Delta E = \left(\Delta N_{ms} + \Delta N_{cs}\lambda + \Delta N_{mc}\lambda\right) B \quad \text{.....(2)}$$

We choose values of λ ranging from 10 to 50 and, examine the collapse of copolymers containing increasingly solvophobic *c*-units in non-polar solvent. In this work, we term the units that interact with an interaction parameter of λB as *c*-units while the other chain units are termed *m*-units. As $\lambda >> 1$ in our model system, ΔE is dominated by *c*-*c* contact energy.

For a chain comprising *N* units, *N* MC moves represent one MC step (MCS). In our work, we calculate mean square end-to-end distance, $\left\langle R^2 \right\rangle$ and radius of gyration[10], $\left\langle R_g^2 \right\rangle$ for each MC step, and average these over a large number of MC steps. When the values of $\left\langle R^2 \right\rangle$ and $\left\langle R_g^2 \right\rangle$ do not change appreciably with further MCS, we consider that equilibrium has been reached. We also study equilibration of a model polymer chain with respect to the mean change of energy, $<\Delta E,>$ as a function of MC steps. We observe that $<\Delta E> \sim 0$ by 4×10^6 MC steps. Thus, equilibration of the chain is confirmed using two measures, $\left\langle R_g^2 \right\rangle$ = constant as well as $<\Delta E> = 0$. In Figure 3.1, $\left\langle R_g^2 \right\rangle$ is plotted as a function of MC steps for a homopolymer with $N = 128$ at $B = 0$ and it is observed that the value of $\left\langle R_g^2 \right\rangle$ does not change appreciably beyond 4×10^6 MC steps. For $B > 0$ also, we observe equilibration both in terms of $\left\langle R_g^2 \right\rangle$ and $<\Delta E>$ by 4×10^6 MC steps (Figure 3.2). Equilibration studies for a model random copolymer ($N=128$, $\lambda=20$, $x=12.5\%$) are presented in Figure 3.3.

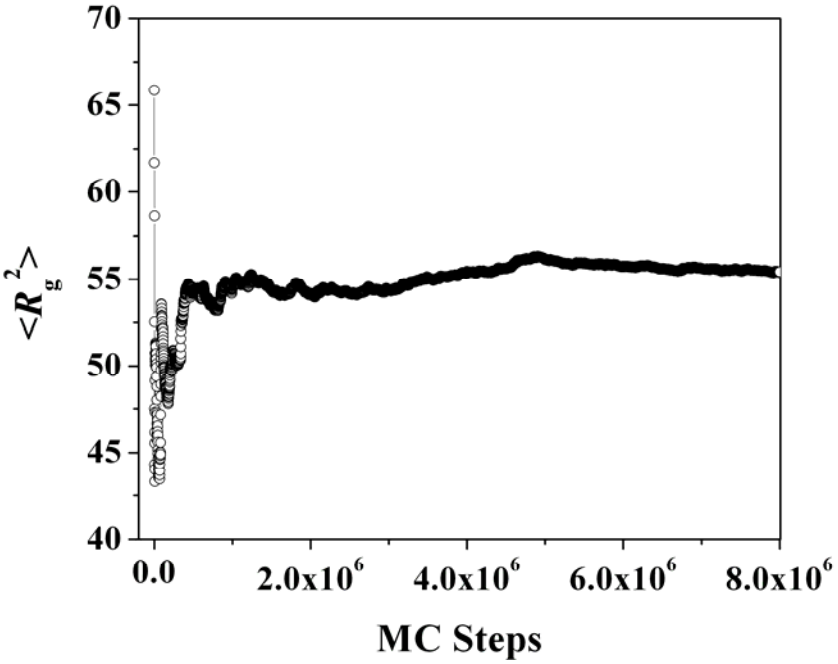

Figure 3.1: Change in $\left\langle R_g^2 \right\rangle$ as a function of MC steps for a homopolymer (N = 128) at B = 0

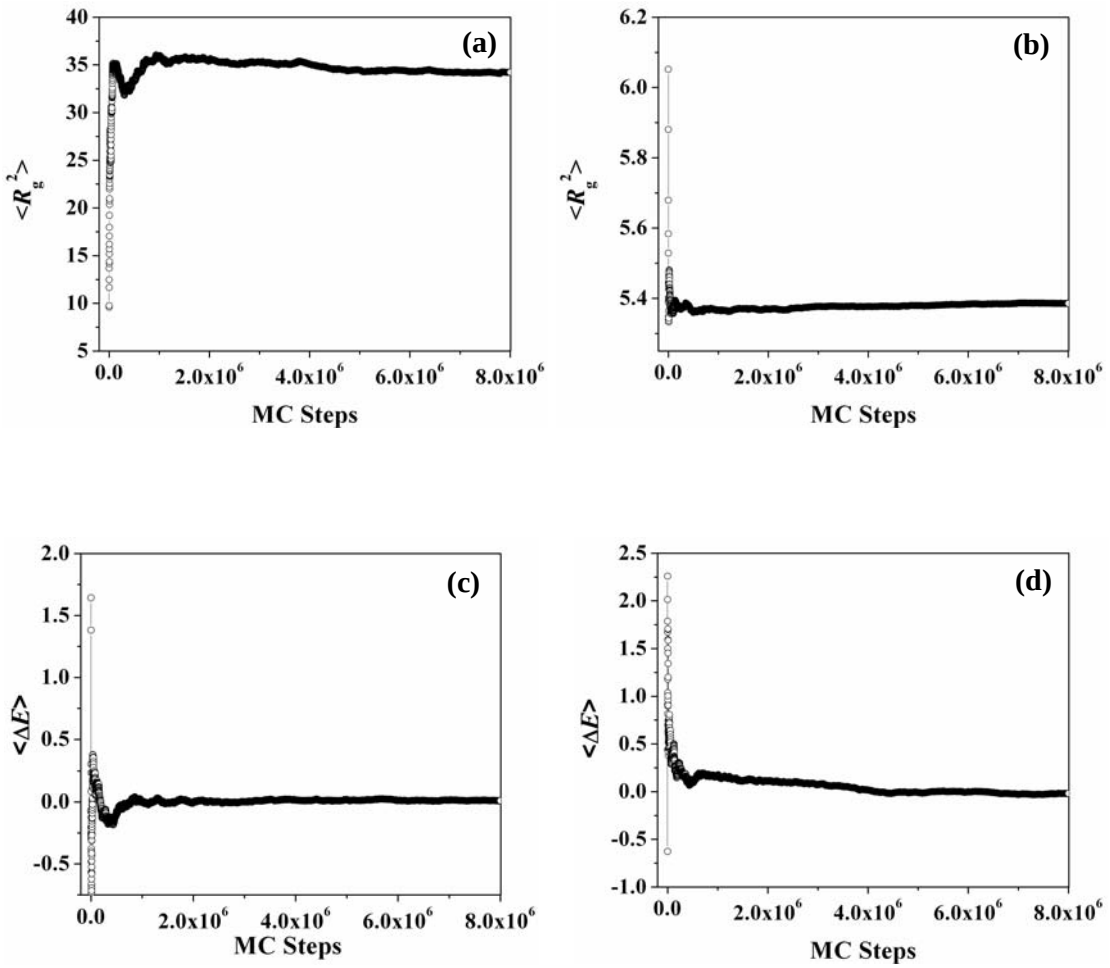

Figure 3.2: Evolution of $\left\langle R_g^2 \right\rangle$ and <ΔE> for a homopolymer (N = 128). (a) and (b) present $\left\langle R_g^2 \right\rangle$ at B = 0.03 and B = 0.1 respectively while (c) and (d) present <ΔE> at B = 0.03 and B = 0.1 respectively.

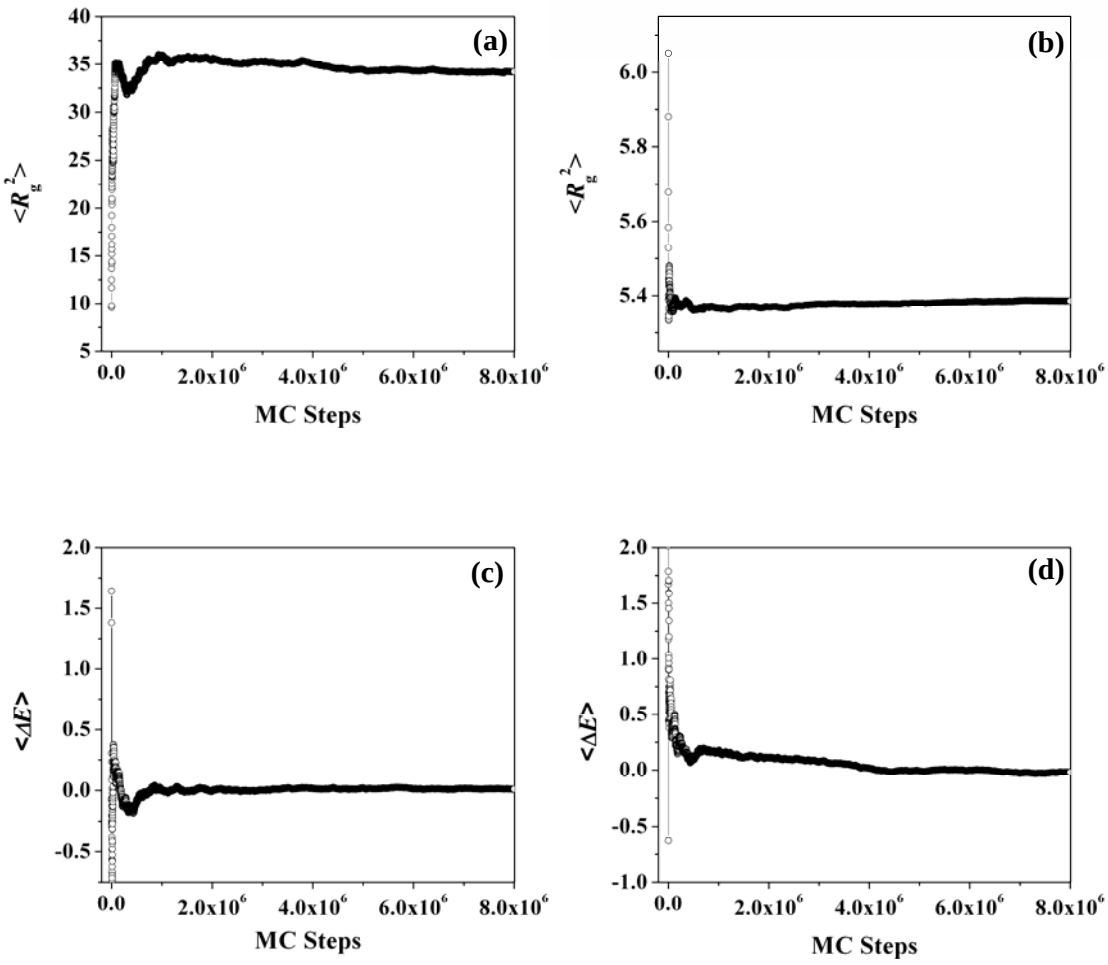

Figure 3.3: Evolution of $\left\langle R_g^2 \right\rangle$ and <ΔE> for a random copolymer (N = 128, λ = 20, x = 12.5%). (a) and (b) present $\left\langle R_g^2 \right\rangle$ at B = 0.02 and B = 0.1 respectively while (c) and (d) present <ΔE> at B = 0.02 and B = 0.1 respectively.

As mentioned earlier, $\langle R_g^2 \rangle$ values represent averages over quenched disorder. However, we find that, over most of the *B*-range investigated, the error bars (standard deviation) for $\langle R_g^2 \rangle$ are typically of the size of the symbol used to plot the data, and thus, simulations of different chains are quantitatively nearly identical. In the *B*-range between theta and collapse, the error bars are about 15% – this value does not affect any of the trends that we discuss.

We describe the spatial distribution of *c*-units by calculating the radius of gyration of only the *c*-units, $\langle R_{gc}^2 \rangle$. Thus, if the *c*-units form a compact aggregate, the *c*-unit radius of gyration is smaller than that of the entire chain.

We have also investigated the evolution of the shape of the polymer chain by calculating the principal components of the shape tensor. The shape tensor S^2 can be written as:

$$S^2 = \begin{bmatrix} S_{xx} & S_{xy} & S_{xz} \\ S_{yx} & S_{yy} & S_{yz} \\ S_{zx} & S_{zy} & S_{zz} \end{bmatrix}, \quad \text{.....(3)}$$

where, $S_{xx} = \frac{1}{N}\sum_{i=1}^{N}(x_i - x_{cm})^2$ and $S_{xy} = \frac{1}{N}\sum_{i=1}^{N}(x_i - x_{cm})(y_i - y_{cm})$, x_i and x_{cm} are the *x*-coordinate of i^{th} unit and center of mass, respectively.

The eigenvalues of the shape tensor yield the three principal moments of *S*, and represent the shape of the molecule. The eigenvalues (averaged over a large number of conformations) are represented as $\langle S_i^2 \rangle$, where, i = 1, 2 and 3; the shape factors, L_i^2, given by the ratios, $\langle S_i^2 \rangle \Big/ \sum_{i=1}^{3} \langle S_i^2 \rangle$, provide information about the shape of the molecule. For an isotropic structure, L_i^2 = 1/3.

We begin the simulation by placing a polymer chain on the lattice in a regularly folded state. This initial structure is equilibrated at $B = 0$ (viz., at effectively high temperatures or under athermal[33,46] conditions) using the DMC algorithm. For an isotropic polymer coil, the ratio of $\langle R^2 \rangle$ to $\langle R_g^2 \rangle$ is 6. Our simulation data shows that $\langle R^2 \rangle / \langle R_g^2 \rangle$ = 6.25 ± 0.05, as against 6.3694 ± 0.002 for self avoiding walk (SAW) polymer chains[47] after equilibration. The polymer solution is then "cooled" to $B = 0.2$, by increasing B (for a homopolymer, the step size is 0.005 while for copolymers, the step size is smaller and depends on λ and x) and the structure of the chain is analyzed after equilibration at each value of B. For chains of size $N = 64$, for example, 4×10^6 MCS have been performed at each cooling step. The first 2×10^6 MCS equilibrate the chain, and the subsequent 2×10^6 MCS have been averaged to calculate $\langle R^2 \rangle$, $\langle R_g^2 \rangle$ and $\langle S_i^2 \rangle$. Larger chain sizes (N = 128, 256 and 512) are similarly simulated. However, for larger N, a larger number of MCS are performed at each cooling step. We have investigated the swelling of collapsed chains on heating, viz., we decrease B from 0.195 to 0. The $\langle R_g^2 \rangle$ values follow the same trend during heating and cooling indicating that equilibrium is achieved at each step during our simulations, viz., our simulations represent slow cooling experiments.

3.3. Results and Discussions

3.3.1. Accounting for the Effect of Overall Solvophobicity on Copolymer Collapse

We have simulated single chain collapse for a series of random copolymers with varying *c*-unit content, x (x = 0, 6.25, 12.5, 25, 37.5, 50, 87.5 and 100%, $N = 128$, $\lambda = 20$; Figure 3.4a) and, with varying λ (λ = 10, 20, 30, 40 and 50, $N = 128$, x = 12.5%; Figure 3.4b). With increase in *c*-unit content, the decrease in the size of the copolymer chain occurs at progressively lower values of B (viz., higher effective temperatures), and the transition is

more abrupt, viz., the transition takes place over a narrower range of B (Figure 3.4a). Similarly, with an increase in λ, (viz., increased c-c attraction), there is an enhanced driving force for copolymer collapse and the chain collapses at lower values of B and over a narrower B range (Figure 3.4b). The results in Figures 3.4a,b (influence of x and λ), clearly indicate that the transition from coil to globule state for a copolymer, is mainly driven by c-c attraction. Since the c-units are more solvophobic compared to m-units, an increase in either x or λ, leads to an increase in the overall solvophobicity of the copolymer chain. Therefore, the abrupt collapse of copolymers at lower values of B observed in Figures 3.4a, b is anticipated. However, these data do not differentiate between the effects of overall solvophobicity from those of the copolymer chain microstructure. For example, a polymer containing 100% of the c-units should exhibit qualitatively similar collapse behavior as a homopolymer of the m-units. Since the effective attraction between units of the homopolymer of c-units is λB, a plot of $\left\langle R_g^2 \right\rangle$ versus B^* ($=\lambda B$, see Equation 2) is expected to be identical with the collapse behavior observed for a homopolymer of m-units. Therefore, we attempt to separate out the influence of the overall increase in solvophobicity by appropriately rescaling B for each copolymer studied.

We rescale the B axis by matching the theta points for the various copolymers as follows:

$$B^* = \left(B_\theta^h / B_\theta^c\right) B \qquad \text{.....(4)}$$

where, the scale factor, B_θ^h / B_θ^c is the ratio of the theta value of B for the homopolymer to that for the copolymer.

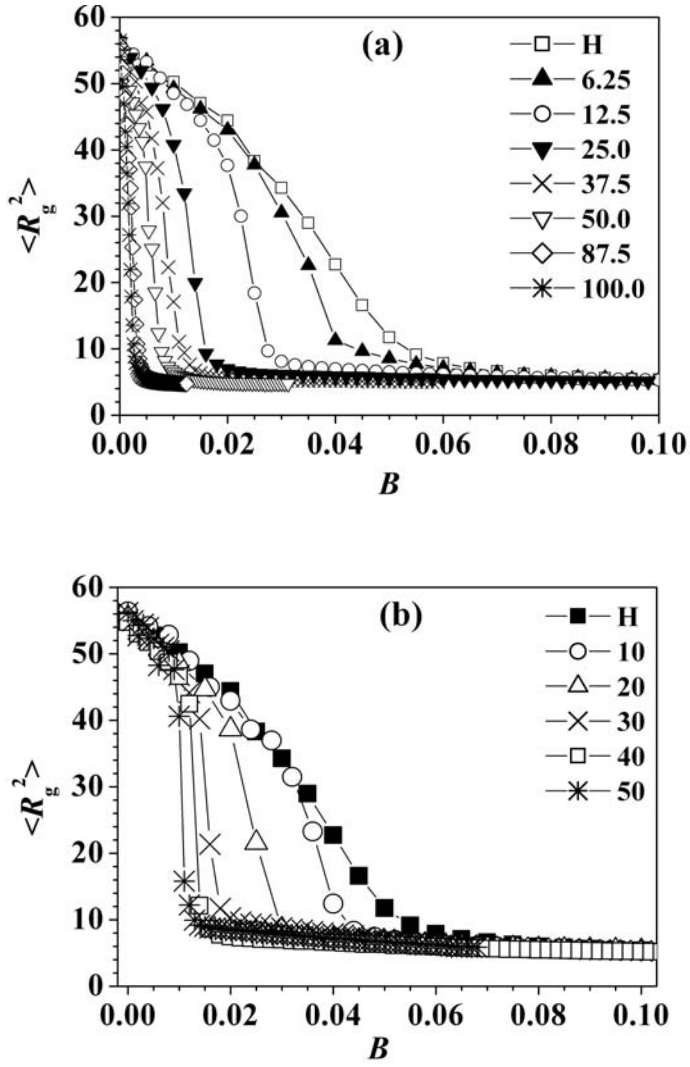

Figure 3.4. Effect of (a) *c*-unit content, *x* (for λ = 20) and (b) λ (for *x* = 12.5%) on collapse of a random copolymer (*N* = 128). H stands for homopolymer. The lines joining the points are meant only as a guide to the eye.

According to Flory[5], the theta state is an "ideal" state where polymer chain is said to attain its unperturbed dimensions. The mean square radius of gyration scales linearly with the chain size, (N-1). Thus, the ratio $\left\langle R_g^2 \right\rangle / (N-1)$, is a constant, independent of chain length. We use this principle to estimate the theta value of B in a manner analogous to Hu[10]: we simulate chains of different length (N = 32, 64, 128, 256 and 512) and obtain the theta value as the value of B at which $\left\langle R_g^2 \right\rangle / (N-1)$ coincides for all N. Strictly, a unique theta point is defined only for $N \rightarrow \infty$; for a finite length chain, we obtain instead a "theta region" that approaches the unique theta temperature[48] as $N \rightarrow \infty$. For a homopolymer, we estimate a theta region of $B = 0.027 \pm 0.001$, at which the normalized chain size is $\left\langle R_g^2 \right\rangle / (N-1) = 0.29 \pm 0.01$ (Figure 3.5a). The B_θ and theta-value of $\left\langle R_g^2 \right\rangle / (N-1)$ obtained here closely match those obtained previously[10]. Similarly, we have calculated the theta region for a copolymer ($\lambda = 20$, $x = 12.5\%$) as $B = 0.019 \pm 0.001$ at which $\left\langle R_g^2 \right\rangle / (N-1) = 0.29 \pm 0.01$ (Figure 3.5b). Since both *m*-units and *c*-units occupy one lattice site in our simulations, the normalized value of the chain coil size, $\left\langle R_g^2 \right\rangle / (N-1)$ at the theta region is the same for homo– and copolymers and is equal to 0.29 ± 0.01. We have verified this value of the normalized chain size for copolymers with x = 6.25%, 25%, 37.5%, 50% and 87.5% for $\lambda = 20$. Therefore, for the other copolymers, we conveniently estimate the theta region as the B value at which $\left\langle R_g^2 \right\rangle / (N-1) = 0.29$. We estimate B^* for each of the copolymers mentioned above and present this data in Figure 3.6. We find that our values closely match with those calculated using the formulation of Chen and co-workers[49] except at low x and λ. For example, for x = 6.25% and $\lambda = 10$, B^* calculated according to the formulation of Chen yields a value of

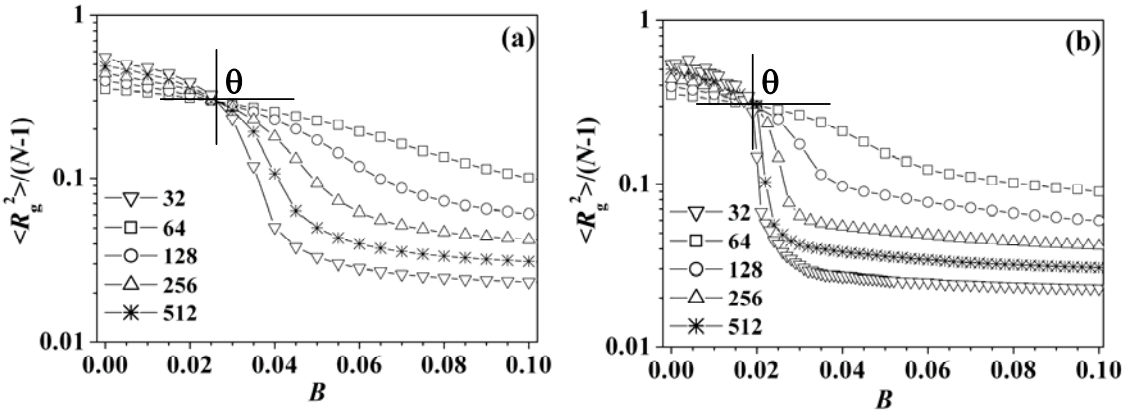

Figure 3.5. Change in the mean square radius of gyration (scaled by the number of chain segments), $\langle R_g^2 \rangle / (N-1)$ as a function of *B* for (a) homopolymer and (b) random copolymer (*x* = 12.5 %, λ = 20). The theta point is determined at the point where $\langle R_g^2 \rangle / (N-1)$ is equal for chains of different length – data for *N* = 32, 64, 128, 256 and 512 are shown as squares, circles, triangles, stars and inverted triangles respectively. The lines joining the points are meant only as a guide to the eye. The θ-value of *B* is as indicated. Note that the scaled value of the θ-chain size is the same for homo- and copolymers.

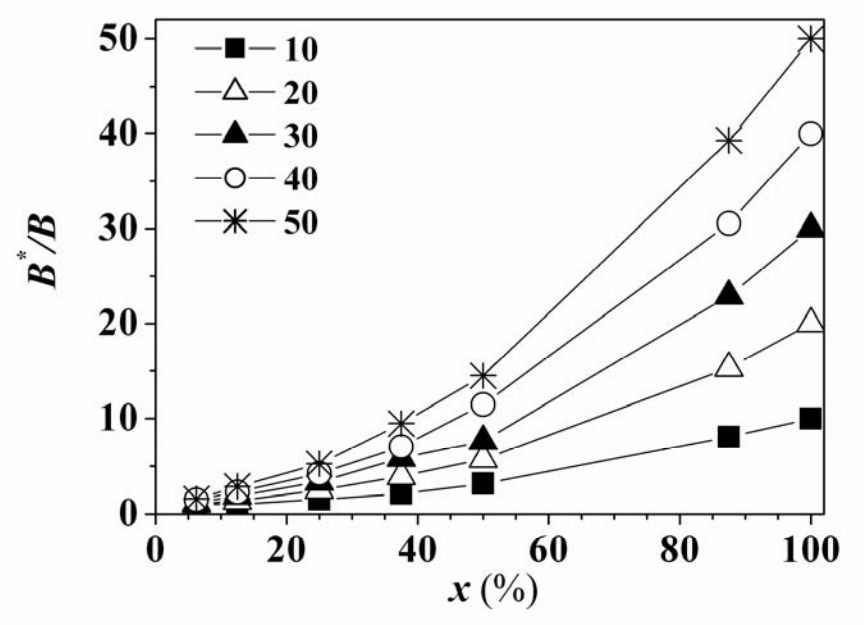

Figure 3.6. The scale factor, B^*/B for copolymers (N = 128) as a function of *c*-unit content for various values of λ. The lines joining the points are meant only as a guide to the eye.

0.977*B*, which is aphysical since, collapse of a copolymer with attractive comonomer unit cannot take place at effective temperatures that are lower than for the corresponding homopolymer.

3.3.2. Influence of Copolymer Microstructure

We first investigate the collapse of copolymers with varying comonomer content at λ = 20, plotted against our rescaled B^* (Figure 3.7, compare with the data in Figure 3.4a). Our data demonstrate that the sizes of the copolymer chains are similar in the expanded state ($B^* < B^*_\theta$) and in the collapsed state ($B^* >\sim 0.08$), independent of x (Figure 3.7). The effect of the copolymer microstructure is evident only in a B^* range between the theta region and collapse, where the size of a copolymer deviates from that of the homopolymer. To investigate the effect of the copolymer microstructure at various x and λ, we plot the ratio of the size ($\left\langle R_g^2 \right\rangle$) of the homopolymer to that of the copolymer at B^* = 0.034, intermediate between the theta and collapsed states (Figure 3.8). We have selected this value of B^* arbitrarily, such that the effects of copolymer microstructure are clearly evident. For $x >\sim 50\%$, for all values of λ, the ratio of the size of the homopolymer to that of the copolymer is ~1 (Figure 3.8). For $x <\sim 50\%$, for λ = 10, this ratio does not deviate much from 1, but for higher values of λ, the deviation is pronounced and reaches a maximum between 12.5 to 25% for all λ values investigated. Thus, the collapse transition becomes steeper (viz., takes place over a narrower range of B^*) as *c*-unit content increases up to x = 12.5 or 25%, depending on the value of λ, and then becomes less steep, and is qualitatively similar to homopolymer collapse, for values of $x >\sim 50\%$, for the λ values investigated.

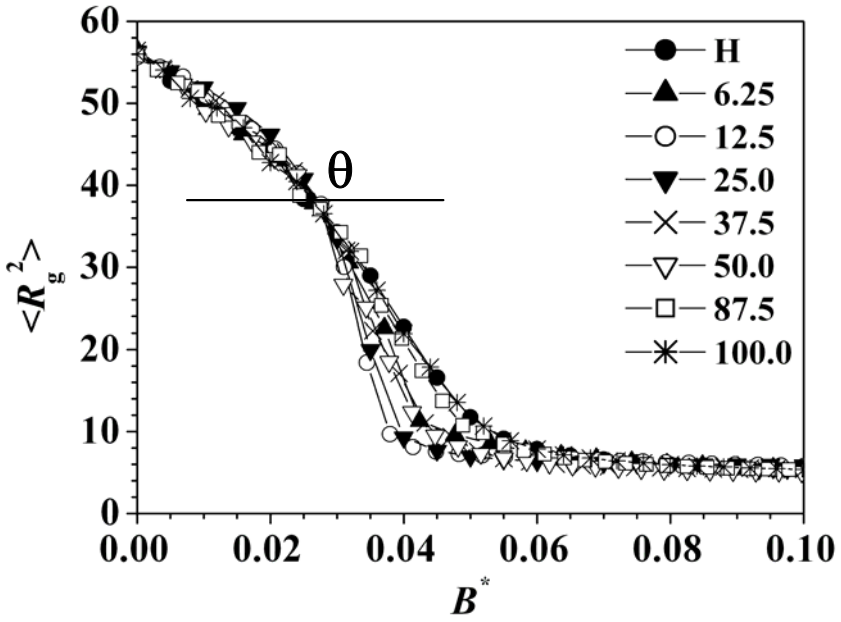

Figure 3.7. Effect of *c*-unit content on collapse of a random copolymer (N = 128, λ = 20) compared at equal theta by appropriately scaling B^* as described in eqn (4). H stands for homopolymer. The lines joining the points are meant only as a guide to the eye.

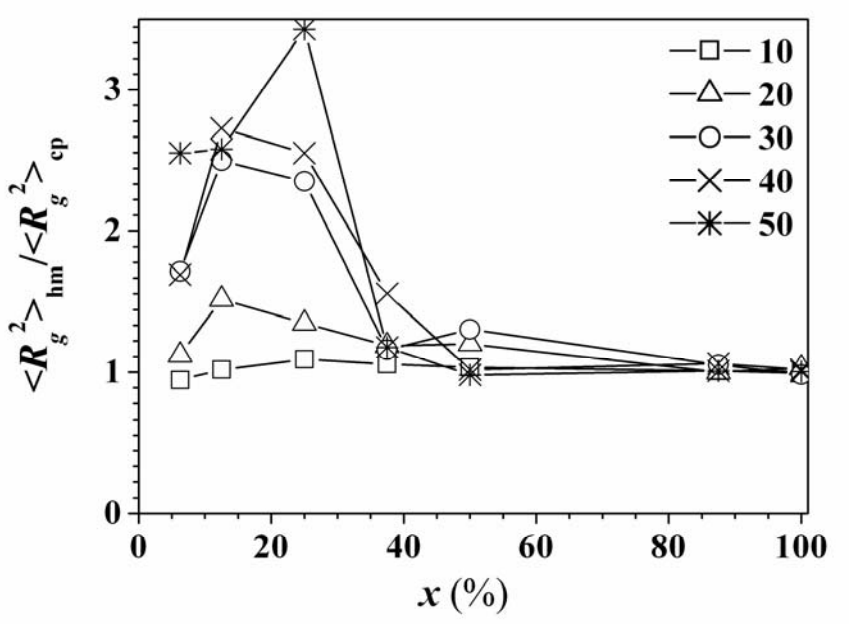

Figure 3.8. Change in the ratio of mean square radius of gyration of homopolymer to copolymer (N = 128) as a function of x at B^* = 0.034 for various values of λ. The lines joining the points are meant only as a guide to the eye.

As copolymer collapse is driven by the strong attraction between *c*-units, we examine the average number of *c*-*c* contacts (*CC*) as a function of x and λ in the expanded coil state ($B^* = 0.01$), in the collapsed state ($B^* = 0.08$) and in the intermediate state ($B^* = 0.034$). In the high temperature expanded coil state (low B^*), we expect that *CC* should scale as x^2, while in the compact collapsed globule state (high B^*), the *c*-units are expected to be aggregated and therefore we anticipate that the number of *c*-*c* contacts should scale as x (the scaling in the globule state is expected to hold strictly only for globules containing a large number of *c*-units). When we plot the ratio of CC/x as a function of x, at $B^* = 0.01$ for copolymers containing various *c*-unit contents, we observe that this number approximately scales with x, while at $B^* = 0.08$, CC/x is almost independent of x at higher x (Figure 3.9). Interestingly, at $B^* = 0.034$, the number of *c*-*c* contacts exhibits non-monotonic behavior in the range of x where we observe the effects of copolymer microstructure on collapse (Figure 3.9). This strongly indicates that the rapid collapse in the copolymer size (relative to the homopolymer) that we observe for the copolymers is driven by the formation of a larger than average number of *c*-*c* aggregates.

Before we discuss the implications of these results, we present data for collapse of copolymers containing 12.5% *c*-units as λ is increased from 10 to 20, 30, 40 and 50 ($N = 128$, Figure 3.10). The sizes of the copolymer chains are plotted versus B^* obtained by rescaling B by B_θ^h / B_θ^c. Again, we find that the collapse is steeper as we go from the homopolymer to copolymers with increasing values of λ. However, for $\lambda > 30$, the initially abrupt decrease in $\left\langle R_g^2 \right\rangle$ beyond theta transitions to a slower decrease before a compact globule is formed (Figure 3.10).

For $\lambda = 30$, 40 and 50 the average coil size is higher relative to the homopolymer even at $B^* = 0.1$ where we expect the chains to have completely collapsed. This effect is not an

artifact of our simulations since the percentage of accepted MC moves is similar for λ = 20 and 50 (viz. above and below λ = 30). Also, we do not observe any hysteresis in the size of the copolymer chain when we reheat and expand collapsed copolymer chains even with λ = 50. We believe that the large *c*-*c* attraction at λ > 30 may lead to the formation of a *c*-unit aggregate that prevents the chain from contracting rapidly to form a more compact conformation.

3.3.3. Comparison with Literature

Our results accord qualitatively with experimental studies that have observed that copolymers collapse over a narrower temperature interval relative to the corresponding homopolymers (Figure 3.4). For example, it has been reported that collapse of a copolymer of styrene and methyl methacrylate (MMA) in isoamylacetate, is more abrupt compared to collapse of poly(methyl methacrylate) (PMMA)[14]. Also, while polystyrene (PS) has a theta temperature of 18.5^{o}C in a nonpolar solvent, decalin (cis:trans 60:40), a polar copolymer of polystyrene sulfonic acid (PSSA, with a sulfonation level of 2 mol %) shows a theta temperature of 151^{o}C[50]. Thus, B^{*}/B for the pair of PS and PSSA can be calculated as $(T_{\theta}^{PSSA}/T_{\theta}^{PS})$~1.45. From Figure 3.6, we can estimate that this corresponds to a $\lambda \approx 30$ at x = 2%. Thus, it appears that the range of λ values considered in our work is appropriate to model the collapse of copolymers containing polar comonomers (solvophobic *c*-units) in apolar solvents.

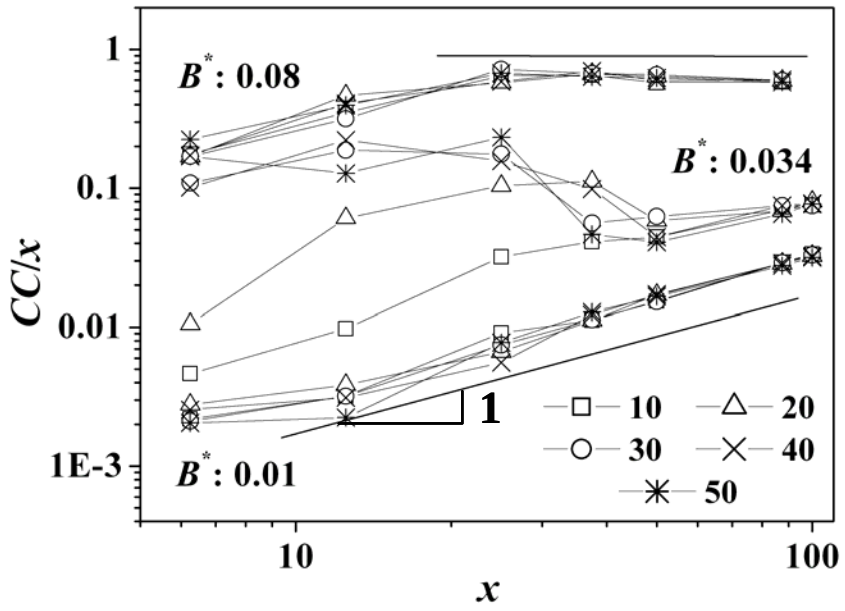

Figure 3.9. Change in the ratio of number of *c*-*c* contacts (*CC*) to *c*-unit content (*x*) for copolymers (*N* = 128) as a function of *c*-unit content for various values of λ at B^* = 0.01 (expanded coil), 0.034 (intermediate between theta and collapse), 0.08 (collapsed globule). Line with slope of 1 is shown near the data for B^* = 0.01 as a guide to the eye. The lines joining the points are meant only as a guide to the eye.

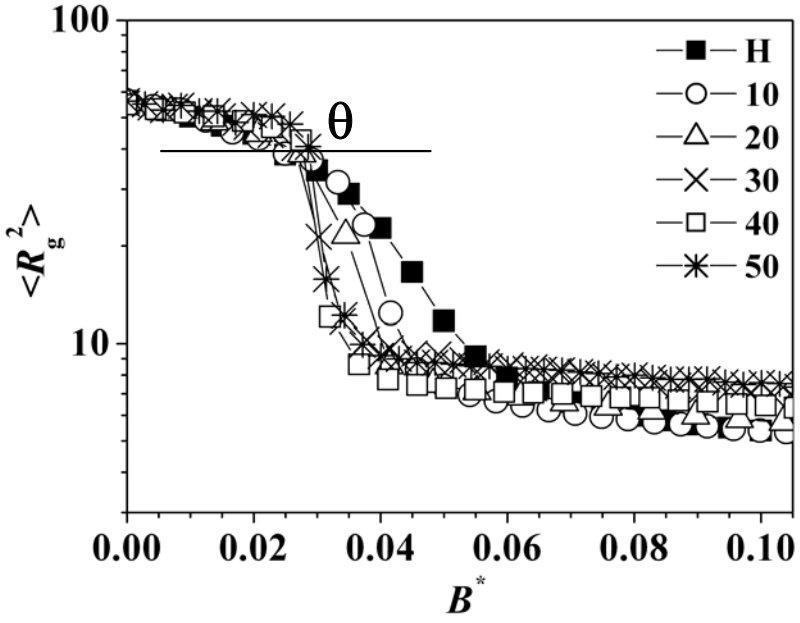

Figure 3.10. Effect of λ on collapse of a random copolymer (N = 128, x = 12.5%). The polymers are compared at equal theta by plotting versus the appropriately scaled B^*. H stands for homopolymer. The lines joining the points are meant only as a guide to the eye.

Our results also match with the predictions of Ganazzoli[12] who theoretically showed that copolymers collapse more abruptly as compared to homopolymers, but that, as expected, the behavior of a "copolymer" at x = 100% is qualitatively similar to that of a homopolymer. Theory indicates that copolymer collapse is a first order transition while flexible homopolymers collapse through a smooth second order transition[7]. We do not probe the order of the collapse transition in our simulations; however, the decrease in $\left\langle R_g^2 \right\rangle$ for the copolymer during collapse is observed to be steeper relative to that for homopolymers (Figure 3.7), even after accounting for the increase in overall solvophobicity of the copolymers.

Simulations suggest that polymer chains collapse via the formation of an initial dense nucleus surrounded by a partially collapsed chain[10]. Collapse proceeds as this nucleus grows by reeling in chain units. In homopolymers, monomers near the surface of the initial nucleus are reeled in[2]. In copolymers, the initial nucleus is made up of *c*-units, and collapse is driven by the net attraction of *c*-units to the nucleus[2,12]. Simulation data suggest that this structural difference underlies the change from second order collapse in homopolymers to first order in copolymers[12,26]. Our data too suggest a structural origin for the relatively abrupt collapse of copolymers: we observe that values of λ and x that lead to abrupt collapse are related to an increased number of *c*-*c* contacts in the intermediate state that precedes the formation of the final collapsed globule (Figure 3.9). Therefore, we expect that an exploration of the spatial structure of the copolymer chain as it collapses may yield valuable insights into the influence of copolymer microstructure on the collapse transition. This is investigated in the next section.

3.3.4. Structure of the Copolymer Chain during Collapse

In this section, we examine the structure of the copolymer chain as it transitions from an expanded coil at low B^* through the theta condition to the final collapsed globule at high B^*. We focus on a copolymer with N = 128, x = 12.5% and λ = 20, viz., a copolymer that undergoes an abrupt collapse relative to the corresponding homopolymer and present results for the tructure of the chain as the value of B^* is increased.

A comparison between the density of the entire copolymer chain (defined as the number of units, N, divided by $\left\langle R_g^2 \right\rangle^{3/2}$, a measure of the chain volume) and the density of only the c-units (defined as the number of comonomers, N_c, divided by the $\left\langle R_{gc}^2 \right\rangle^{3/2}$, a measure of the volume occupied by the c-units) provides insights into the structure of the copolymer chain as B^* is increased. For B^* below the theta value, m-units and c-units are distributed equally densely in space (Figure 3.11a). However, slightly above the theta value of B^*, the c-unit density increases abruptly. At this same B^* value, the overall density of the polymer chain also exhibits an equally abrupt but smaller increase. However, while the c-unit density plateaus after the abrupt increase, the remainder of the chain continues to densify (Figure 3.11a). Thus, as B^* increases, the c-units aggregate, driven by their strong repulsion for the m-units and the solvent. The abrupt increase in the overall chain density observed in Figure 3.8a is also driven by the formation of this c-unit aggregate. It is interesting to compare this behavior with that of a chain with N = 128, x = 50% and λ = 20 (Figure 3.11b), viz. a chain that effectively behaves like a homopolymer (Figure 3.7). For this copolymer, the increase in the density of c-units parallels that in the density of the entire chain – beyond

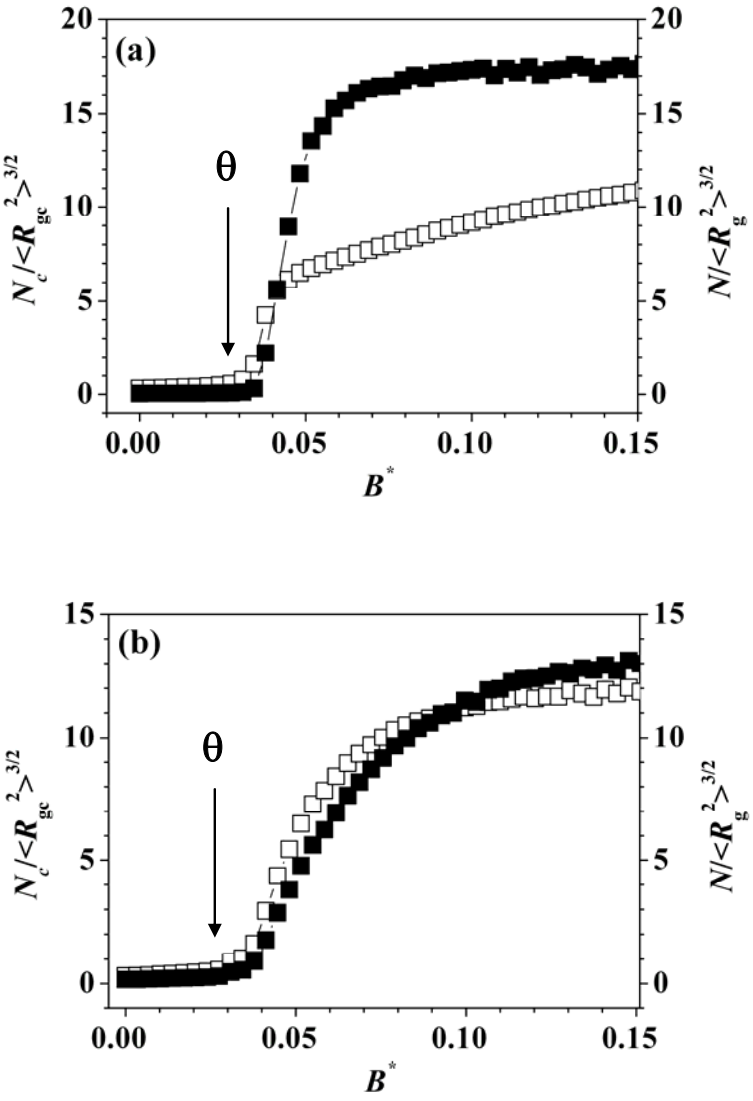

Figure 3.11. Comparison of the density (as defined in the text) as a function of B^* for a random copolymer N = 128, λ = 20 (a) x = 12.5 %,; (b) x = 50%. Filled symbols represent the density of the *c*-units while the empty symbols represent the density of the entire chain. The θ point is as indicated.

the theta point, both densities increase. This densification is rapid initially (but not as rapid as for the low *x* copolymer) and then continues gradually.

Snapshots of the copolymer equilibrated at various B^* values indicate that the chain is expanded at $B^* = 0$ (Figure 3.12a). At $B^* \sim 0.0276$, near the theta state, *m*-unit and *c*-units stay solvated (Figure 3.12b). However, at $B^* = 0.041$, above the theta value, the *c*-units collapse to form a dense core, that is surrounded by *m*-units that remain solvated (Figure 3.12c). These *m*-units then begin collapsing (Figure 3.12d, $B^* = 0.055$) and finally form a dense globule (Figure 3.12e, $B^* = 0.138$) that retains the *c*-core–*m*-shell structure that originates near the theta state.

Our data demonstrate that copolymer collapse proceeds via a two-stage process, first forming a dense *c*-unit aggregate (the "core"), and subsequently compacting, at higher B^*, by aggregation of *m*-units. The formation of the core (aggregate of *c*-units) is abrupt and happens at B^* slightly greater than B^*_θ. At theta, and for B^* values slightly greater than theta, the *m*-sequences between *c*-units remain solvated around the dense *c*-unit core. This configuration appears to be similar to the "flower-like" intermediate state that has been recently observed to precede collapse in poly(N-isopropylacrylamide)-polyethyleneoxide graft copolymers[22]. Finally, the shell of *m*-units then collapses slowly around the *c*-unit core to form the final core-shell globular structure.

We analyze the shape of the copolymer chain as it collapses, using the ratio of the eigenvalues (L_i^2) of the shape tensor, S^2. We plot the change of L_i^2 with B^* for the entire copolymer chain ($N = 256$, $\lambda = 20$, $x = 12.5\%$, Figure 3.13a), for the *c*-units in the same copolymer chain (Figure 3.13b), and for the corresponding homopolymer ($N = 256$, Figure 3.13c).

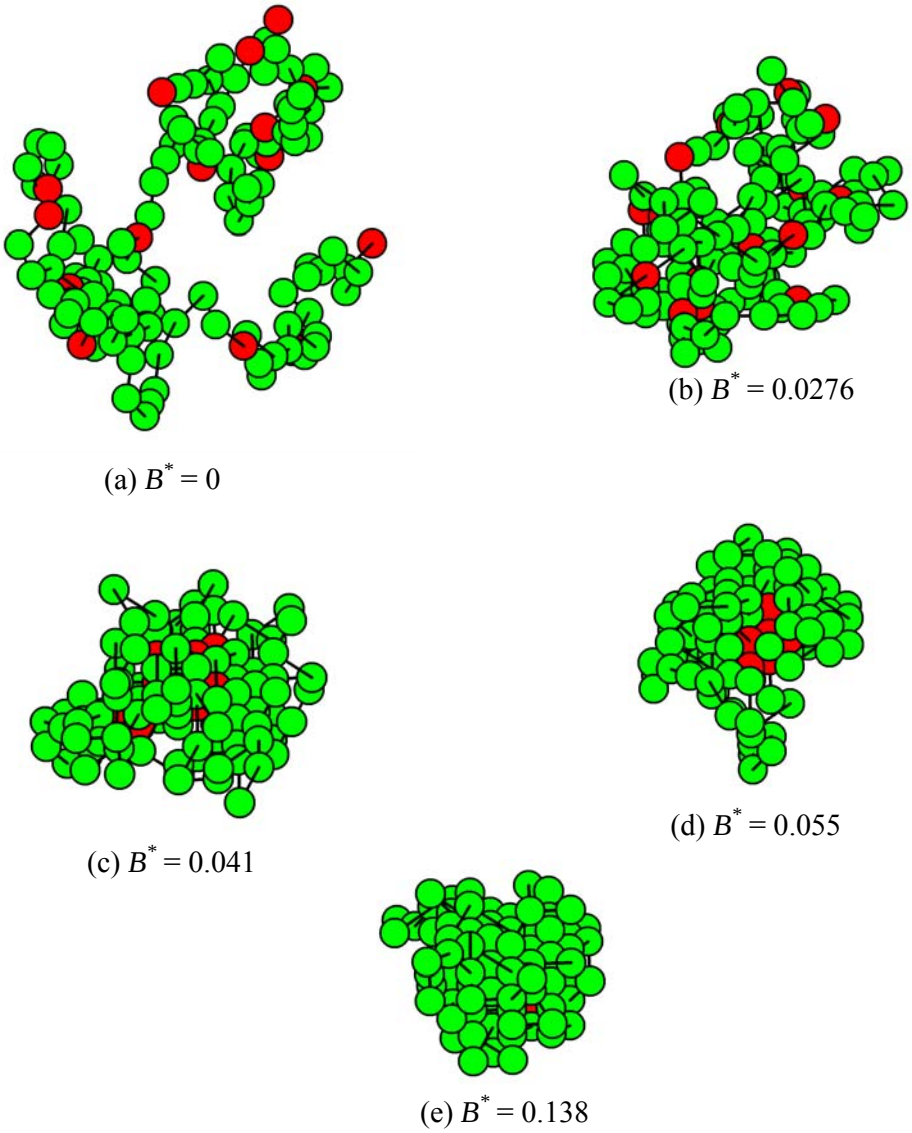

Figure 3.12. Snapshots of the structural evolution a random copolymer chain (N = 128, x = 12.5%, λ = 20) during collapse. *m*-units and *c*-units are represented by green and red symbols respectively. B^* = 0.0276 represents the snapshot at theta state.

In the expanded coil state, homo- and copolymer chains are extended. Topological connectivity of the units along the polymer chain leads to an anisotropic shape with shape factors, L_i^2, in the ratio of 14.1:2.94:1. The shape factors change above B_θ^*, and approach each other as the chain begins to collapse (Figures 3.13a,c). The change in the shape factors is gradual for the homopolymer relative to the copolymer. Even in the collapsed globule state, we observe that L_i^2 are not equal, viz., the globule is not spherical. Rather, we obtain an ellipsoidal core-shell structure with shape factors, L_i^2 in the ratio of 1.62:1.25:1 (Figure 3.13a).

In our simulations, the anisotropy that we observe is affected by the discreteness of the lattice used. However, the final globule is predicted to be anisotropic by molecular dynamics[51] and Monte Carlo simulation[52] studies, even for the case of homopolymer collapse. These values for the copolymer anisotropy from our simulations accord well with homopolymer theory[53] and previous simulations[52]. The shape of the final globule state of copolymer is similar to that of a homopolymer (compare Figure 3.13a and 3.13c). For a copolymer, collapse is mediated by the formation of a core consisting of *c*-units. From the shape factors only for the *c*-units comprising the core, we observe that the compact *c*-unit core is essentially isotropic (Figure 3.13b). Thus, the picture that emerges is that during collapse, the *c*-units aggregate to form an isotropic core that is surrounded by incompletely collapsed *m*-units in the copolymer chain. These *m*-units slowly approach an isotropic shape with increase in B^*, but for the B^* values investigated here, the entire chain remains ellipsoidal.

Finally, we contrast the behavior observed for the copolymer with $N = 128$, $x = 12.5\%$ and $\lambda = 20$ (Figure 3.12) with a copolymer chain having a higher *c*-content ($N = 128$, $x = 50\%$

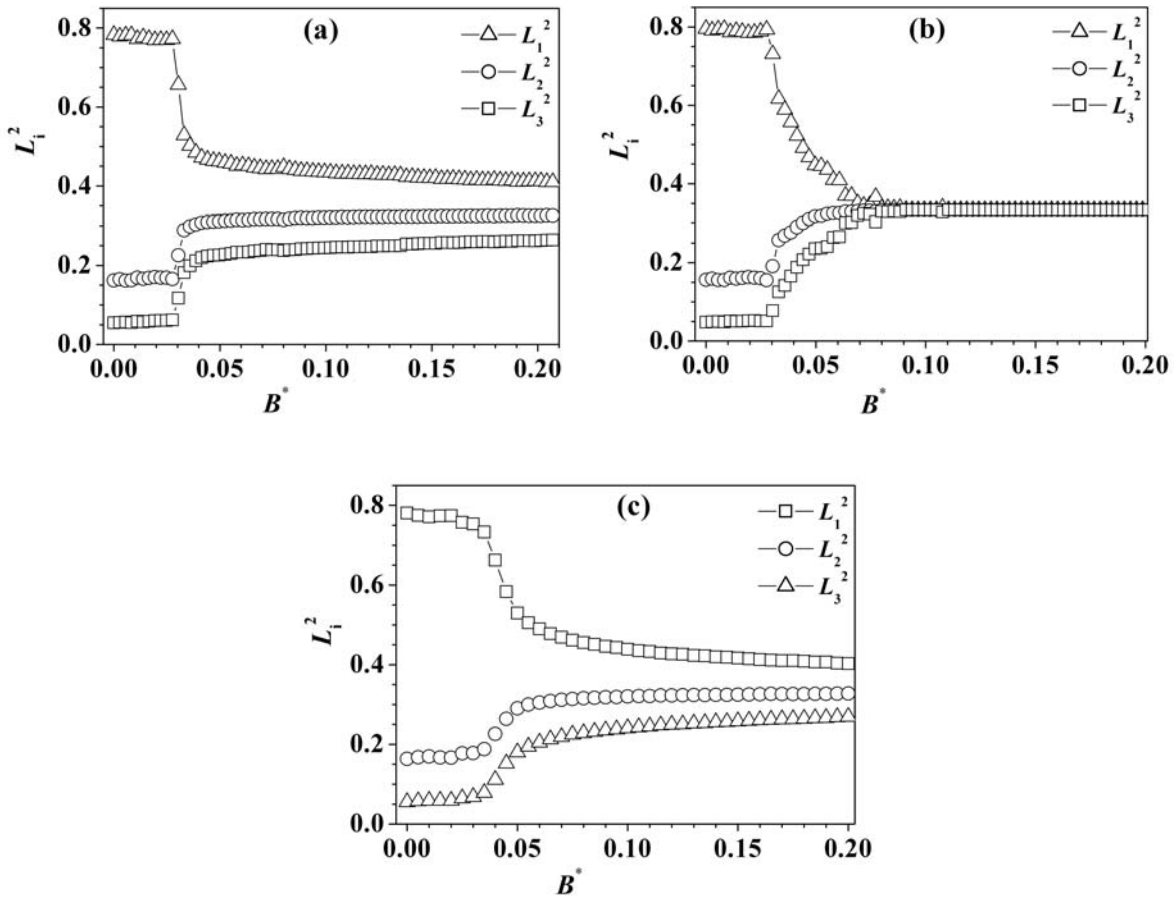

Figure 3.13. Change in the shape factors as a function of B^* for (a) copolymer (N = 256, x = 12.5%, λ = 20), (b) for the c-unit core and (c) for a homopolymer (N = 256). The lines joining the points are meant only as a guide to the eye.

and λ = 20, Figure 3.14) that collapses in a manner that is qualitatively similar to homopolymers (see Figure 3.7). As the chain with higher x is cooled to the theta value, the chain conformation appears similar to that observed for the chain with x = 12.5% (compare Figure 3.12b with 3.14a, B^* values closest to the B_θ^* we selected). When B^* is increased to ~ 0.041, in the region between theta and collapse, we observe that unlike the formation of a well-defined core-shell structure in the x = 12.5% copolymer (Figure 3.12c), the copolymer with x = 50% does not exhibit any microphase separation and does not collapse (Figure 3.14b). The final collapsed state for the polymer with x = 50% exhibits a core-shell morphology (Figure 3.14c). However, this structure is not as clearly defined as in the case of the polymer with x = 12.5% (Figure 3.13e). These qualitative differences have been illustrated in Figure 3.11a (x = 12.5%) and 8b (x = 50%) for quantitative comparison.

Therefore, it appears that the effect of copolymer microstructure is evident only in cases where the collapse happens via the formation of a well-defined core-shell structure. We note here that we are comparing the spatial structure of copolymers at the same B^*, viz., after accounting for the effect of the overall solvophobicity. For chains with increased x, it appears that the only effect of the *c*-units is to increase the overall solvophobicity, and apart from this, the collapse is qualitatively similar to that of a homopolymer. Hu[10] has claimed that even homopolymer chains exhibit an internal "microphase segregation" between a compact core and a disordered, crumpled shell during collapse. In the case of copolymers containing a "small" percent of highly mutually attractive *c*-units, this core-shell microphase separation happens between a compact *c*-unit core and an *m*-unit shell. The formation of this microsegregated structure appears to be responsible for the qualitative change in behavior for copolymer collapse relative to homopolymers. With increase in x or λ, the behavior of the copolymer chain is

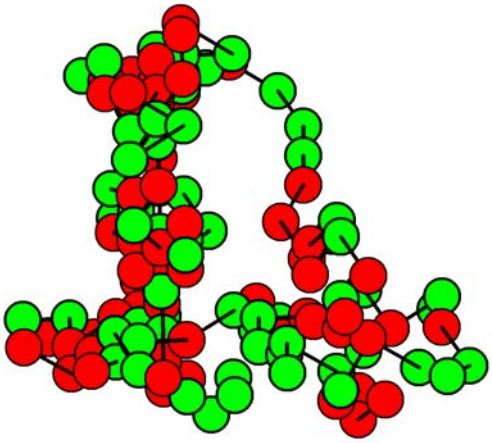

(a) $B^* = 0.034$

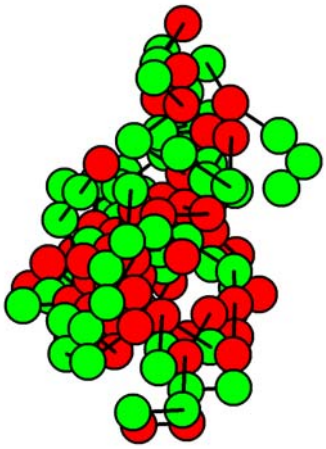

(b) $B^* = 0.041$

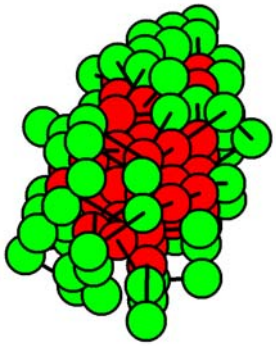

(c) $B^* = 0.11$

Figure 3.14. Snapshots of the structural evolution a random copolymer chain (N = 128, x = 50%, λ = 20) during collapse. m-units and c-units are represented by empty and filled symbols, respectively. B^* = 0.034 represents the snapshot at near the theta state.

dominated by the *c*-units. Therefore, these chains simply behave like homopolymers with a higher solvophobicity, and the effect of copolymer chain microstructure is no longer apparent.

3.3.5. Effect of Chain Length

In this last section, we examine the effect of the chain size, *N*, on copolymer collapse. We have seen that for "small" *c*- content (for example, $x = 12.5\%$ at $N = 128$ and $\lambda = 20$), the *c*-units in the copolymer undergo a microphase separation beyond the theta region and aggregate to form a compact core surrounded by a shell of *m*-units. The formation of this core-shell structure makes the collapse from the theta state more abrupt relative to that for a homopolymer. It is interesting to examine the effect of chain length on microphase separation, viz., on the formation of this core-shell structure. This will provide insight as to whether this microphase separation persists at, and influences the "true" phase transition, viz. for chains of infinite *N*. Our simulation technique limits the chain sizes that we can probe. However, we obtain a qualitative understanding of the effect of chain size by varying *N* (*N* = 32, 64, 128 and 256). We see that the variation in the number of *c*-*c* contacts with x is essentially identical and scales with x^2 for the range of *N* in the expanded coil state, viz., at $B^* = 0.01$ (Figure 3.15). For clarity, in Figure 3.15, we plot only the results for $N = 32$ and 256 and note that the data for the other chain lengths are qualitatively similar. In the collapsed globule state ($B^* = 0.16$, we choose $B^* = 0.16$ rather than 0.08, since chains with $N = 32$, undergo a significant decrease in their size beyond $B^* = 0.08$), the number of *c*-*c* contacts increases approximately linearly with x for all *N*; as the number of *c*-units increases with *N*, the number of *c*-*c* contacts also increases with increasing *N* (Figure 3.15). At both, $B^* = 0.01$ and 0.16, the increase in the number of *c*-*c* contacts is monotonic. However, in the intermediate state between theta and collapse, $B^* = 0.034$, we observe that the number of

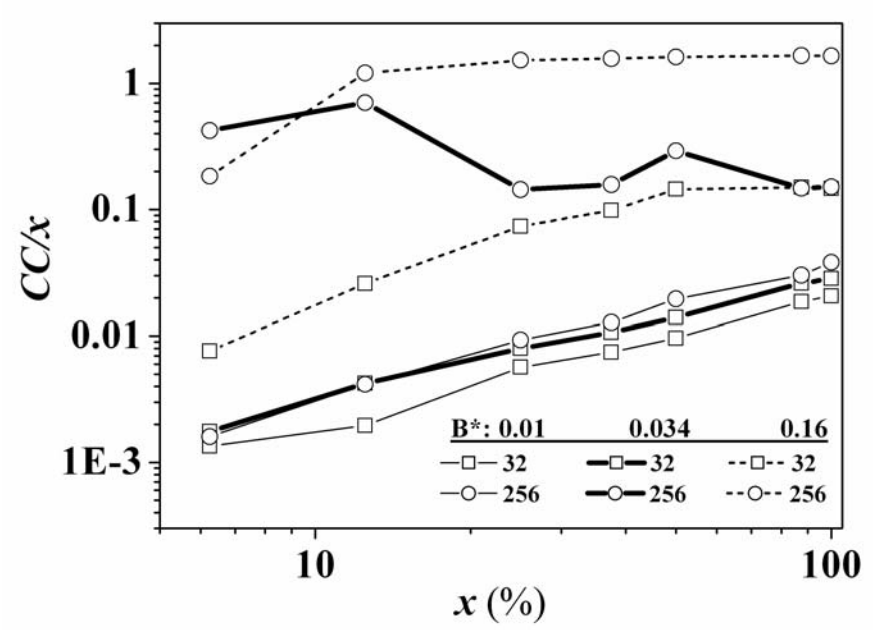

Figure 3.15. Change in the value of *CC*/x for copolymers (λ = 20) with various chain lengths (*N* = 32 and 256) as a function of x and at B^* = 0.01, 0.034 and 0.16. We highlight the data for B^* = 0.034 using bold lines. The lines joining the points are meant only as a guide to the eye.

c-*c* contacts is non-monotonic with a higher number of contacts at $x < 50\%$ (Figure 3.15). As seen previously, this is a signature of the formation of the *c*-unit aggregate core. Therefore, it appears that the effect of copolymer microstructure at *c*-unit content, $x < 50\%$, persists with increase in *N*. This is strongly indicative that the formation of a *c*-unit aggregate core and *m*-unit shell happens even at larger *N* and that this microphase segregation leads to a more abrupt collapse transition. This result accords with theoretical predictions of a change in the order of the "true" collapse transition from second order for homopolymers to a steeper first order transition for copolymers[12]. Our data also suggest that for higher *x*, the copolymer behaves essentially like a homopolymer and the order of the phase transition then returns to second order.

Finally, we examine the shape of the collapsed globule at $B^* = 0.16$ (for $N = 32$, 64, 128, 256 and 512). We have observed that the globules are not isotropic (Figure 3.13a). This is true not only for copolymers, but also for homopolymers (Figure 3.13c). The anisotropy is more pronounced at low *N* and the shape factors approach each other as *N* increases (Figure 3.16). It appears that at infinite *N*, the collapsed globule tends to $L_i^2 = 1/3$. We have seen that a copolymer with $N = 256$, $x = 12.5\%$ and $\lambda = 20$ exhibits a core shell structure, with a compact, isotropic core comprising *c*-units surrounded by an ellipsoidal shell of *m*-units (Figure 3.13). The anisotropy in the overall shape of the copolymer (Figure 3.16) is similar to that observed for homopolymers and follows the same trend with increasing *N*, viz. it approaches a more isotropic shape as *N* increases. Thus, there appears to be no specific role of the copolymer microstructure on the final shape of the collapsed globule, viz., it affects only the "path" between the theta and globule states.

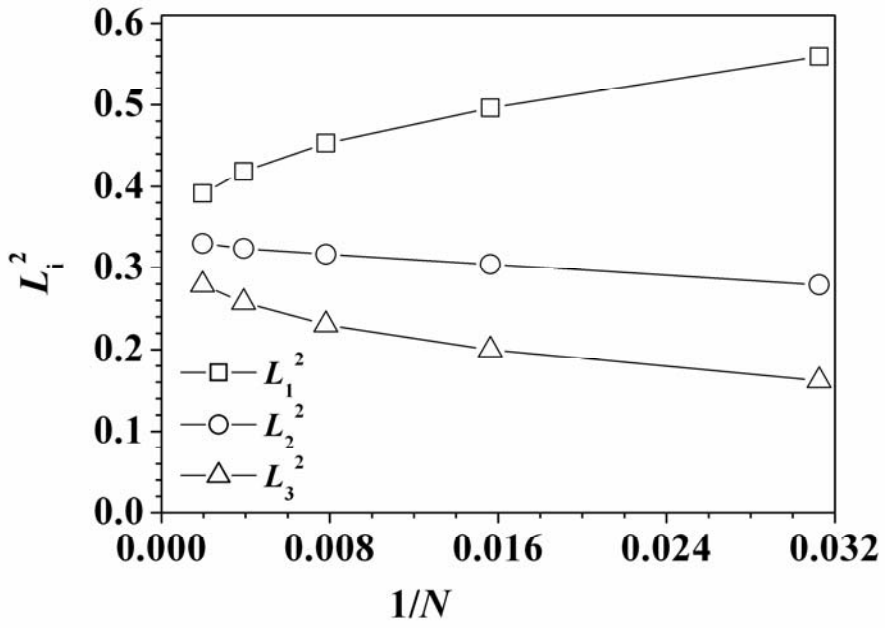

Figure 3.16. Change in the shape factors as a function of 1/*N* for a random copolymer (*x* = 12.5%, λ = 20) for *N* = 32, 64, 128, 256 at B^* = 0.16. The lines joining the points are meant only as a guide to the eye.

3.4. Summary

We describe the collapse of a copolymer chain as it is cooled from an expanded coil state through the theta region to a collapsed globule using dynamic Monte Carlo lattice simulations. The salient features of our investigations are:

1. We model the collapse of copolymers containing solvophobic *c*-units (e.g., polar *c*-units in nonpolar solvents) in a Flory-like approach
    a. We choose a higher penalty for an *m*-*c* or a *c*-*s* contact relative to an *m*-*s* contact.
    b. The high effective *c*-*c* attraction, leads to an increase in the overall solvophobicity of the chain relative to a homopolymer, and therefore, copolymers collapse abruptly and at higher effective temperatures relative to homopolymers.
2. We compare polymers at the same solvophobicity by rescaling the collapse data so as to match the theta temperatures of these polymers. The rescaled data reveal that:
    a. In the high temperature region from the expanded coil state to theta, enthalpic interactions between chain units are unimportant and homo- and copolymer chains show the same collapse behavior, after normalizing (scaling) out the overall solvophobicity.
    b. The overall solvophobicity is normalized empirically, by rescaling the *B* axis to make coincident the theta point for the various copolymers.
    c. Beyond the theta point, copolymers containing < 50% *c*-units collapse over a narrower region and at higher effective temperatures.
    d. Copolymers with higher *c*-content, behave in a manner that is qualitatively similar to homopolymers, when the overall solvophobicity is normalized.

3. Our results point to an interesting structural origin to the influence of copolymer chain microstructure on collapse.
    a. For copolymers with < 50% *c*-units, the *c*-units aggregate due to their strong mutual attraction to form a dense isotropic core as the chain is cooled below theta, thus exhibiting distinct *c*-core – *m*-shell morphology.
    b. The anisotropic *m*-unit shell that surrounds the *c*-unit core is "fluffy" and densifies on further cooling. The collapsed core-shell globule is anisotropic, but the anisotropy decreases with increase in chain length.
    c. Our data suggest that the aggregation of the comonomers to form a core-shell structure in copolymers containing < 50% *c*-units persists as the chain length is increased.
    d. Copolymers containing more than 50%, *c*-units are dominated by the mutual attraction of *c*-units and behave essentially like homopolymers having a higher effective solvophobicity.
    e. The solvophobicity-normalized copolymer microstructure affects only the path or mechanism of the collapse, as the solvent quality becomes poorer. It does not affect the final shape of the collapsed globule.

References

(1) Dill, K. A. *Biochemistry* **1985**, *24*, 1501-1509.

(2) Pande, V. S.; Grosberg, A. Yu.; Tanaka, O. *J. Chem. Phys.* **1997**, *107*, 5118-5124.

(3) Pande, V. S.; Rokhsar, D. S. *Proc. Natl. Acad. Sci. USA* **1998**, *95*, 1490-1494.

(4) de Gennes, P. G. *Scaling Concepts in Polymer Physics*; Cornell University Press: Ithaca, New York, 1979.

(5) Flory, P. J. *Principles of Polymer Chemistry*; Cornell University Press: Ithaca, New York, 1953.

(6) Baysal, B. M.; Karasz, F. E. *Macromol. Theory Simul.* **2003**, *12*, 627-645.

(7) Grosberg, A. Yu.; Kuznetsov, D. V. *Macromolecules* **1992**, *25*, 1970-1979.

(8) Ma, J.; Straub, J. E.; Shakhnovich, E. I. *J. Chem. Phys.* **1995**, *103*, 2615-2624.

(9) Grassberger, P.; Hegger, R. *J. Chem. Phys.* **1995**, *102*, 6881-6899.

(10) Hu, W. *J. Chem. Phys.* **1998**, *109*, 3686-3690.

(11) Timoshenko, E. G.; Yu.A.Kuznetsov, Yu. A.; Dawson, K. A. *Phys. Rev. E* **1998**, *57*, 6801-6814.

(12) Ganazzoli, F. *J. Chem. Phys.* **1998**, *108*, 9924-9932.

(13) Lantman, C. W.; MacKnight, W. J.; Higgins, J. S.; Peiffer, D. G.; Sinha, S. K.; Lundberg, R. D. *Macromolecules* **1988**, *21*, 1339-1343.

(14) Karal-Yllmaz, O.; Gurel, E. E.; Kayaman-Apohan, N.; Baysal, B. M.; Karasz, F. E. *Polymer* **2001**, *42*, 9433-9440.

(15) Chu, B.; Ying, Q.; Grosberg, A. Yu. *Macromolecules* **1995**, *28*, 180-189.

(16) Chu, B.; Wang, Z. *Macromolecules* **1989**, *22*, 380-383.

(17) Wu, C.; Zhou, S. *Macromolecules* **1995**, *28*, 5388-5390.

(18) Wu, C.; Zhou, S. *Macromolecules* **1995**, *28*, 8381-8387.

(19) Wu, C.; Zhou, S. *Phys. Rev. Lett.* **1996**, *77*, 3053-3055.

(20) Wu, C.; Wang, X. *Phys. Rev. Lett.* **1998**, *80*, 4092-4094.

(21) Wu, C.; Qiu, X. *Phys. Rev. Lett.* **1998**, *80*, 620-622.

(22) Zhang, G.; Winnik, F. M.; Wu, C. *Phys. Rev. Lett.* **2003**, *90*, 035506.

(23) Yu, J.; Wang, Z.; Chu, B. *Macromolecules* **1992**, *25*, 1618-1620.

(24) Vasilevskaya, V. V.; Klochkov, A. A.; Lazutin, A. A.; Khalatur, P. G.; Khokhlov, A. R. *Macromolecules* **2004**, *37*, 5444-5460.

(25) Raos, G.; Allegra, G. *J. Chem. Phys.* **1997**, *107*, 6479-6490.

(26) Bastolla, U.; Frauenkron, H.; Grassberger, P. *J. Mol. Liq.* **2000**, *84*, 111-129.

(27) Pande, V. S.; Grosberg, A. Yu.; Joerg, C.; Tanaka, T. *Phys. Rev. Lett.* **1996**, *76*, 3987-3990.

(28) Bastolla, U.; Grassberger, P. *Phys. Rev. E* **2001**, *63*, 031901-1-031901-12.

(29) Garel, T.; Leibler, L.; Orland, H. *J. Phys. II France* **1994**, *4*, 2139-2148.

(30) Kantor, Y.; Kardar, M. *Europhys. Lett.* **1994**, *28*, 169-174.

(31) Grassberger, P.; Hegger, R. *Europhys. Lett.* **1995**, *31*, 351-356.

(32) Hu, W.; Mathot, V. B. F.; Frenkel, D. *Macromolecules* **2003**, *36*, 2165-2175.

(33) Chanda, M. *Advanced Polymer Chemistry: A Problem Solving Guide*; Marcel Dekker: New York, 2000.

(34) Mayo, F. R.; Lewis, F. M. *J. Am. Chem. Soc.* **1944**, *66*, 1594-1601.

(35) Hiemenz, P. C.; Lodge, T. P. *Polymer chemistry*; CRC Press: Boca Raton, 2007.

(36) Kremer, K.; Binder, K. *Comput. Phys. Rep.* **1988**, *7*, 259-310.

(37) Carmesin, I.; Kremer, K. *Macromolecules* **1988**, *21*, 2819-2823.

(38) Shaffer, J. S. *J. Chem. Phys.* **1994**, *101*, 4205-4213.

(39) Metropolis, N.; Rosenbluth, A. W.; Rosenbluth, M. N.; Teller, A. H.; Teller, E. *J. Chem. Phys.* **1953**, *21*, 1087-1092.

(40) Nishimura, Takuji; Matsumoto, Makoto *http://www. math. sci. hiroshima-u. ac. jp/~m-mat/MT/emt. html* **2002**.

(41) Grassberger, P. *Phys. Rev. E* **1997**, *56*, 3682-3693.

(42) Koga, T. *Eur. Phys. J. E* **2005**, *17* , 381-388.

(43) Paul, W.; Müller, M. *J. Chem. Phys.* **2001**, *115*, 630-635.

(44) Hu, W. B.; Frenkel, D. *J. Phys. Chem. B* **2006**, *110*, 3734-3737.

(45) Cowie, J. M. G. *Polymers: Chemistry and Physics of Modern Materials*; Nelson Thornes: U. K., 2001.

(46) Polanowski, P.; Jeszka, J. K. *Langmuir* **2007**, *23*, 8678-8680.

(47) Smith, N. C.; Flemming, R. J. *J. Phys. A: Math. Gen.* **1975**, *8*, 929-937.

(48) Domb, C. *Polymer* **1974**, *15*, 259-262.

(49) Chen, T.; Changjun Peng, C.; Liu, H.; Hu, Y. *Fluid Phase Equilib.* **2005**, *233*, 73-80.

(50) Chakrabarty, K.; Seery, T. A. P.; Weiss, R. A. *Macromolecules* **1998**, *31*, 7385-7389.

(51) Tanaka, G.; Mattice, W. L. *Macromolecules* **1995**, *28*, 1049-1059.

(52) Tanaka, G.; Mattice, W. L. *Macromol. Theory Simul.* **1996**, *5*, 499-523.

(53) Šolc, K. *J. Chem. Phys.* **1971**, *55*, 335-344.

Chapter 4

Pathway to Copolymer Collapse in Dilute Solution: Uniform versus Random Distribution of Comonomers

4.1. Introduction

As solvent quality decreases, monomer-monomer attraction drives a polymer to collapse from a solvated expanded coil state to a compact globule[1-6]. When a polymer chain contains mutually attractive ("sticky") *co*-monomer units, the phase behavior of the chain is richer compared to homopolymers. Theory and simulations show that collapse of flexible random copolymers is preceded by microphase separation due to aggregation of the sticky comonomers, and that the chain can exhibit frozen, folded and collapsed states depending on its stiffness, the "stickiness" of comonomer interactions and on the distribution of comonomers along the chain (viz. chain microstructure)[3,7,8].

It is interesting to examine the role played by copolymer microstructure on collapse – especially since copolymers with precisely tailored microstructures can now be experimentally realized using recent advances in synthetic techniques[9]. There are relatively few reports that investigate how copolymer microstructure influences collapse. Interestingly, these studies already indicate the important role of comonomer distribution in determining the path to the collapsed state. In experiments on PNIPAM chains grafted with polystyrene "stickers" in aqueous solution, Zhang et al.[10] showed that copolymers with equi-spaced stickers formed an ordered coil prior to collapsing "cooperatively"; while, in contrast, random

copolymers did not form this intermediate structure and collapsed over a wider temperature range[6,10]. Recently, telechelic star copolymers were shown to collapse into "watermelon-structures" by aggregation of the terminal sticky comonomers[11]. Such microstructure-controlled pathways to collapse have important technological implications since they provide opportunities to rationally control the architecture of nanoparticles prepared by intramolecular crosslinking during collapse of single copolymer chains[12,13]. The two-letter copolymer collapse problem also represents a simplified version of protein folding[14,15]. In proteins, amino acid sequences are not random, but are designed to ensure collapse and cooperative folding of the protein into its unique native state[16-19], often via well-defined intermediate states[20-22]. Interestingly, simulations indicate that copolymers with specially designed protein-like sequences created by "coloring" monomer units on the outside of a homopolymer globule [5,23,24] exhibit abrupt transitions relative to random copolymers, and form soluble globules rather than precipitating.

Motivated by these reports, we investigate the influence of chain microstructure on the pathway to collapse, for a copolymer comprising two types of units: monomer *m* and co-monomer *c*. We consider the case where *c*-units are "sticky" and compare copolymers with a uniform (or periodic) distribution of comonomers (viz. systems with quenched order, termed U) with random copolymers (viz. systems with quenched disorder, termed R). U and R polymer structures are indicated schematically in Figure 4.1a. Uniform copolymers contain only one monomer sequence length (viz. number of *m*-units between consecutive *c*-units) whereas for random copolymers, there is a distribution of *m*-unit sequence lengths, with shorter sequences having higher probability compared to the longer sequences (Figure 4.1b).

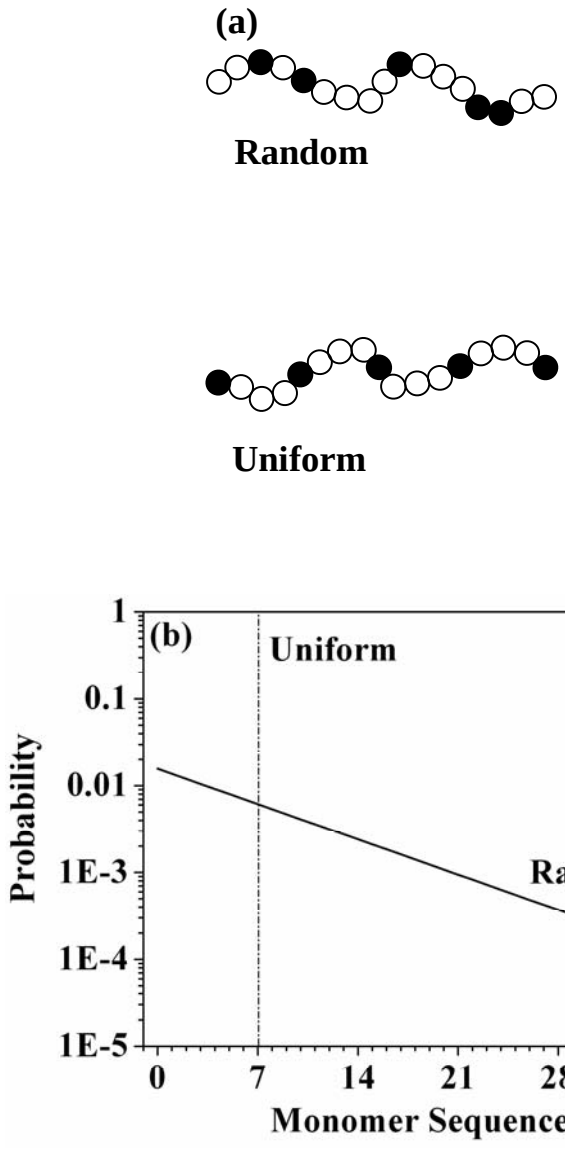

Figure 4.1: (a) Schematic representation of chain microstucture for uniform and random copolymers. (b) Calculated probability distribution of *m*-unit sequence length (length of *m*-units between consecutive *c*-units) for random copolymers contrasted with that for uniform copolymers (where there is only one fixed monomer sequence length).

We have recently reported[25] (reference cited and Chapter 3) dynamic Monte Carlo simulations of the collapse of flexible, nearly-random copolymers and have demonstrated that in these copolymers, collapse happens via aggregation of *c*-units, and that the fraction of *c*-units dictates collapse behavior. Collapse of chains containing a high *c*-unit fraction (greater than about 50%) is qualitatively identical to a homopolymer with a higher effective solvophobicity. Such copolymers collapse by localized "crumpling" along the entire chain, thus leading to behavior that is qualitatively like a homopolymer with a higher effective solvophobicity. In contrast, copolymers with a lower fraction of *c*-units (less than about 50%) exhibit "copolymer-ness", viz. the collapse transition is qualitatively different as compared to homopolymers. In this case, *c*-units microphase separate from *m*-units to aggregate into a core, leading to an abrupt collapse transition. In this Chapter, we focus exclusively on chains that exhibit such "copolymer-ness" and examine the effect of comonomer distribution on copolymer collapse.

4.2. Model and Simulation Technique

We use dynamic Monte Carlo (MC) simulations with Metropolis sampling to investigate collapse of copolymer chains on a cubic lattice of size 64 × 64 × 64. Our copolymer chains comprise monomer units, *m*, and comonomer units, *c*. Sites not occupied by the copolymer contain solvent molecules, *s*.

We consider the case where *c*-units repel both solvent and *m*-units. This is representative of an apolar polymer chain containing polar *co*-monomer units collapsing in an apolar solvent. Both *m*-units and *c*-units are solvophobic, and collapse is driven by effective *m*-*m* and *c*-*c* attractions. *c*-units are significantly more solvophobic relative to *m*-units, and are therefore, effectively "sticky". We use a Flory-like approach[26] wherein the "exchange" energy penalty to create an extra *m*-*s* contact is given by $B_{ms} = B$. B is directly related to

Flory's χ parameter[26]. All energies are normalized by kT, where k is Boltzmann's constant and T is the absolute temperature. For sticky *c*-units, the enhanced *m*-*c* or *c*-*s* interaction energy (relative to *m*-*s* interactions), results in a higher energy penalty to create additional *m*-*c* or *c*-*s* contacts, given by $B_{mc} = B_{cs} = \lambda B$, where the stickiness parameter, $\lambda > 1$.

The simulation scheme and the microrelaxation moves used in our MC algorithm are as described in the previous Chapter, where we ensure that there is no bond crossing, and that the excluded volume criterion is satisfied. The energy for a chain depends on the number of contacts between dissimilar units and the change in energy for a single MC move, is $\Delta E = \frac{1}{2}\sum_{\alpha \neq \beta} \Delta N_{\alpha\beta} B_{\alpha\beta}$, where $\alpha, \beta \in \{m, c, s\}$, and $\Delta N_{\alpha\beta}$ represents the net change in nearest neighbor contacts between α and β. We equilibrate copolymer chain on the lattice at $B = 0$ ($T = \infty$), and progressively increase B in steps of 0.0025 to simulate cooling. Our work is representative of equilibrium slow cooling experiments, since we observe no hysteresis between heating (decreasing B) and cooling (increasing B) runs. At each B, we relax the sample over 4×10^6 MC steps and calculate structural properties over the subsequent 4×10^6 MC steps. The radius of gyration of the chain and the *c*-*c* pair correlation function, g(r) are calculated as described in the previous Chapter.

Here, we examine copolymer chains of size, $N = 128$ containing 12.5% *c*-units with $\lambda = 20$ (we also state our findings for $\lambda = 10$, 50, N=512 and for 25% *c*-units). We have previously shown[25] that a random copolymer with this composition exhibits "copolymer-ness", viz. in such chains, a microphase-separated *c*-unit-core *m*-unit-shell intermediate forms as the chain collapses abruptly between the θ state ($B_\theta \approx 0.02$, the B range where $\left\langle R_g^2 \right\rangle \sim N$) and collapse ($B > 0.1$). As mentioned above, copolymer chains containing a large fraction of "sticky" *c*-units (greater than 50%) do not show "copolymer-ness" and collapse by "crumpling" locally rather than via a core-shell intermediate[25]. Therefore, it appears intuitive

that the influence of the chain architecture (R vs. U) on the collapse behavior should decrease as the fraction of *c*-units increases above 50%. This is indeed verified by our simulations (Figure 4.2). Here, we restrict our discussion to a chain composition that exhibits "copolymer-ness".

We generate a new random microstructure for each R-chain simulation and average over 50 different representations of the quenched disorder. U chains with the same composition have 7 *m*-units that separate two consecutive *c*-units. For U-chains, we simulate sequences of $(cm_7)_{16}$, $m(cm_7)_{15}cm_6$, $m_2(cm_7)_{15}cm_5$ and $m_3(cm_7)_{15}cm_4$, and present data averaged over at least 15 runs. The variability in chain microstructure within each R-chain as well as across the 50 chains simulated results in higher error bars relative to U copolymers.

We first present a detailed analysis of the collapse of R- and U- chains with $N = 128$ containing 12.5% *c*-units with $\lambda = 20$. Subsequently, we examine the influence of chain length on the collapse transition for R- and U- chains. We also briefly discuss the effects of *c*-unit concentration (within the "copolymer-ness" range) and λ.

4.3. Results and Discussion

4.3.1. $N = 128$, $x = 12.5\%$, $\lambda = 20$

We follow the collapse of the copolymer chain on cooling from $B = 0$, by monitoring the change in specific heat, C_v, calculated from energy fluctuations. As the copolymer collapses, solvophobic units aggregate, leading to an enthalpic gain that gives rise to a peak in C_v. Therefore, we examine C_v for the copolymers as a function of scaled

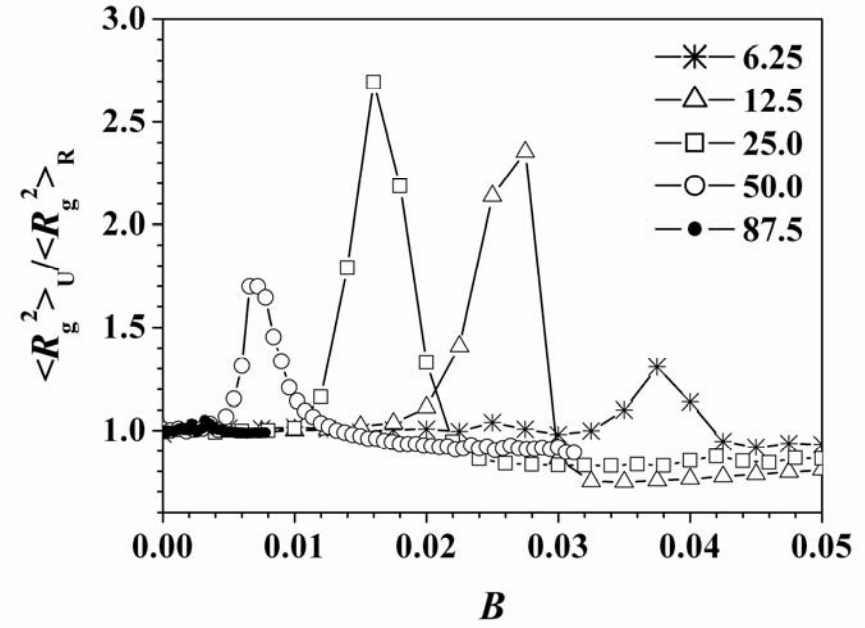

Figure 4.2: Ratio of the $\langle R_g^2 \rangle$ for U to that for R for chain of N = 128, λ = 20, with varying *c*-unit content as shown in the figure. The lines joining the points are meant only as a guide to the eye.

temperature, $T^* = B^{-1}$ (Figure 4.3). We observe that the C_v peak for U copolymers is at a higher B (viz. lower T^*), as compared to R (peak onset at $T^* \approx 40$ for U, $T^* \approx 60$ for R). Further, for U chains, C_v is sharply peaked (since the step size in our simulations appears to be inadequate to resolve the peak in C_v, we estimate $C_v^{max} \approx 500$ and full width at half maximum, FWHM ≈ 10 T^* units) relative to R chains ($C_v^{max} \approx 250$, FWHM ≈ 18 T^* units). Thus, chain microstructure strongly influences collapse. The narrow, sharply peaked C_v for U is suggestive of a "latent heat" associated with a "cooperative" collapse[27], when compared with R, where the enthalpy associated with collapse is spread over a wider temperature range. We compare our results with those of Zhang *et al*.[10], who examined a copolymer of PNIPAM grafted with styrene chains (DP of PNIPAM between successive styrene blocks ~ 500; styrene content in the copolymer ~ 4%). The calorimetric experiments of Zhang *et al*. appear similar to our C_v results and show that collapse of the PNIPAM copolymers is associated with a sharp peak in C_p, compared with a weak, broad peak for random copolymer collapse. Zhang *et al*.[10] claim that the uniform copolymer (*but not* the random) forms a phase-separated core-shell structure that they term an ordered coil. The formation of the ordered coil precedes collapse and is resolved as a shoulder to the C_p peak from collapse. However, our earlier work[25] indicates that in our simulations, random copolymers too undergo intramolecular phase separation into a *c*-unit core-*m*-unit shell structure as they collapse, for *c*-unit concentrations < ~ 50%. Therefore, the origin of the difference in the behavior of R and U copolymers observed in our study does not arise from the presence (or absence) of an intermediate microphase-separated state, since both R and U copolymers show intramolecular microphase separation. Rather, the difference in the behavior of the R and U copolymers results from the *structure* of this microphase separated intermediate state, the temperature at

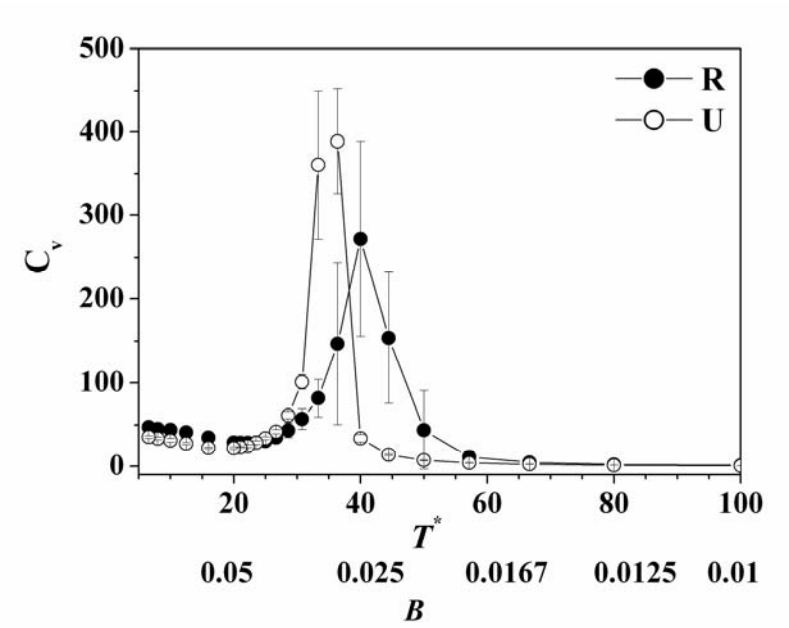

Figure 4.3: Change in specific heat, C_v as a function of T^* (= B^{-1}) for R and U copolymers. The lines joining the points are meant only as a guide to the eye.

which it is achieved and the *path* taken to achieve it. To investigate the intermediate structures formed by R and U chains, we now examine their structural evolution during collapse.

On cooling (viz. increasing B), expanded copolymer chains contract via the θ condition to a collapsed globule. As previously [25], we determine the θ state as the B value where $\left\langle R_g^2 \right\rangle \sim N$. For both R and U copolymers, $B_\theta = 0.021 \pm 0.001$. For $B < B_\theta$, excluded volume interactions dominate, and $\left\langle R_g^2 \right\rangle_{\mathrm{U}} = \left\langle R_g^2 \right\rangle_{\mathrm{R}}$ (Figure 4.4). As B increases above B_θ, the copolymer $\left\langle R_g^2 \right\rangle$ decreases due to the effective solvophobicity of m and c units. The decrease of $\left\langle R_g^2 \right\rangle$ follows different trends for R and U chains. $\left\langle R_g^2 \right\rangle_{\mathrm{R}}$ initially decreases rapidly from B_θ to $B \approx 0.025$, and then decreases gradually for higher B. $\left\langle R_g^2 \right\rangle_{\mathrm{U}}$ decreases more abruptly, but at higher B (≈ 0.025) relative to R chains and, there is no significant decrease beyond $B \approx 0.03$. Also, for $B \geq 0.03$, $\left\langle R_g^2 \right\rangle_{\mathrm{U}} < \left\langle R_g^2 \right\rangle_{\mathrm{R}}$. The sizes of the R and U copolymers approach each other in the collapsed state, at high B. Thus, the ratio, $\left\langle R_g^2 \right\rangle_{\mathrm{U}} \Big/ \left\langle R_g^2 \right\rangle_{\mathrm{R}} \approx 1$ for $B < B_\theta$, increases to >2 for $B \approx 0.03$, and then rapidly decreases to a value <1, and finally increases to slowly approach 1 at $B = 0.1$ (Figure 4.4, inset).

The specific $\left\langle R_g^2 \right\rangle$–$B$ trajectory followed by a copolymer chain is a function of the c-unit distribution in that chain (grey lines in Figure 4.4 indicate the collapse trajectories for chains having different random c-unit distributions). For U chains, this trajectory is independent of the precise chain microstructure (whether $(cm_7)_{16}$, $m(cm_7)_{15}cm_6$, $m_2(cm_7)_{15}cm_5$ or $m_3(cm_7)_{15}cm_4$), and the standard deviation from the "average" trajectory is smaller than the symbol size in Figure 4.4. For R chains, the different microstructures randomly generated for

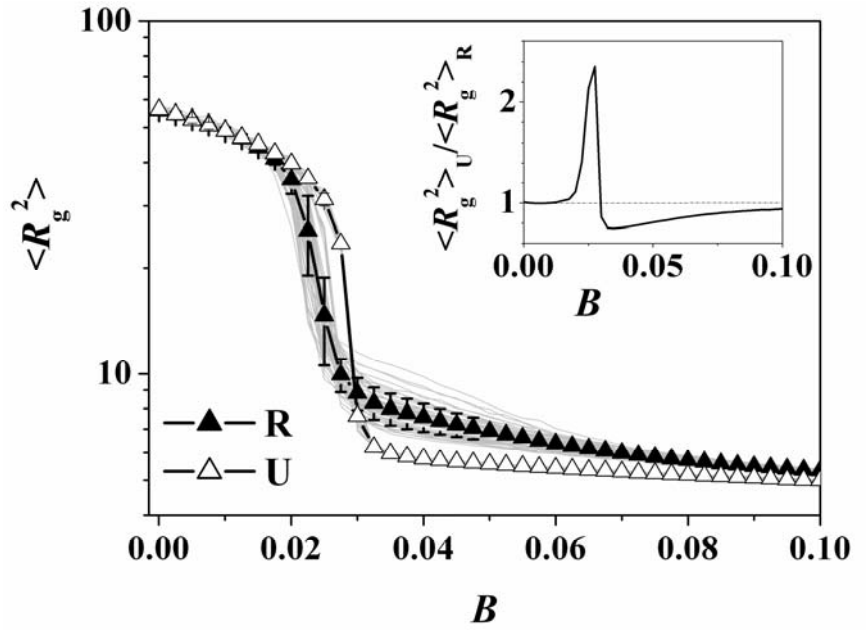

Figure 4.4: Decrease in copolymer $\langle R_g^2 \rangle$ as a function of *B* for R and U chains. The grey lines represent data for independent simulations – the $\langle R_g^2 \rangle$ for these data represent averages over a large number of Monte Carlo steps. As explained in the description of the simulation technique, the bold lines represent averages over 50 chain realizations for R and 15 chain realizations for U copolymers. The error bars for U copolymers are smaller than the size of the symbols used. The inset shows the ratio of the $\langle R_g^2 \rangle$ for U to that for R. The lines joining the points are meant only as a guide to the eye.

the 50 simulations, yield significantly different trajectories. However, the average trajectory for the R-chains is distinctly different from that for U-chains. We quantify the randomness of the chain microstructure by defining a randomness index, δ, using approximate entropy concepts[28-30]. According to this, δ = 0.00 for the U chains, while δ ~ 0.15 to 0.35 for the R microstructures generated. We do not observe any obvious correlation between the $\langle R_g^2 \rangle$–*B* trajectory exhibited by specific random copolymer microstructures and their δ values.

It is interesting to examine the range of δ from U (δ=0) to R chains, by arbitrarily changing the position along the chain of one or two *c*-units. Chains with one point-mutation (δ ≈ 0.04) show an $\langle R_g^2 \rangle$–*B* trajectory that is very close to that for U (Figure 4.5). For chains with two point mutations (δ≈ 0.08) too, the $\langle R_g^2 \rangle$–*B* trajectory is close to that for U - however, we can clearly observe a systematic transition away from a U-like trajectory and towards a R-like trajectory with increase in δ. Thus, chains with δ close to 0 collapse along an $\langle R_g^2 \rangle$–*B* trajectory similar to U while chains with δ > ~ 0.15 show a random copolymer-like collapse.

The initial rapid decrease in $\langle R_g^2 \rangle$ for copolymers containing sticky comonomers is associated with the formation of a microphase-separated intermediate with a collapsed "core" of *c*-units surrounded by a solvated shell of *m*-units. We compute the *c*–*c* pair correlation function at the nearest neighbor shell, g(1), by averaging the fraction of *c*-units adjacent to other *c*-units over a large number of chain configurations. g(1) represents the mean square concentration fluctuation of *c*-units (viz., g(1) is proportional to the integral invariant for scattering from *c*-units). An increase in g(1) indicates *c*-unit aggregation. We observe a more abrupt increase in g(1) for U copolymers, at higher *B* relative to R chains (Figure 4.6). Beyond $B \approx 0.03$, we cannot resolve differences between g(1) for R and U.

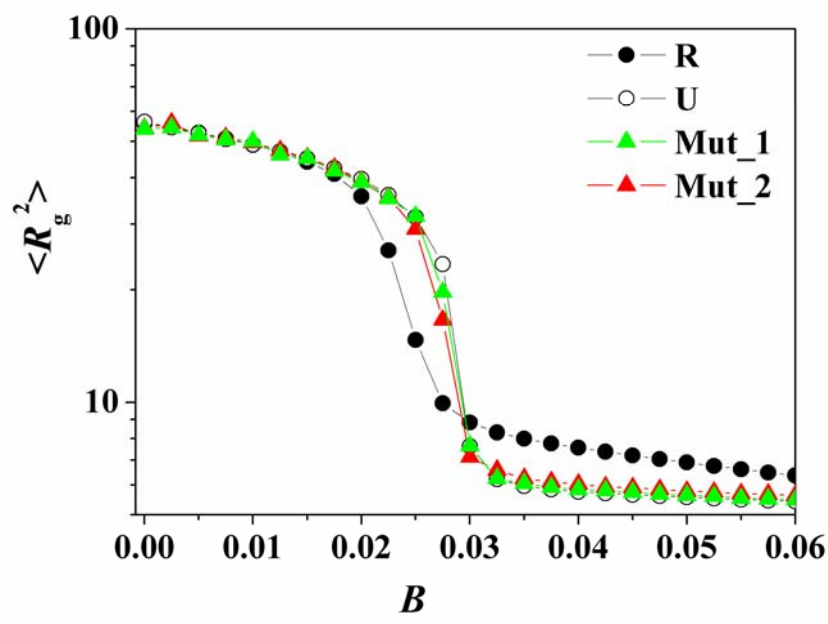

Figure 4.5: Change in $\left\langle R_g^2 \right\rangle$ as a function of for R, U, one-point and two-point mutated copolymer chain (N = 128, c = 12.5%, λ = 20). The lines joining the points are meant only as a guide to the eye.

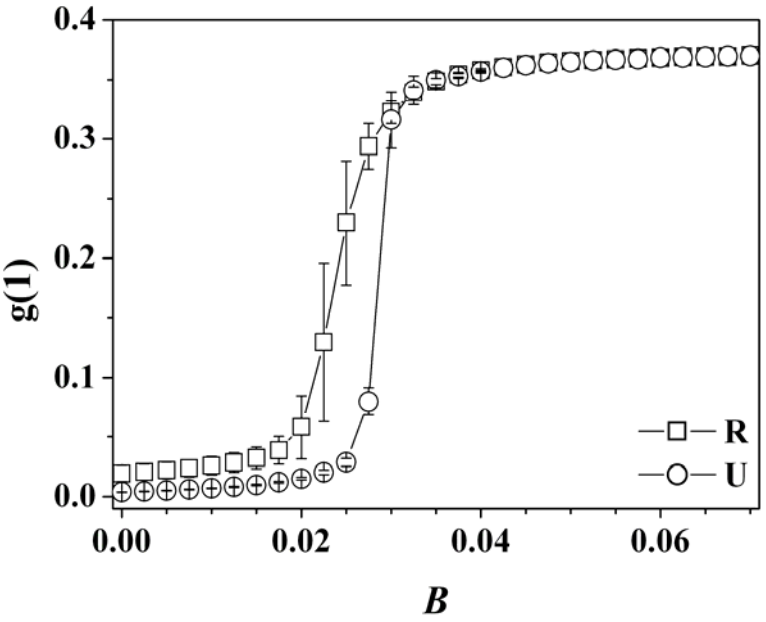

Figure 4.6: Comparison of the comonomer pair distribution function, g(1) as a function of *B* for R and U copolymers. The lines joining the points are meant only as a guide to the eye.

Comparing Figures 4.4 and 4.6 with Figure 4.3 reveals that the C_v peak corresponds to the *B*-interval where the copolymer $\langle R_g^2 \rangle$ undergoes an initially abrupt decrease and, where g(1) increases. Taking together the trends in $\langle R_g^2 \rangle$ and g(1) (Figures 4.4 and 4.6), indicate that the rapid decrease in the size of the copolymer chain beyond B_θ is due to the aggregation of *c*-units. Aggregation of *c*-units happens at lower *B* for R copolymers relative to U – however, for U, the *c*-units aggregate abruptly, over a shorter *B* interval. The formation of the *c*-unit aggregate is essentially complete by $B \approx 0.03$ and decrease in the chain size beyond $B \approx 0.03$ is due to collapse of solvated *m*-units. $\langle R_g^2 \rangle$ for U copolymers does not decrease significantly beyond $B \approx 0.03$, while R copolymers continue to densify gradually. This suggests that while the onset of aggregation of *c*-units for U copolymers happens only at higher *B*, this results in the formation of a nearly collapsed ordered compact intermediate.

We now explain the differences between the aggregated *c*-unit intermediates of the R and U copolymers. When sticky comonomers form aggregates, the enthalpy of *c*-*c* attraction decreases the free energy, while the loss of conformational entropy due to loop formation increases the free energy. The probability of M_i chain units in a flexible, self-avoiding chain forming a loop in the coil state can be written as[31]:

$$W_i \sim M_i^{-3.71\nu} \quad \text{.....(1)}$$

where ν is the universal scaling exponent, and $M_i >> 1$. We have verified this relation by calculating the fraction of self-avoiding chains forming loops in simulations at $B = 0$ ($\nu = 0.58$). Surprisingly, we observe that the relation provides a reasonable estimate of the loop formation probability even at small M_i ($M_i \geq 3$). From equation 1, it is clear that the

entropy penalty for loop formation, S ~ ln(W_i), increases with M_i, viz. short loops can form more readily. For U copolymers, two consecutive *c*-units in the chain are always separated by seven *m*-units. However, for R copolymers, at least some *c*-units are separated by less than seven *m*-units, and have a correspondingly lower entropic barrier to aggregation. Thus, we anticipate that R copolymers will rapidly form initial aggregates involving *c*-units separated by only a small number of *m*-units.

We calculate $\langle M \rangle$, the average loop length separating aggregated *c*-units (viz. clusters of *c*-units) as a function of *B* (averaged over 4×10^6 MC steps, and over 50 chain microstructures for R and 15 chains for U) by estimating the distribution of the cluster size (see Appendix for detail description algorithm and results of cluster size distribution). At B = 0, there is no enthalpic gain associated with *c*-*c* aggregation and therefore, formation of *c*-aggregates is governed only by entropy of loop formation. At B = 0, our simulation results give $\langle M \rangle \approx 3.67$ for R while, $\langle M \rangle \approx 13.15$ for U. At B = 0, most of the *c*-aggregates are dimers (≈ 72% of aggregates for R and ≈ 95% for U), since the chance of three or more *c*-units aggregating is small. If, for simplicity, we assume that *c*-units aggregate to form only dimers, then we can estimate $\langle M \rangle$ at B = 0 by averaging over all possible R microstructures as:

$$\langle M \rangle = \frac{\sum_{i=0}^{N_m}\sum_{j=0}^{N_c-2} N_{ij} W_{i+j+1} M_{i+j+1}}{\sum_{i=0}^{N_m}\sum_{j=0}^{N_c-2} N_{ij} W_{i+j+1}} \quad \text{.....(2)}$$

where $N_{ij} = \frac{\left[{}^{(i+j)}C_j\right](N-i-j-1)!}{(N_m-i)!(N_c-j-2)!}$ is the number of ways in which a copolymer chain of N_m *m*-units and N_c *c*-units can contain a sub-segment with i *m*-units and j *c*-units between terminal *c*-units, and W_{i+j+1} is estimated using equation 1, with ν = 0.58 at B = 0. $N_{ij}W_{i+j+1}$

represents the number of ways in which a *c*-dimer can form a loop containing *i* *m*-units and *j* *c*-units. From eq. 2, we obtain $\langle M \rangle$ = 2.33 at B = 0. For U copolymers, the *c*-units are uniformly spaced and M_i takes values of 8, 16, 24, etc. In this case, we calculate $\langle M \rangle$ = 12.95. Given the assumptions made to simplify our calculations, our estimates for $\langle M \rangle$ are in reasonable accord with the simulation data for both R and U copolymers. Thus, the relevant barrier to aggregation of *c*-units is the conformational entropy loss associated with loop formation, unlike in Halperin's analysis of intramolecular micelle formation in copolymers[32].

As B increases above 0, the enthalpic contribution from association of sticky *c*-units stabilizes *c*-aggregates, compensating for the entropy loss due to loop formation. Therefore, as B increases, larger loops form and $\langle M \rangle$ increases (Figure 4.7). Increasingly large aggregates involving more *c*-units are formed, changing the distribution of *c*-unit aggregates. As B exceeds B_θ ($\approx$ 0.02), the enthalpy of *c*-unit association dominates the free energy leading to microphase separation. Microphase separation is complete beyond $B \approx 0.03$; all the *c*-units are incorporated into a core and $\langle M \rangle$ tends to N_m/N_c (= 8) for both R and U copolymers.

The copolymer microstructure determines the pathway along which microphase separation proceeds between B_θ and collapse. When *m*-units and *c*-units are not covalently enchained, *c*-units condense abruptly in a "gas-liquid" transition at a well-defined B, where the enthalpy of *c*-unit interactions overwhelms the translational entropy of a "gas" of *c*-units. Topological constraints due to chain connectivity shift and broaden this phase separation and, the formation of *c*-aggregates is now determined by a balance of enthalpy of *c*-unit interactions and entropy of loop formation (rather than translational entropy): for U, *c*-units

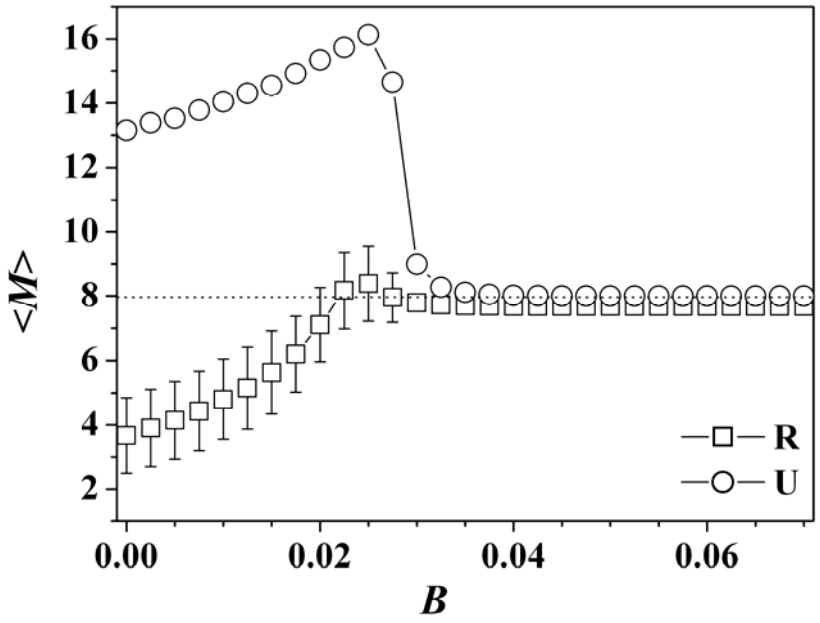

Figure 4.7: Comparison of the average loop length, $\langle M \rangle$ as a function of *B* for *c*-unit aggregates of R and U copolymers. In the final collapsed state, $\langle M \rangle$ approaches the ratio of *m*-units to *c*-units (N_m/N_c) indicated by the broken horizontal line. The lines joining the points are meant only as a guide to the eye.

aggregate to form a core over a relatively narrow *B*-range (0.025-0.03) and $\langle M \rangle$ decreases abruptly from ~16 to 8, while for R, microphase separation is initiated immediately above B_θ and continues until $B \approx 0.03$. Thus, the regular chain microstructure in a uniform copolymer determines the balance of *c*-unit aggregation enthalpic gain and loop formation entropy penalty such that *c*-unit core-formation is postponed to higher *B* relative to random copolymers, and then happens abruptly, to form a compact intermediate state. In comparison, random copolymers microphase-separate over a broader *B*-range, forming an intermediate with a fluffy *m*-unit shell surrounding the *c*-unit core.

4.3.2. Effect of Chain Length, *N*

We now examine whether the difference in the behavior of R and U copolymers persists to higher chain lengths, since a "true" thermodynamic phase transition is only defined in the limit of infinite chain length. Our simulations become increasingly expensive with increasing *N* – therefore, there are practical limitations to the chain lengths that we can simulate. Here, we present collapse data for a series of random and uniform copolymers with increasing *N* from 64 to 128, 256 and 512, with 12.5% *c*-units and $\lambda = 20$ (Figure 4.8).

With increase in *N*, collapse of chains from the coil to globule state happens over an increasingly narrower range of *B* [33]. We observe that, for all *N* investigated, the onset of collapse for R copolymers is at lower *B* relative to U copolymers, similar to the case that we have analyzed in detail. Thus, at *B* values where the random copolymer starts to collapse, viz. $\langle R_g^2 \rangle_R$ start to decrease, the uniform copolymer is still relatively swollen. At these *B* values, the ratio

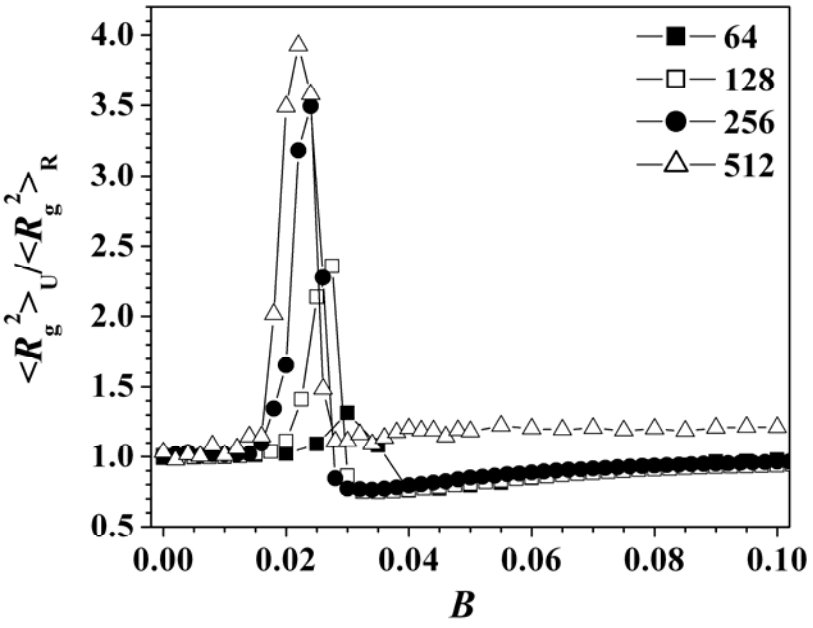

Figure 4.8: Ratio of the $\left\langle R_g^2 \right\rangle$ for U to that for R for chains of different sizes, N = 64, 128, 256 and 512. The lines joining the points are meant only as a guide to the eye.

$\left\langle R_g^2 \right\rangle_{\mathrm{U}} / \left\langle R_g^2 \right\rangle_{\mathrm{R}}$ increases above 1; we observe that the peak value of $\left\langle R_g^2 \right\rangle_{\mathrm{U}} / \left\langle R_g^2 \right\rangle_{\mathrm{R}}$ increases with N, from around 1.3 for $N = 64$ to around 4 for $N = 512$ (Figure 4.8).

As B is further increased, $\left\langle R_g^2 \right\rangle_{\mathrm{U}} / \left\langle R_g^2 \right\rangle_{\mathrm{R}}$ decreases from its peak value and drops to a value less than 1 for $N = 64$, 128 and 256, viz. the size of the uniform copolymer decreases below that for the random as both chains approach a fully collapsed state (Figure 4.8). However, for the chain with $N = 512$, $\left\langle R_g^2 \right\rangle_{\mathrm{U}} / \left\langle R_g^2 \right\rangle_{\mathrm{R}}$ does not decrease below unity after the peak, and $\left\langle R_g^2 \right\rangle_{\mathrm{R}} \leq \left\langle R_g^2 \right\rangle_{\mathrm{U}}$ in the B range where U and R chains collapse. Our analysis in the previous section shows that the decrease in $\left\langle R_g^2 \right\rangle_{\mathrm{U}} / \left\langle R_g^2 \right\rangle_{\mathrm{R}}$ to below 1 after the peak is indicative of the compactness of the core-shell structure formed during collapse for U copolymers relative to R. We now examine the collapse of copolymer chains with $N = 512$ to understand the difference in behavior relative to shorter chains.

The excluded volume of chain segments emanating from a comonomer aggregate makes it unlikely for a chain to be able to form a single core for large N (for which the number of c-units is correspondingly large). Using a scaling argument, Orlandini and Garel[34] have shown that, for collapse of multi-block copolymers with both A and B blocks having a length of p, a single solvophobic core is formed for $p > O(N^{1/3})$ while multiple cores form for $p < O(N^{1/3})$. Multicanonical Monte Carlo simulations of periodic AB block copolymers with asymmetric A and B blocks [35] show that above a critical value of chain length, N, these copolymers collapse into structures with multiple cores – however, with further decrease in temperature, the increase in comonomer mutual attraction drives coalescence of these multiple cores to form a single comonomer aggregate.

In our simulations, we see differences in the tendency to form multiple cores for R and U copolymers. For random copolymers, only a single core is formed during collapse in all our simulations (N up to 512). For the corresponding uniform copolymers, a single core is

formed during collapse of chains with N = 64, 128 and 256; however, chains with N = 512 have formed two distinct cores[36] in every single simulation run (see for example, a snapshot from a typical run in Figure 4.9). The multiple core structure for the U copolymer with N = 512 forms immediately after the decrease in $\left\langle R_g^2 \right\rangle$ (viz. $B \approx 0.025$) and the multiple cores are retained as B is increased to 0.1 (viz. we do not observe the cores coalescing even at B values substantially higher than the onset of collapse). We note here that the inability of the multiple core structure to transform into a single core even at high B in our simulations could result from an artifact of the lattice Monte Carlo scheme employed. However, these results clearly indicate the influence of chain architecture (R versus U) on the structure of the intermediate state formed during collapse.

Thus, the structure of the intermediate core-shell state is different for R and U copolymers for N = 512. Due to the formation of multiple cores, the intermediate structure for the U copolymer is not more compact than the corresponding R copolymer, in contrast to what is observed for shorter chains. However, even though R chains form one core and U chains form two for N = 512, the *pathway* to the intermediate core-shell structure is still determined by chain microstructure in the same way as in the case analyzed in detail (N = 128). Thus, for N = 512, the C_v for U chains is sharply peaked and narrow relative to R chains ($C_v^{max} \approx 3000$, FWHM ≈ 5 T^* units for U chains relative to $C_v^{max} \approx 700$, FWHM ≈ 28 T^* units for the corresponding R chains; Figure 4.10, compare with Figure 4.3). Further, the increase in g(1) is significantly more abrupt for the U copolymer during collapse relative to

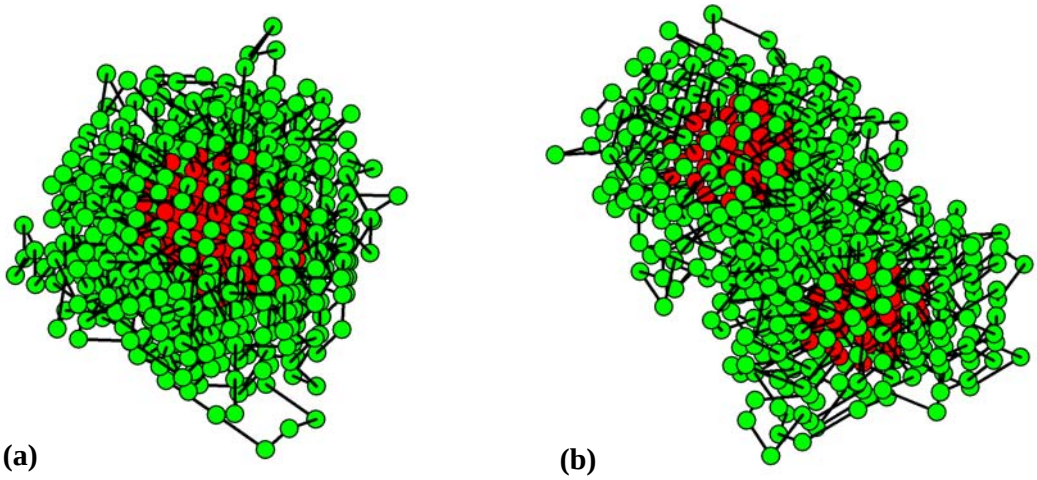

Figure 4.9: A snapshot in the collapsed globular state (B = 0.1) for (a) random and (b) uniform copolymers with N = 512, x = 12.5% and λ = 20. The U chain shows the formation of two distinct cores (shown here, containing 27 and 32 *c*-units).

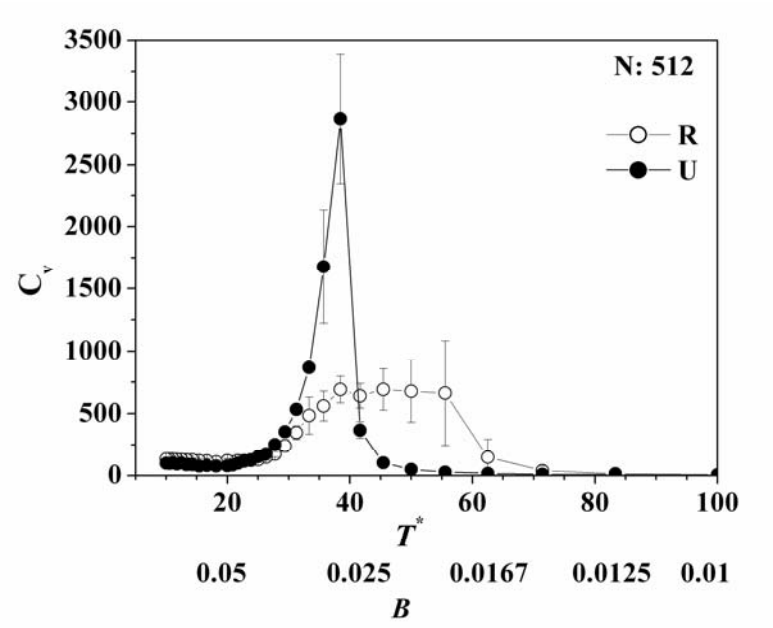

Figure 4.10: Comparison of change of specific heat, C_v, as a function of T^* (= B^{-1}) for R and U copolymers for chain length, N = 512, at x = 12.5% and λ = 20. The U copolymer shows a narrow, steep peak in C_v relative to the corresponding to R copolymers. The lines joining the points are meant only as a guide to the eye.

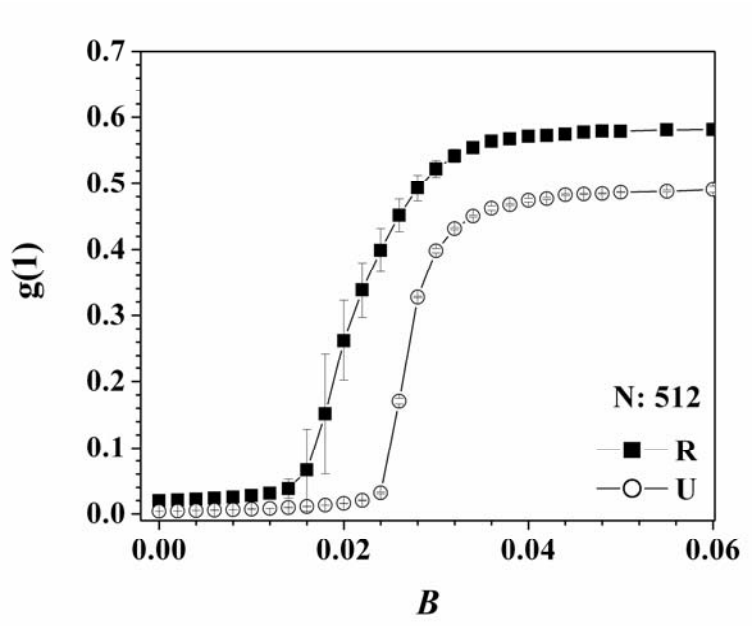

Figure 4.11: Comparison of change of g(1) as a function of *B* for R and U copolymers for *N* = 512, at *x* = 12.5% and λ = 20. U copolymer shows a relatively sharp increase in g(1) compared with the corresponding R copolymers. The magnitude of g(1) of U is higher than R due to the formation of multiple cores in the collapsed state in U copolymers. The lines joining the points are meant only as a guide to the eye.

the R chains (Figure 4.11, compare with Figure 4.6). This indicates that for $N = 512$ too, the core-shell intermediate structure forms via an abrupt aggregation of *c*-units to form a compact, ordered core for U chains, while R chains follow a gradual process of comonomer aggregation.

Our data strongly suggest that the chain microstructure-controlled difference in the pathway to collapse for U chains relative to R chains persists to higher chain lengths. The periodic structure of the U chain leads to *c*-unit aggregation being delayed to higher B relative to the corresponding R chain. However, the aggregation of comonomers in the first stage of the chain collapse happens abruptly for U chains, over a narrower range of B, relative to R chains.

4.3.3. Effect of *c*-Unit Concentration and λ

Initial simulations on copolymers containing different comonomer fraction (25% *c*-units) and for different values of λ ($\lambda = 10, 50$), indicate that the difference in pathways to the intermediate state during collapse of R and U chains described in this work is preserved (Figure 4.12a,b). For U chains with $N = 512$, $x = 25\%$ and $\lambda = 20$, we observe the formation of either two or three comonomer cores in the intermediate state during collapse. We are unable to obtain multiple core structures during collapse of R copolymers in any of our simulations. However, we anticipate that increasing excluded volume constraints on chains with even larger N than we have simulated, may lead to multiple core structures for R copolymers also. Thus, we speculate that for large N, both R and U chains will collapse into a string of core-shell "flowers", and that the chain microstructure will determine the details of the local *c*-unit aggregation process, similar to the finite chain lengths simulated here.

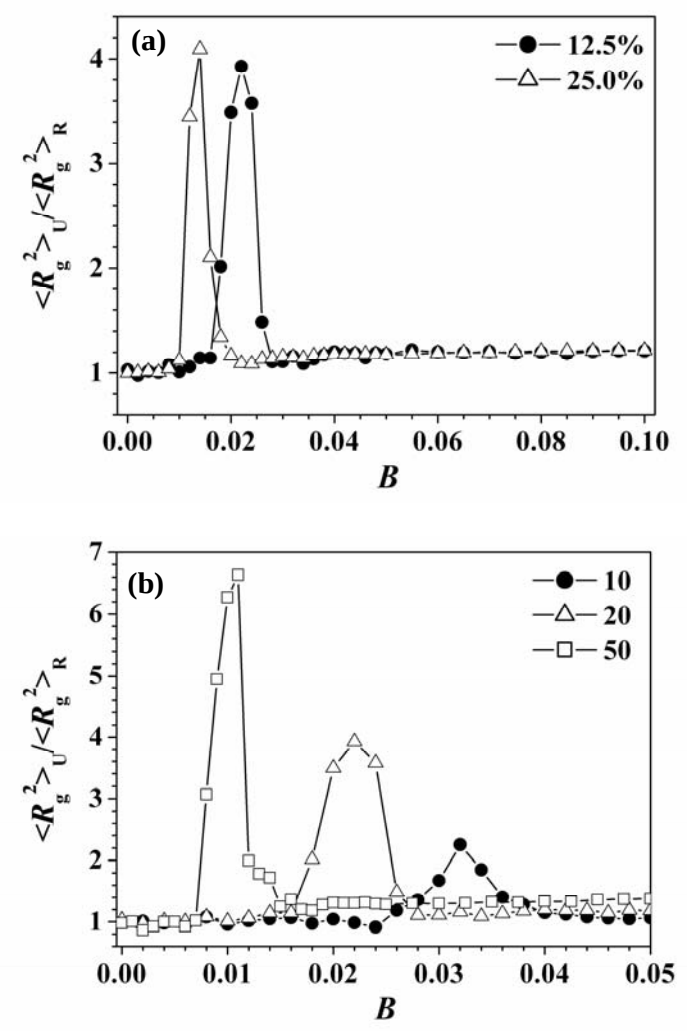

Figure 4.12: Ratio of the $\left\langle R_g^2 \right\rangle$ for U to that for R for N = 512. (a) λ = 20, c = 12.5% and 25.0%; (b) c = 12.5%, λ = 10, 20 and 50. The lines joining the points are meant only as a guide to the eye.

4.4. Summary

We examine the dilute solution collapse of copolymers containing a small fraction of "sticky" (viz. mutually attractive) comonomers using dynamic Monte Carlo simulations. Copolymer chain microstructure (viz. the distribution of comonomer units along a copolymer chain) plays an important role in determining the path to the collapsed state. Our results indicate that uniform copolymers (comonomer units arranged periodically along the chain) collapse at lower temperatures relative to random copolymers – however, the collapse of uniform copolymers is abrupt as compared with random copolymers.

Copolymer collapse for both, uniform and random copolymers happens via an intermediate core-shell structure, comprising a core of sticky comonomers surrounded by a solvated monomer shell. The formation of this intermediate structure can be explained as the expected interplay of the enthalpy of comonomer-comonomer interactions with the entropic penalty for the formation of loops when comonomers aggregate. Our work suggests that the regular chain microstructure of a uniform copolymer leads to the abrupt, formation of a compact, nearly-collapsed ordered intermediate core-shell state; the random copolymer microstructure leads to the formation of intermediates with "fluffy" monomer shells, over a wider temperature range. This difference in the aggregation behavior of *c*-units during collapse of uniform and random copolymers persists to higher chain lengths. We observe the formation of multiple core intermediate structures during collapse of uniform copolymers at $N = 512$, but not for the corresponding random copolymer.

References

(1) Baysal, B. M.; Karasz, F. E. *Macromol. Theory Simul.* **2003**, *12*, 627-645.

(2) Chu, B.; Wang, Z. *Macromolecules* **1989**, *22*, 380-383.

(3) Grassberger, P.; Hegger, R. *Europhys. Lett.* **1995**, *31*, 351-356.

(4) Hu, W. *J. Chem. Phys.* **1998**, *109*, 3686-3690.

(5) Khokhlov, A. R.; Khalatur, P. G. *Physica A* **1998**, *249*, 253-261.

(6) Wu, C.; Wang, X. *Phys. Rev. Lett.* **1998**, *80*, 4092-4094.

(7) Sfatos, C. D.; Gutin, A. M.; Shakhnovich, E. I. *Phys. Rev. E* **1993**, *48*, 465-475.

(8) Timoshenko, E. G.; Kuznetsov, Yu. A.; Dawson, K. A. *Phys. Rev. E* **1998**, *57*, 6801-6814.

(9) Baughman, T. W.; Wagener, K. B. *Adv. Polym. Sci.* **2005**, *176*, 1-42.

(10) Zhang, G.; Winnik, F. M.; Wu, C. *Phys. Rev. Lett.* **2003**, *90*, 035506.

(11) Verso et al., F. L. *Phys. Rev. Lett.* **2006**, *96*, 187802-1-187802-4.

(12) Harth et al., E. *J. Am. Chem. Soc.* **2002**, *124*, 8653-8660.

(13) Mecerreyes et al., D. *Adv. Mater.* **2001**, *13*, 204-208.

(14) Dill et al., K. A. *Protein Sci.* **1995**, *4*, 561-602.

(15) Pande et al., V. S. *Curr. Opin. Struct. Biol.* **1998**, *8*, 68-79.

(16) Anfinsen, C. B. *Science* **1973**, *181*, 223-230.

(17) Socci, N. D.; Onuchic, J. N. *J. Chem. Phys.* **1995**, *103*, 4732-4744.

(18) Shakhnovich, E. I. *Phys. Rev. Lett.* **1994**, *72*, 3907-3910.

(19) Irbäck, A.; Peterson, C.; Potthast, F. *Proc. Natl. Acad. Sci. USA* **1996**, *93*, 9533-9538.

(20) Abkevich, V. I.; Gutin, A. M.; Shakhnovich, E. I. *J. Chem. Phys.* **1994**, *101*, 6052-6062.

(21) Fersht, A. R. *Proc. Natl. Acad. Sci. USA* **1995**, *92*, 10869-10873.

(22) Kolinski, A.; Madziar, P. *Biopoly* **1997**, *42*, 537-548.

(23) Khokhlov, A. R.; Khalatur, P. G. *Phys. Rev. Lett* **1999**, *82*, 3456-3459.

(24) van den Oever, J. M. P.; Leermakers, F. A. M.; Fleer, G. J.; Ivanov, V. A.; Shusharina, N. P.; Khokhlov, A. R.; Khalatur, P. G. *Phys. Rev. E* **2002**, *65*, 041708-1-041708-13.

(25) Dasmahapatra, A. K.; Kumaraswamy, G.; Nanavati, H. *Macromolecules* **2006**, *39*, 9621-9629.

(26) Flory, P. J. *Principles of Polymer Chemistry*; Cornell University Press: Ithaca, New York, 1953.

(27) Shakhnovich, E. I. *Curr. Opin. Struct. Biol.* **1997**, *7*, 29-40.

(28) Pincus, S.; Singer, B. H. *Proc. Natl. Acad. Sci. USA* **1996**, *93*, 2083-2088. (Our calculations are based on a block length of 8 units.)

(29) Pincus, S. M. *Proc. Natl. Acad. Sci. USA* **1991**, *88*, 2297-2301.

(30) Moody, George B. *http://www. physionet. org/physiotools/ApEn/* **2001**.

(31) des Cloizeaux, J. *J. Phys. (Paris)* **1980**, *40*, 223-238.

(32) Halperin, A. *Macromolecules* **1991**, *24*, 1418-1419.

(33) Tanaka, G.; Mattice, W. L. *Macromol. Theory Simul.* **1996**, *5*, 499-523.

(34) Orlandini, E.; Garel, T. *Eur. Phys. J. B* **1998**, *6*, 101-110.

(35) Koga, T. *Eur. Phys. J. E* **2005**, *17* , 381-388.

(36) We state that *c*-units aggregate into distinct (multiple) cores when there is no nearest neighbor contact between any two units selected from different cores

Appendix

Cluster Size Distribution and Application to Collapse Transition

A.1. Introduction

In the main text (Chapter 4), we have shown that, with increase in B (viz. by reducing the effective temperature), the "sticky" units of comonomer units in the copolymer chain aggregate, and subsequently, the chain collapses. We have also shown that the distribution of c-units along the chain, determines the progression of intermediate states, on the path to the collapsed globular state. Clearly, as the copolymer collapses, the sticky comonomer units aggregate to form c-unit clusters, and form core/s depending on the chain microstructure (sequence distribution of c-units along the chain and chain size[*]). We can obtain deeper insights into the collapse process by examining the manner in which the comonomer aggregates form and evolve into core/s. This involves characterizing the size distribution of clusters of c-units at each temperature stage along the path to the collapsed state. The average loop length, $<M>$, described in Chapter 3, also comes from the analysis of the cluster size distribution. In this Appendix, we describe the algorithm that we have implemented to calculate the cluster size distribution (CSD), and present results on the CSD from our simulations on R and U copolymers.

A cluster of size n is a contiguous object comprising n numbers of c-units, such that each c-unit has at least one nearest neighbor c-unit. The CSD provides the information on the

[*] We have observed the formation of multiple cores at higher chain length ($N = 512$) for U copolymer.

relative frequency of appearance of clusters of different sizes. While clusters of all sizes are possible at all *B*, we expect to observe clustering of *c*-units only at high *B* (low temperature) where the enthalpy of *c*-*c* contacts dominates the free energy. At high *B* (viz. low effective temperature), above the theta point, the chain is expanded and the *c*-units are dispersed to form a "gas" of *c*-units connected by the covalent links between chain units. With increase in *B* (viz. on lowering the effective temperature), the enthalpy of *c*-unit interactions drives clustering and changes the CSD from the $B = 0$ state. Finally, above the theta point, we observe the formation of a large cluster of *c*-units.

It is reasonable to expect that the evolution of the CSD will be a function of the chain microstructure. We have already described the difference in behaviors of the collapse transitions of R and U copolymers in the Chapter 4. The presence of short *m*-sequences in R copolymers facilitates the formation of clusters at relatively high temperature (low *B* value) compared to U copolymers. CSD data provide a more detailed characterization of the thermodynamic pathway being followed by R and U copolymers towards the collapse transition. In the following section, we will describe the algorithm for the estimation of CSD, followed by results and discussion.

A.2. CSD –Algorithm

As mentioned in Chapter 4, at each *B*, we use 4×10^6 MC steps for equilibration and calculate the CSD over the subsequent 4×10^6 MC steps. We calculate the probability, $P(n)$, to form a *c*-unit cluster of size, n from the CSD. We now describe the methodology for the CSD calculation.

We sequentially scan each *c*-unit in the chain and for each *c*-unit, we find the number of nearest neighbor *c*-units. In this step we always use periodic boundary condition to avoid anomalous boundary effects. This is implemented as in the following example. If we find q1 *c*-units present at the nearest neighbor positions of the first *c*-unit along the chain, then we

designate this as our first cluster with size (q1+1) and assign cluster index, CI = 1 to the (q1+1) *c*-units. Then, we examine the next *c*-unit along the chain and determine the number, q2, of nearest neighbor *c*-units. If the second *c*-unit is already labeled with index, CI, then all q2 nearest neighbor *c*-units are also assigned the same index. If this *c*-unit is not labeled with an index, but one of the q2 neighbors is labeled with an index, CI, then all the *c*-units will be labeled with the index CI, and the (q2+1) *c*-units will become a part of the aggregate with the index CI. If any neighboring *c*-unit is labeled with more than one index, then the lowest index value is used to label all q2+1 units. If none of the q2+1 *c*-units carry any label, then this will represent a new cluster and a new label (the last cluster sequence index, incremented by 1), will be assigned to all the *c*-units present in this aggregate. Each *c*-unit along the chain is scanned in this manner, and is assigned a unique label, representing the cluster that it belongs to. Thus, a single scan of the *c*-units yields the entire distribution of clusters in the system.

Once all the *c*-units are labeled, we generate a histogram of the number of clusters and their corresponding sizes. Here, the size of the cluster specifies the total number of *c*-units bearing the same index. We calculate the cluster size histogram and average over an ensemble of 4×10^6 MC steps, to generate the CSD. The size of the cluster is designated by *n* and the corresponding frequency by w(n). We then calculate the probability of the formation of an *n*-mer cluster as $P(n) = w(n)/\sum w(n)$. The plot of $P(n)$ vs. n is used to study the microphase separation within the collapsing copolymer and to investigate the effect of sequence distribution. We also calculate the number of *c*-*c* contacts ($N_{cc}(n)$) for every cluster and average over an ensemble of 4×10^6 MC steps.

We schematically illustrate the CSD calculation algorithm in Figure A.1. The representation is restricted to a 2D lattice and, 16 *c*-units are placed on this lattice. For clarity, we do not depict the backbone monomer units that connect the *c*-units in our

schematic. *c*-units along the chain, counted from one end of the chain are ennumerated as C1, C2, etc. As described previously, we scan the *c*-units starting from C1, all the way to the last *c*-unit along the chain. In Figure A.1, the first *c*-unit (C1) does not have any *c*-unit at its neighboring sites. Hence it is considered as a cluster of size 1; this is the first cluster wtith a cluster index, CI = 1. C2 has four *c*-units (5, 6, 9 and 10) at its neighboring sites, and neither C2 not the neighboring *c*-units bear a cluster label. Hence, this is designated as the second cluster (CI = 2) with a size of 5. Similarly, C3 has two (4 and 13) neighboring *c*-units, and forms a cluster of size 3 (with a cluster index, CI = 3). Since C4 has two *c*-units already labeled with CI = 3, it too takes the same label. C5 has two (2 and 10) and C6 has three (2, 9 and 10) nearest neighbors, that already form part of the second cluster. C7 has two (8 and11) neighboring *c*-units, and it forms a 3-mer cluster (CI = 4). C8 has two (7 and 11) *c*-units, already included in cluster with CI = 4. C9 has three (2, 6 and 10) and C10 has three (2, 6 and 9) units that are already part of a cluster with CI = 2. C11 has two (7 and 8) units that are already included in cluster-4 (CI = 4). C12 has two (13 and 15) neighboring units and forms a 3-mer cluster. Since C13 is already labeled with CI = 3, all the neighboring units to C12 are labeled with the cluster index, CI = 3. This now forms a 5-mer (3, 4, 12, 13 and 15) cluster. C14 has one neighbor (16), and it forms a 2-mer cluster (cluster-5, CI = 5). C15 has two (12 and 13) units that are already included in cluster, CI = 3. C16 has only one (14) neighboring c-unit and is included in cluster, CI = 5. Thus, the cluster size distribution is calculated as follows:

Cluster no.	*n*
1	1
2	5
3	5
4	3
5	2

n	w(*n*)
1	1
2	1
3	1
4	0
5	2

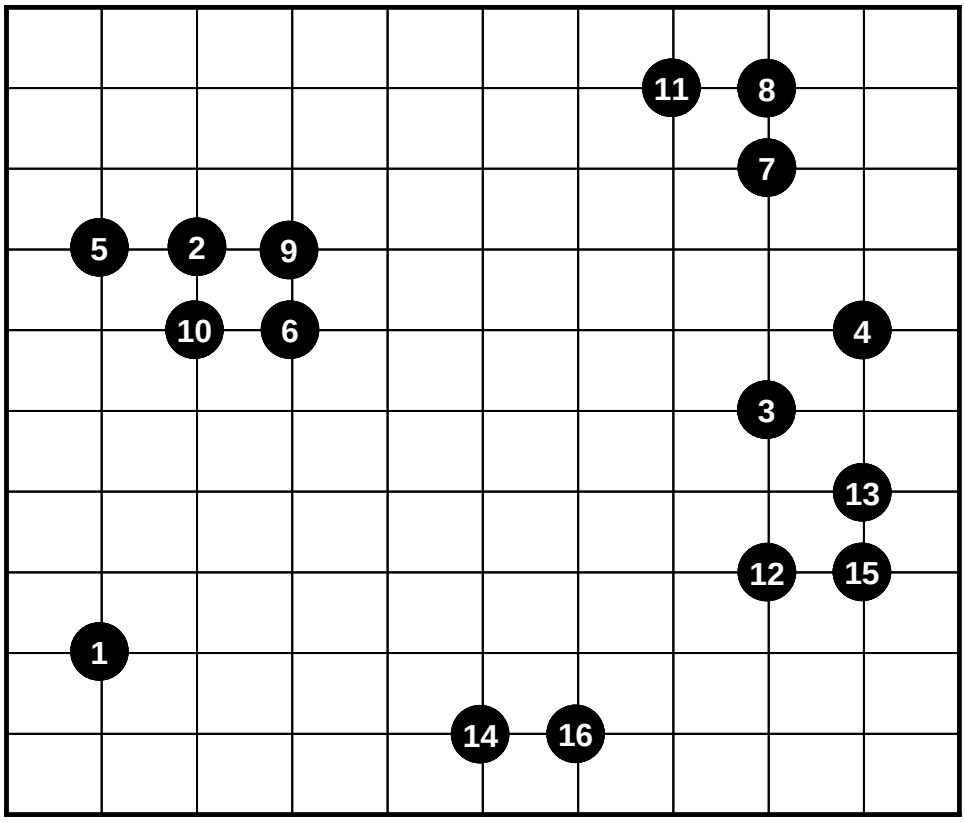

Figure A.1. Schematic representation of the estimation of cluster size distribution (CSD). Only *c*-units are shown in the above schematic for clarity.

A.3. Results and Discussions

We present the results ($P(n)$ vs. n) for the chain size, N = 128, containing 12.5% c-units with λ = 20 for both, R and U copolymers. We compare the results of $P(n)$ for R and U copolymers in Figures A.2 to A.4 for B = 0.01 to 0.04. The error bars in the graphs are the standard deviations for data from 30 and 15 simulations of R and U copolymers, respectively. We note that the Metropolis weighting scheme that we use, does not efficiently sample relatively low probability conformations that do not contribute significantly to the calculation of average quantities. This results in the observed large error bars for low probability cluster sizes. In addition, the larger error bars for R copolymers (relative to U) arise from averaging over 30 random copolymer chains, each with an independent, random comonomer distribution.

Discussion on the Nature of $P(n)$-n Plot:

For $B \leq 0.02$ (Figure A.2 a-d), the $P(n)$ values decrease monotonically with n for both, R and U copolymers. A majority of the c-units are dispersed, viz., form clusters of size = 1. This is as expected, since the low B (effectively high temperature) state corresponds to a "gas" of c-units connected via the backbone. As described in chapter 4, below the theta point ($B < B_\theta$), the enthalpic gain due to c-c aggregation is not sufficient to overcome the entropy loss due to the loop formation. As a result, only relatively few c-units form aggregates, while the majority of c-units exist as single entities. Comparing R and U chains, we observe that, for any value of n, the R copolymer has a higher value of $P(n)$ compared with U. Thus, R copolymers have a higher tendency to form aggregates when compared with U, even in the coil state ($B \leq 0.02$). We have described this behavior with the help of the $<M>$ value in the chapter 4. Briefly, the distribution of m-segment lengths in the R chain implies that there are always c-units that are separated by only a few m-units and these can readily loop to form a

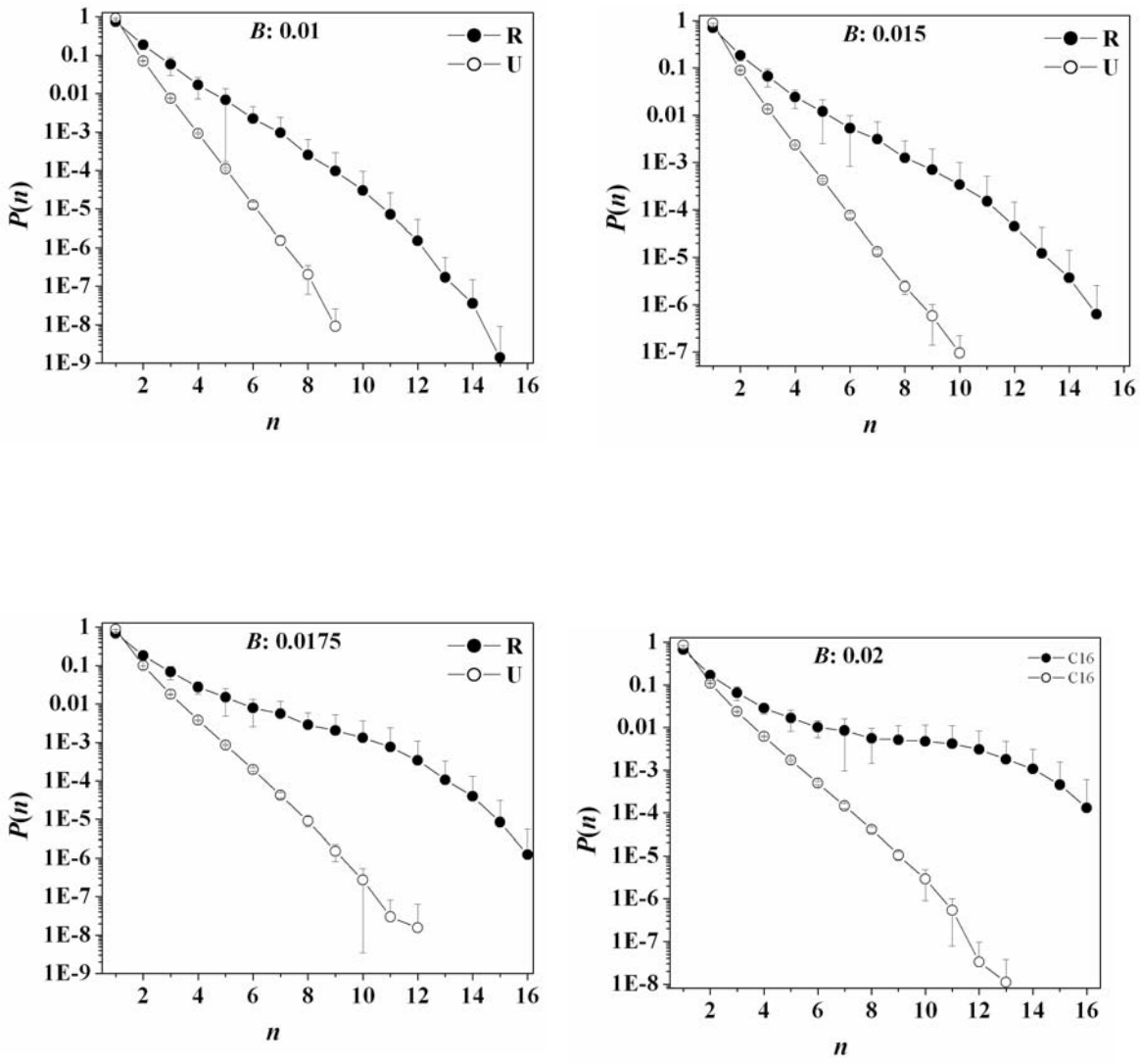

Figure A.2. *P*(*n*) vs. *n* for R and U copolymer at *B* = 0.01 (a), 0.015 (b), 0.0175 (c) and 0.02 (d). The connecting lines are meant to guide the eyes.

cluster. This is not possible in the U-chain where all *c*-units are uniformly spaced along the chain and the *m*-sequence length between comonomer units is higher than the corresponding average length in R copolymers.

At B = 0.0225 (Figure A.3a), R shows a non-monotonic behavior whereas U still shows a monotonic decrease. For all sizes of clusters (except n=1), R has a higher probability than U copolymer. At B = 0.025 (Figure A.3b), U copolymers show higher values of $P(n)$ for n = 1 to 6 relative to R. This trend shows that the tendency to form higher size clusters increases for U relative to R copolymer with increase in B. However, at this B, U copolymers show a monotonically decreasing probability for clusters of larger sizes, unlike R copolymer. At B=0.0275 (Figure A.3c), both R and U show a non-monotonic trend. U has a higher values of $P(n)$ than R, for n = 1 to 10, but has a lower value of $P(n)$ for n >10. The probability of formation of a 16-mer cluster is smaller by 2 orders of magnitude than for R copolymer. On further cooling, at B = 0.03 (Figure A.3d), both R and U copolymer show a similar trend and larger size clusters are now more probable than smaller ones. As cooling proceeds, smaller size clusters disappear while larger ones grow. and we see a depletion in the value of $P(n)$ for the intermediate ranges of n (Figures A.4a, b, c and d). Finally, R and U copolymers yield only one cluster with 16 comonomers at the collapsed globule state (B>0.04). At higher B value, larger clusters are more stable than the smaller ones.

As the cooling proceeds, more *c*-units aggregate to form larger size aggregates. In the coil state (B<0.02), the probability of clustering decreases dramatically with with cluster size since enthalpic gain from *c*-*c* aggregation is much less compared to entropic loss from loop formation. However, as B increases (viz., decreasing temperature), the enthalpic gain overcomes the entropic loss and larger clusters form.

Since the clusters are at thermodynamic equilibrium state, we estimate the free energy for the cluster formation, $F(n)$ of size n from the following relation:

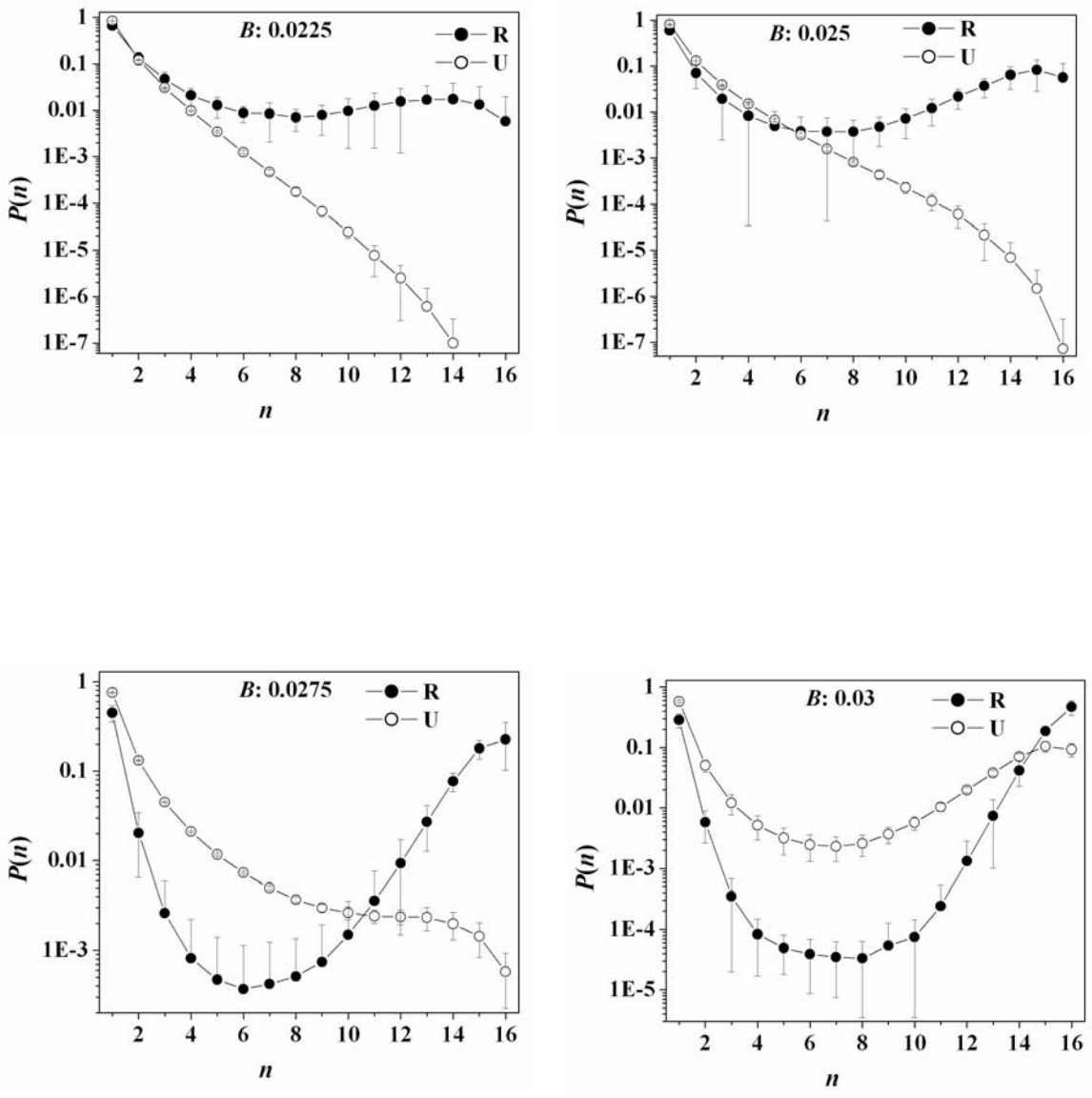

Figure A.3. *P*(*n*) vs. *n* for R and U copolymer at *B* = 0.0225 (a), 0.025 (b), 0.0275 (c) and 0.03 (d). The connecting lines are meant to guide the eye.

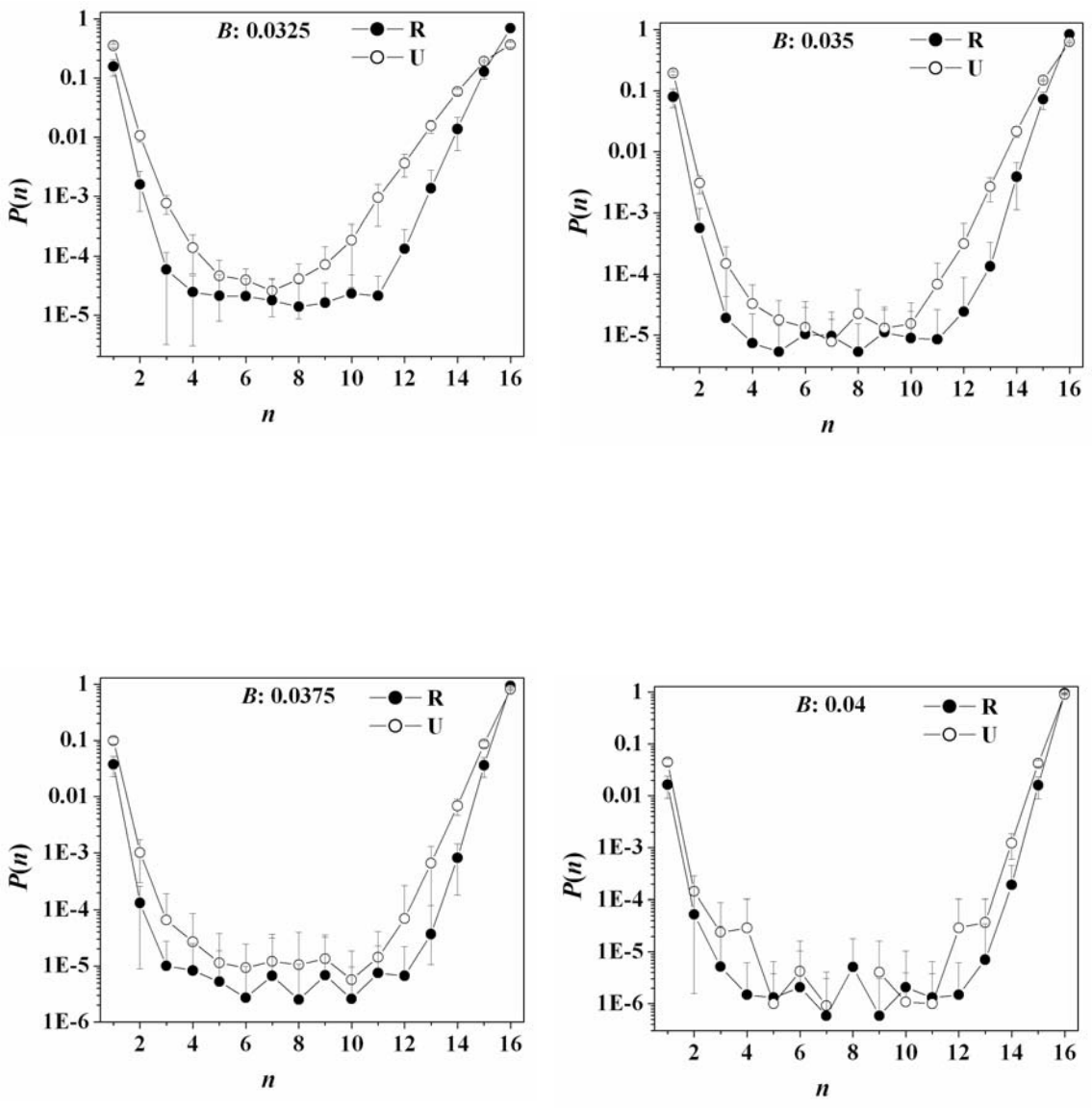

Figure A.4. *P*(*n*) vs. *n* for R and U copolymer at *B* = 0.0325 (a), 0.035 (b), 0.0375 (c) and 0.04 (d). The connecting lines are meant to guide the eye.

$$-F(n)/T = H(n)/T - S(n) \approx \ln[P(n)], \quad \text{..... (1)}$$

where $H(n)$ and $S(n)$ represent the enthalpy and entropy of a cluster of size n. The enthalpy is estimated by multiplying the number of *c*-*c* pair contact in each cluster ($N_{cc}(n)$)by the energy per contact (ε_{cc}), i.e., $H(n) = N_{cc}(n) * \varepsilon_{cc}$. It is difficult for us to estimate the entropy of loop formation in our simulations. However, we note that the free energy at $B = 0$ comes only from the entropic contribution. Thus, at $B = 0$, we can re-write equation 1 as:

$$-F(n)_0/T = S(n)_0 \approx \ln[P(n)_0] \quad \text{.....(2)}$$

In the coil state, the free energy is dominated by the entropic contribution and the enthalpy of *c*-*c* contacts relatively unimportant. As an approximation, we assume that the entropic contribution to the free energy at $B < B_\theta$ is given by the free energy at $B = 0$. Thus, we estimate the free energy for $B>0$ from

$$-F(n)/T = \ln[P(n)] = H(n)/T - S(n)_0 = N_{cc}(n) * \varepsilon_{cc}/T - S(n)_0 \quad \text{.....(3)}$$

We fit the $P(n)$ values obtained our simulations at each B with the expression (3), to obtain ε_{cc}, as a fitting parameter. We present the simulation data and the fits to $P(n)$ in Figure A.5 for B = 0.01, 0.015, 0.0175 and 0.02. We are able to obtain a reasonable fit to $P(n)$ for $B < 0.02$, viz. below the θ-point. However, the values of ε_{cc} obtained from these fits decrease with B, and further, the fitted values are significantly different for U and R copolymers (Figure A6). Since ε_{cc} represents the energy per *c*-*c* contact, scaled with kT, we do not expect any B-dependence. We believe that this reflects the B-dependence of the entropy that we have neglected in our highly simplified analysis. Beyond theta, i.e., $B > 0.02$, the enthalpy of *c*-*c* contacts dominate as the chain collapses and $S(n) \neq S(n)_0$. Therefore, we cannot use (3) to model the simulation data. However, the values of $S(n)_0$ and ε_{cc} from high

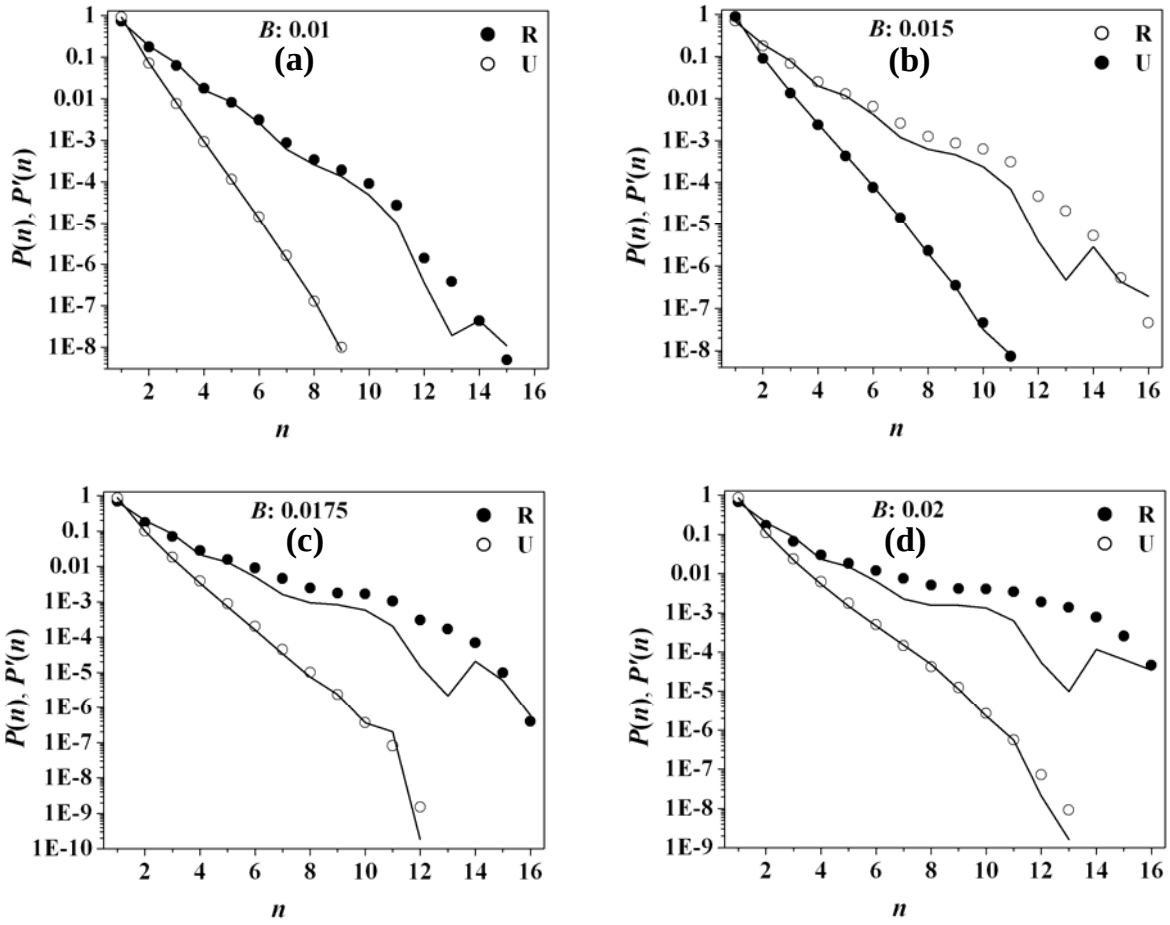

Figure A.5. $P(n)$ **(data points) and the fit (continuous lines) for R and U copolymer at *B* = 0.01 (a), 0.015 (b), 0.0175 (c) and 0.02 (d).**

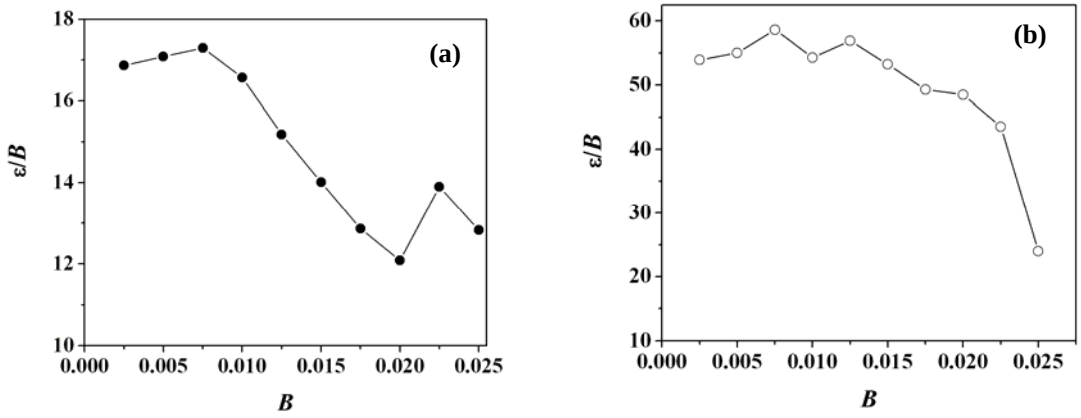

Figure A.6. Variation of ε_{cc}/B as a function of *B* for (a) R and (b) U copolymer

T (low *B*) data can be employed to refine the modeling and to estimate $S(n)$ as a function of *B*.

We have observed that the trend of $P(n)$ becomes a non-monotonic function of *n* as *B* is increased beyond 0.02 (viz. beyond theta), as larger clusters form. The gradual progression of a monotonic to a non-monotonic distribution of $P(n)$ vs. *n*, demonstrates the formation of larger clusters at the cost of the smaller clusters. The non-monotonic trend for R, spans a wider range of *B* compared to U copolymer – as recognized earlier in Chapter 4, the U copolymer collapses more abruptly than the R copolymer. The co-existence (existence of small and large size clusters with appreciable probability) range of *B* for U is smaller than for R and this is dictated by the chain microstructure. In case of R copolymer, the core formation happens in a gradual manner unlike for the U copolymer, where the collapse happens more abruptly and cooperatively. The gradual collapse in R copolymer widens the co-existence region in terms of *B*.

Chapter 5

Polymer Crystallization in the Presence of "Sticky" Additives

5.1. Introduction

Additives are a class of materials that are added to a parent polymer, typically during compounding, so as to impart desired properties without modifying the molecular architecture of the polymer.[1] All commodity polymers, without exception, are supplied in additivated form. Additives are used to impart a variety of functionalities. For example, antioxidants are used in almost all polymers, to inhibit their oxidative degradation; lubricants are used to promote flow; antistatic compounds are used to prevent build-up of static charge on the surface of the polymeric part; nucleating agents are used to provide surfaces for heterogeneous nucleation of semicrystalline polymers; plasticizers are used to depress the polymer glass transition temperature, T_g, etc. Additives that modify bulk properties of a polymer, such as antioxidants, nucleating agents, etc., need to be uniformly dispersed in the polymer to be effective, while additives such as antistatic agents, that modify surface properties, need to "bloom" to the surface during processing.

Additives that are used to rigidify polymers are called antiplasticizers. We classify antiplasticizers into two kinds, depending on the mode of rigidification. The first kind of antiplasticizers are bulky molecules that disperse in a polymer, and decrease the available

free volume. This reduction in free volume in the vicinity of antiplasticizers, inhibits chain mobility,[2,3] and typically increases the polymer T_g, thus changing the relaxation spectrum and mechanical properties of the additive-polymer "composite". For example, addition of a large fraction (14% by weight) of nonpolar mineral oil to 1,4-polybutadiene, results in a shift of the α-relaxation to lower frequencies (viz., an increase in T_g), but no change in the β-relaxation, suggesting that local, non-cooperative motions, are not influenced by the additive. Further, there is no change in the shape of the α-relaxation spectrum, and no change in the fragility, suggesting that rigidification of the polymer is effected by an increase in the local friction uniformly along the chain.[4]

The second kind of antiplasticizers are "sticky" molecules, viz., there are attractive interactions between the additive and polymer. For example, Don et al.,[5] report that hydrogen bonding between the carbonyl group of an additive (a polycaprolactone/polycarbonate blend) and the hydroxyl group of the epoxy matrix, results in an increase in the modulus of the epoxy, that correlates with an increase in the activation energy for the β relaxation. Thus, in this system, rigidification of the epoxy, is effected by hydrogen bonding of 2-hydroxypropyl ether groups, localized along the chain. Similarly, Perepechko[6] reports that when a small amount of water is added to polycaproamide, the formation of "short crosslinking bridges" due to water-amide interactions, restricts polymer chain motions, and results in antiplasticization.

There are only very few literature reports that examine the influence of antiplasticizers. Further, most experiments[4-15] such as those described above, and simulations,[16] investigate rigidification of *amorphous* polymers by antiplasticizers. To the best of our knowledge, there are no reports that describe the effect of antiplasticizers on structure formation in semicrystalline polymers. Here, we describe lattice Monte Carlo simulations that probe how crystallinity develops, when "sticky" additives (viz., wherein

there is an attractive interaction between the additive unit and the polymer) are dispersed in the bulk of a semicrystalline polymer. Intuitively, one would imagine that additives that "dilute" a polymer melt and that decrease chain mobility in the melt, would inhibit crystallization, and significantly slow down crystallization kinetics. Accordingly, our results show a monotonic decrease in crystallinity and crystallite dimensions with increase in additive-polymer attraction. However, surprisingly, the change in crystallization kinetics, and the magnitude of the "specific heat" peak at crystallization are non-monotonic with additive-polymer interactions. Thus, our preliminary investigations on the influence of "sticky" additives on polymer crystallization, already reveal interesting, non-intuitive behavior.

We organize this chapter as follows: we describe the model and simulation technique in section 5.2. We discuss our results in the section 5.3 followed by a summary in section 5.4.

5.2. Model and Simulation Technique

In recent years, several Monte Carlo based, rapid chain growth techniques have been developed, such as PERM,[17] CBMC,[18] RES-CBMC,[19] etc. These are suitable for single chain simulations, and cannot be employed for dense systems representing melts. Other algorithms such as the Wormhole Moves Algorithm,[20] are also not suitable for simulation of crystallization of a dense melt, where the same polymer chain could exist in amorphous and crystalline regions. Lattice simulations of dense systems are possible by the Cooperative Motion Algorithm (CMA) by Pakula and coworkers[21,22] and the single site version of the Bond Fluctuation Model[23-26] by Hu et al.[27,28] CMA has been employed for lattice systems with 100% occupancy. However, the time evolution of the morphology, cannot be unambiguously mapped to the simulated Monte Carlo Steps.[23] Therefore, we use a dynamic

Monte Carlo methodology, similar to that of Hu et al.[27-29] to address the crystallization of *homo*polymer melts containing additives. It is worth noting that in their work, Hu et al.[29] were able to successfully reproduce experimentally-observed, nontrivial trends such as the influence of comonomer content on the development of crystallinity on cooling, etc. We now describe our simulation technique in detail.

Our simulations probe dense polymer melts with a lattice occupation density (fraction of lattice sites occupied by additives and polymers) of 0.9375 on a cubic lattice (coordination number = 26) of size 32^3. Monomers and additives occupy one lattice site each. Thus, the simulation box for our unadditivated polymer melt comprises 480 chains, each having 64 monomer units. Additivated systems comprise $(480 - n)$ chains and $64n$ additive units. Thus, a melt containing 1.67% additives is simulated by placing 512 ($= 64 \times 8$) additive units and 472 (=480 - 8) chains on the lattice.

Initially, we place the additives and polymer chains in a regular fashion in the simulation box. We employ a micro-relaxation algorithm, viz. a combination of single site bond fluctuation and slithering diffusion to move the chain units along the lattice sites with periodic boundary conditions.[27,30] Specifically, our algorithm randomly (random number generator, MT19937 [31]) selects a vacant site and attempts to move a monomer or additive from one of the nearest neighboring sites to this vacant site. Depending on the position of unit along the backbone chain, our algorithm selects the appropriate micro-relaxation move. For example, if the selected unit is at a chain-end, then it will attempt to move either by slithering diffusion[24] or by a single site bond fluctuation[25] (cf. end bond rotation), with equal probability. On the other hand, if the selected unit is a non-terminal one, it will attempt to move by a single site bond fluctuation.[25] The moves chosen for the polymer chain are physically realistic; evidence from the literature indicates that such Monte Carlo simulations are capable of faithfully describing polymer chain dynamics in a melt from large length

scales down to an effective bond[23,32,33]. For additives, only a single site move is performed. Combination of these moves are known to produce faster relaxation in such a highly dense system.[26] We enforce excluded volume interactions and disallow bond crossings[32]. Such a scheme satisfies detailed balance, and precludes "locked-in" states which chain-growth self-avoiding walk (SAW) algorithms may face.[24,34]

The success of attempted moves is governed by the Metropolis[35] scheme with a probability, $p = \exp(-\Delta E/kT)$, where ΔE is the change of energy for the transition from the old to new conformation, k is the Boltzmann constant and T is the absolute temperature. The change in energy, ΔE, for a move in our simulation is calculated as: $\Delta E/kT = \Delta N_p U_p + \Delta N_c U_c + \Delta N_{ma} U_{ma}$, where, ΔN_p, ΔN_c, and ΔN_{ma} are the net changes in the numbers of non-bonded parallel bonds, collinear bonds and monomer–additive contacts, respectively; U_p, U_c, and U_{ma} are the driving energies (normalized by kT) for pairs of non-bonded parallel bonds, collinear bonds and monomer–additive contacts, respectively. U_{ma} can be considered an additive-monomer exchange energy, and can be expressed using the quasi-chemical approximation[36] as, $U_{ma} = \varepsilon_{ma} - (\varepsilon_{mm} + \varepsilon_{aa})/2$, where ε_{mm}, ε_{aa} and ε_{ma} are the pairwise interactions between *m*-*m*, *a*-*a* and *m*-*a*, respectively.

Thus, in our simulations, polymer crystallization is driven by locally stiffening the chains (by making bonds collinear, via the U_c term) and by arranging polymer chains parallel to each other[37] (via the U_p term). Thus, U_c is used to coarse-grain the bond torsion potential, while U_p is used to coarse grain the enthalpic interactions that drive packing in a crystalline unit cell. Since the atomistic origins of these coarse grained interactions are the same, we assume here that the energies for a pair of bonds to be collinear and to be parallel are equal, i.e. $U_c/U_p = 1$ (Increasing U_c/U_p from 1 to 10 in simulations of unadditivated polymers did not significantly influence either the crystallinity or the lamellar thickness of

the crystals. Therefore, we have performed all our simulations at U_c/U_p = 1). For simplicity, we set the monomer-additive attraction, $U_{ma} = \lambda U_p$, where λ is the "stickiness" parameter, specifying the strength of the monomer-additive attraction, relative to the parallel bond interaction energy. In our work, $\lambda \geq 0$, and higher λ implies stronger monomer-additive attraction.

We begin by equilibrating the system at U_p=0. As U_p, U_c, and U_{ma} are normalized by *kT*. Setting U_p = 0, represents a high temperature state, viz. an athermal melt. At U_p=0, we calculate squares of the instantaneous end to end distances of segments of length *i*, R_i^2 (*i* = *N*, *N*/2, *N*/4 and *N*/8), as a function of MC steps (MCS; one MCS is defined as 0.9375×32^3 MC moves, viz. on average one attempted MC move for each unit, monomer as well as additive, present in the simulation box). We did not observe any appreciable change in the value of R_i^2 beyond 5000 MCS (Figure 5.1). To verify that the athermal melt is at equilibrium after 5000 MCS, we calculate the scaled segmental mean square end to end distance, $\left\langle R_j^2 \right\rangle / j$, for segment lengths *j* (*j* = 1 to *N* - 1) along the chain, and observe that this reaches a plateau with increase in segment length[38] (Figure 5.2). We have checked the scaling relation of $\left\langle R_N^2 \right\rangle$ (*N* = 16, 32, 64 and 128, averaged over 5000 MCS) with chain length, *N*, and have found that the exponent is ~ 0.5, characteristic of a polymer melt.

After equilibration at U_p=0, we progressively increase the value of U_p in steps of 0.05. An increase in U_p can be considered as a decrease in temperature – in our work, we present data as a function of U_p. As at U_p = 0, we allow the sample morphology to develop over 5000 MC steps, and calculate properties as an average over the subsequent 5000 MC steps. In our simulations, we calculate the fractional crystallinity, X_c, "specific heat", C_v

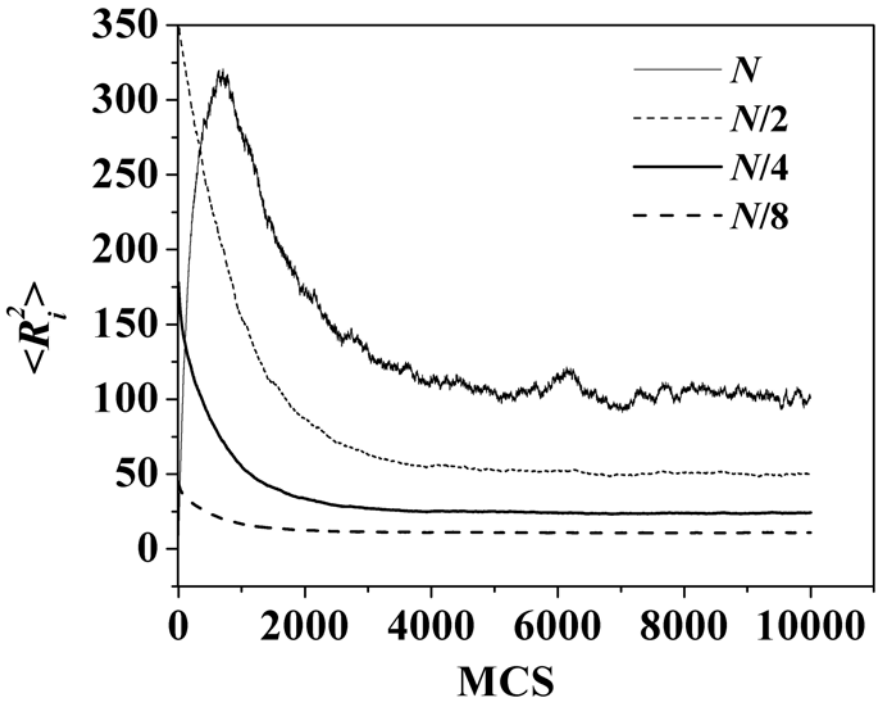

Figure 5.1: Change in segmental square end-to-end distance with number of MCS for the segment length *N*, *N*/2, *N*/4 and *N*/8 for unadditivated polymer. The average has been taken for all possible combination of segment lengths.

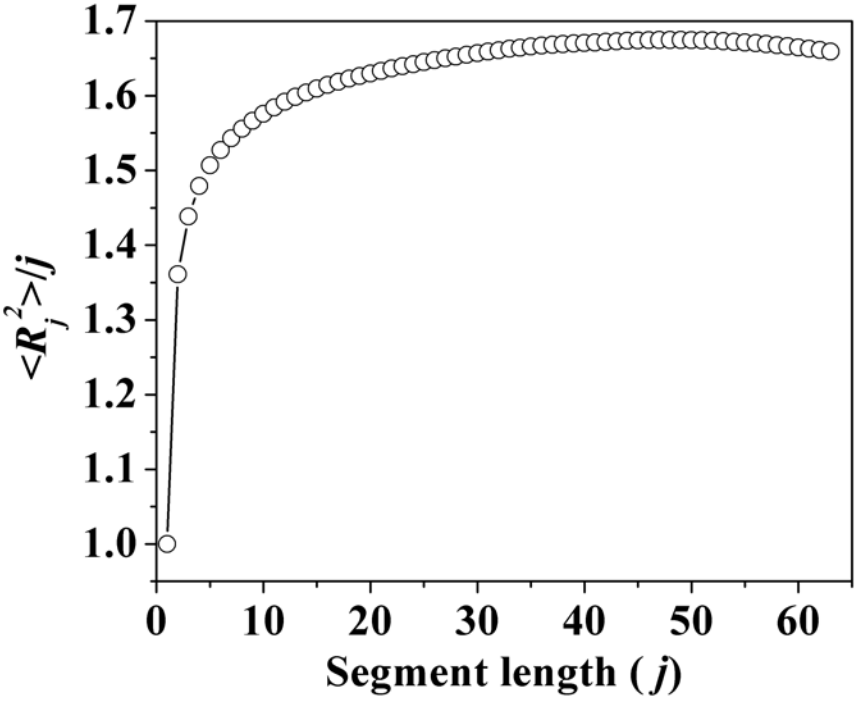

Figure 5.2: Change in mean square segmental end-to-end distance as a function of the segment length, *j* for unadditivated polymer. The lines joining the points are meant only as a guide to the eye.

(described later), additive–monomer pair distribution function and mean square displacement of center of mass, as described below.

Increasing U_p in uniform steps of 0.05 corresponds to a nonlinear cooling profile (since $U_p \sim 1/T$). We have re-run select simulations by cooling at a constant rate (viz. increasing U_p in non-uniform steps at constant $\Delta(1/U_p) = 0.2$. We observe that the results for these two cooling profiles is essentially identical, indicating that the nonlinear cooling rate adopted in our simulations, does not affect the generality of our conclusions.

To monitor the phase transition from a disordered molten state to an ordered crystalline state, we calculate X_c, as a function of U_p. We arbitrarily define a bond as crystalline, if it is surrounded by more than five nearest non-bonded parallel bonds, in a manner similar to Hu.[29] Crystallinity is defined as the ratio of the number of crystalline bonds to the total number of bonds in the system. A crystallite is a contiguous aggregate of crystalline bonds with the same orientation. We characterize crystallites by their size, $\langle S \rangle$ and their thickness, $\langle L \rangle$. The size of a crystallite is the number of crystalline bonds that comprise it. We calculate the distribution of the crystallite sizes and the average crystallite size as a function of U_p. We also calculate the thickness of a crystallite as the average fold length in the chain direction. The average thickness is calculated over all crystallites present in the system and is expressed as the average number of monomer units in the crystal thickness direction.

We calculate the specific heat like property, C_v, in a manner, similar to that for the equilibrium specific heat, viz. from the total energy fluctuations (normalized by the total number of monomer units and additives in the simulation box). Our simulations represent a system that is out of equilibrium – therefore, the energy fluctuation term that we calculate is not the equilibrium specific heat. However, as we calculate properties over a much longer

number of MCS than is required for structural relaxation, we continue to call the calculated energy fluctuation term the "specific heat" and denote it as C_v, for convenience. At the phase transition, C_v shows a peak as fluctuations in energy[39] become large. The U_p value at which we observe a *peak* in C_v on cooling from the melt state, is termed the crystallization U_p, in tune with experimental (calorimetry) convention, even though crystallization takes place over a range of U_p.

The spatial distribution of additives in the system is characterized by calculating the additive-additive (*a*-*a*) and additive-monomer (*a*-*m*) pair distribution functions, g(*r*). These are, respectively, the fraction of additives (or monomers) at a distance *r* from an additive (averaged over all additives). Similarly, to characterize the local environment (crystalline/amorphous) in the vicinity of an additive, we calculate additive–crystalline (*a*-*c*) monomer and additive–non-crystalline (*a*-*nc*) monomer pair distribution functions at $r = 1$.

We have simulated crystallization of polymers containing x = 0.4, 0.83, 1.67, 3.125 and 6.25% of sticky additives. At each additive fraction, we have investigated a range of "stickiness" parameters, λ = 0, 5, 10, 20, 30 and 40. In this parameter range, we encounter attempted moves with a ΔE of up to $45\,kT$. However, the majority of the moves are of less than $10\,kT$ (at least ~60% of possible moves and ~99% of accepted moves in all simulations).

To check that our algorithm is robust against *aphysical* frustration of morphology, we have run test simulations with an artificial Hamiltonian that resets $\Delta E \geq 10\,kT$ to $\Delta E = 10\,kT$. Thus, in these test simulations, attempted moves with energies greater than $10\,kT$ are accepted with an artificially increased probability corresponding to $10\,kT$. We note that this procedure affects only 1% of the accepted moves, and observe that evolution of semicrystalline morphology in these test simulations, is similar to that in our Metropolis DMC simulations – thus, indicating that we do not freeze in aphysical structures in our

simulations that real systems can free themselves from. Further, we always have a healthy fraction of accepted moves in our simulations. In the athermal state (U_p = 0), moves are accepted with a probability of around 18%. As U_p increases, the acceptance rate decreases, but is always above 1%, which is reasonable for DMC of large topologically connected, dense systems such as polymer melts.[32]

Polymer crystallization is a non-equilibrium phenomenon and results in a coexistence of amorphous and crystalline phases over a range of temperatures. The work of Hu et al[29]. has demonstrated that several experimental details of copolymer crystallization can be accurately reproduced by DMC simulations with a similar methodology. Specifically, previous work has demonstrated that DMC simulations faithfully capture the dynamical evolution of semicrystalline microstructure during chain folding[40], sectorization of solution crystals[41] and melting of lamellar polymer crystals[27]. In our work, we "cool" the polymer by reducing U_p in steps of 0.05. Specifying the step size is equivalent to specifying a cooling rate in real experiments. Thus, a step size of 0.01, for example, represents experiments at a slower cooling rate relative to our work. Simulations of the crystallization of unadditivated homopolymers at different cooling rates (U_p step sizes of 0.05, 0.02 and 0.01), show that the crystallinity (defined earlier in this section) increases abruptly, and then saturates as the polymer is cooled. Further, the crystallinity at saturation is a function of cooling rate – higher cooling rates result in lower crystallinity. Thus, the trends from "control experiments" using our simulation system, match reported experimental results.[42]

5.3. Results and Discussion

We begin by describing in detail, the crystallization of a system containing 1.67% additives (viz., 512 additive particles and 472 chains of N = 64; additive units per chain~ $O(1)$), and contrasting it to the behavior of unadditivated polymer. At first, we describe non- isothermal

crystallization on cooling from an equilibrated "high temperature" state (U_p = 0) to U_p = 0.5 with a step size (viz. "cooling rate") of 0.05.

5.3.1 Development of Crystallinity on Cooling

As the polymer is "cooled" from an athermal melt state (viz. U_p is increased from 0), chain segments start "stiffening" (viz. becoming collinear) and, begin aligning parallel to each other. This is a physically realistic representation of polymer crystallization[36] since it is believed that polymer chains first "stiffen" locally into all trans or helical structures that then pack into crystalline unit cells, with chain axes parallel. The additives are well dispersed in the polymer, both, in the melt state (Figure 5.3, U_p = 0) and on cooling into the semicrystalline state (compare Figure 5.3 with Figure 5.9).

For the unadditivated polymer (H) as well as the polymer containing 1.67% additives, there is an abrupt increase in crystallinity at U_p = 0.3 for all λ = 0, 5, 10, 20, 30 and 40 (Figure 5.4), indicating that within the resolution of our simulations, despite the presence of additives, we find no change in the U_p value for the onset of crystallinity; i.e., the additives do not change the "temperature" of crystallization.

For unadditivated polymer and for additivated polymers with low values of λ (λ up to 10), the rapid increase in crystallinity reaches a plateau (by U_p = 0.4). For higher values of λ ($\geq$ 20), the initial increase in crystallinity at the onset U_p is less abrupt, and the crystallinity continues to increase gradually as the sample is cooled to higher U_p (up to U_p = 0.5). The saturation crystallinity, X_c^{sat}, decreases monotonically as the additives become stickier, from ~ 0.77 for the unadditivated polymer and for λ = 0, to 0.765, 0.74, 0.63, 0.46, and 0.43, for λ

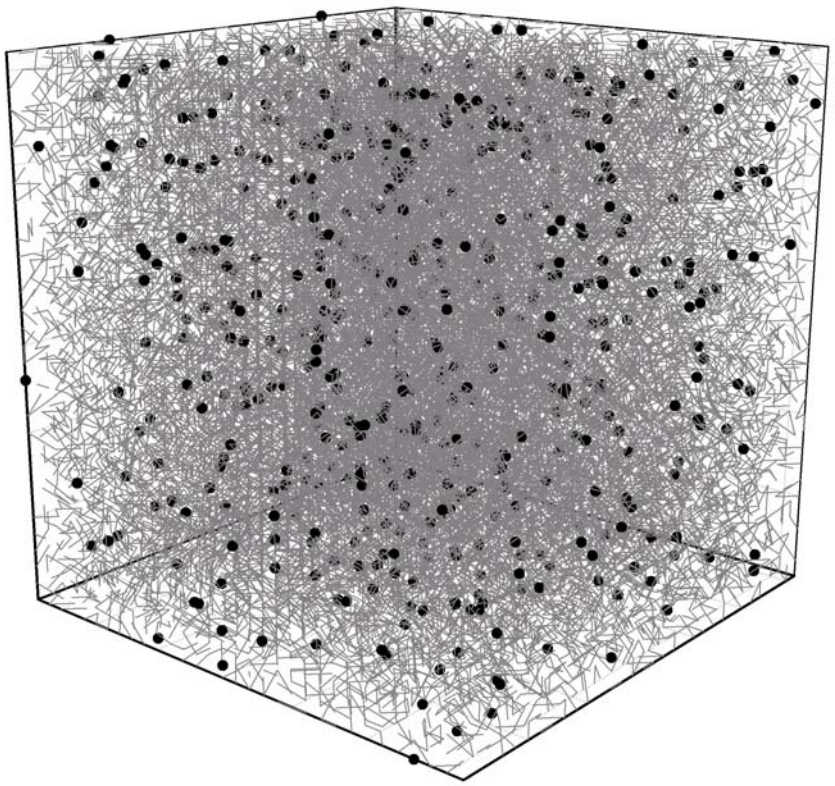

Figure 5.3: Snapshot of the simulation box at U_p = 0 showing the dispersion of the additive in polymer matrix. The filled circles represent the additives (concentration = 1.67%).

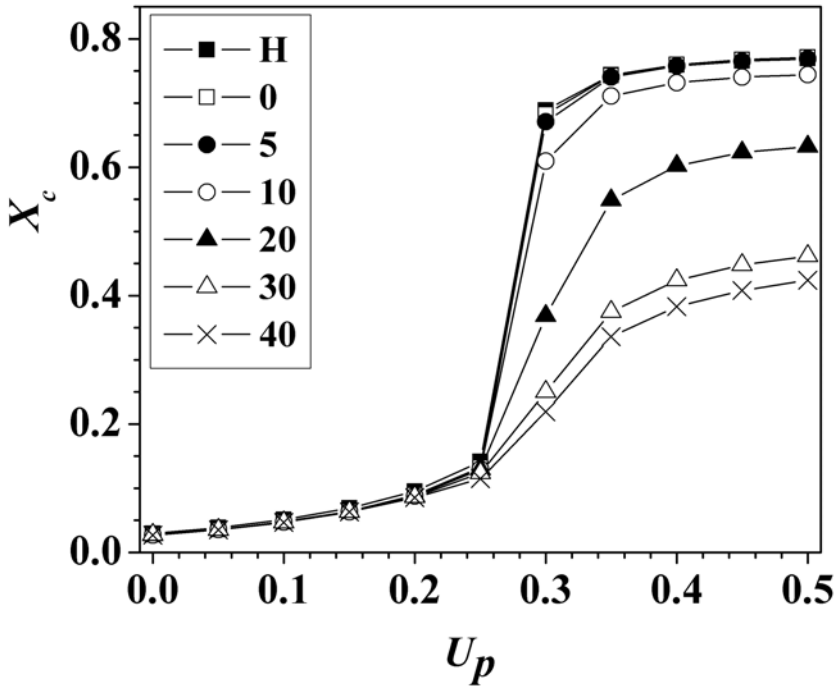

Figure 5.4: Change in crystallinity with U_p for unadditivated (H) and additivated polymers (λ = 0, 5, 10, 20, 30 and 40 ; additive concentration = 1.67%). The lines joining the points are meant only as a guide to the eye.

= 5, 10, 20, 30 and 40, respectively. Thus, as the additives become stickier, they inhibit crystallization: crystallinity decreases and the onset of crystallization is less sharp, relative to unadditivated polymer. Also, reminiscent of copolymers, polymers containing sticky additives ($\lambda \geq 20$), continue to increase their crystallinity on cooling to higher U_p. However, unlike in copolymers, we find no change in the U_p for onset of crystallization with increasing λ (to within the resolution of our simulations). Reheating from $U_p = 0.5$ to $U_p = 0$ with a heating step size of 0.05, shows a hysteresis on melting (Figure 5.5 for H), a characteristic signature of a non-equilibrium first order transition in bulk polymers.

Polymer crystals are out of equilibrium, and the crystallinity that develops in a polymer, depends largely on the conditions of crystallization. To understand how crystallization conditions determine sample crystallinity in the presence of additives, we compare samples where crystallinity develops isothermally after quenching, with the samples discussed previously, viz. where crystallinity evolves on "slow" cooling (in steps of $\Delta U_p = 0.05$).

1. In one simulation, after equilibration at $U_p = 0$, we quench a sample containing 1.67% additives with $\lambda=0$ to $U_p = 0.5$. After annealing for 2.5×10^5 MC steps, a crystallinity of 0.77 is reached, and there is little further evolution of the crystallinity. At $U_p = 0.5$, we abruptly change the value of λ from 0 to 40 for this isothermally crystallized sample and anneal for a further 2.5×10^5 MC steps. On annealing, we observe "melting" and the crystallinity decreases from 0.77 only down to 0.71 (compare with $X_c^{sat} = 0.77$ for a sample with λ = 0 cooled slowly to $U_p = 0.5$ and, $X_c^{sat} = 0.43$ for a sample with $\lambda = 40$ cooled slowly to $U_p = 0.5$).

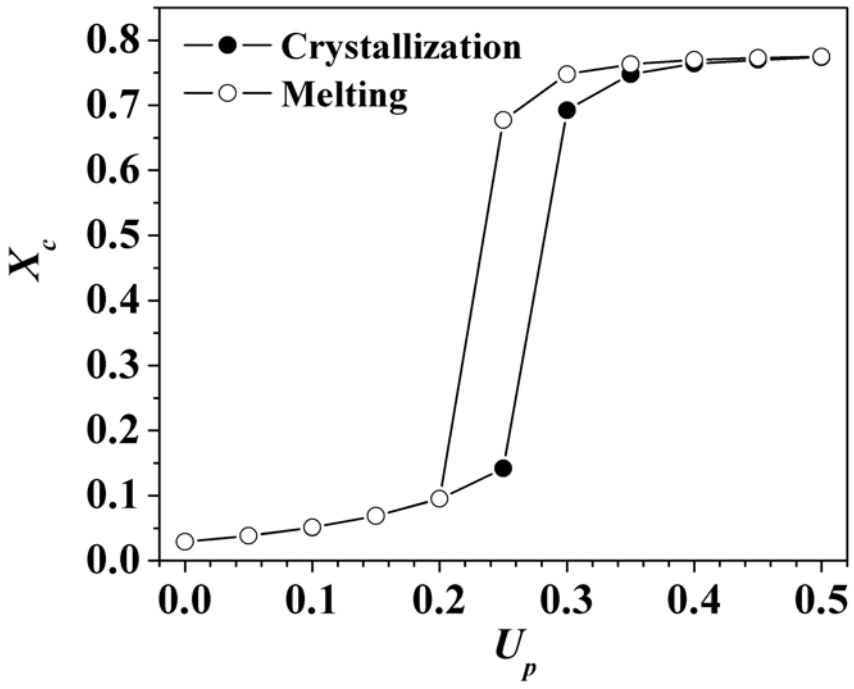

Figure 5.5: Change in crystallinity with U_p for crystallization and melting of an unadditivated polymer, showing hysteresis. The lines joining the points are meant only as a guide to the eye.

2. If, instead, we start with a sample containing 1.67% of $\lambda = 40$ additives, and quench from the high temperature state to $U_p = 0.5$, annealing for 2.5×10^5 MC steps yields a crystallinity of 0.412 (as compared with 0.43 obtained for slow cooling). Now, making the additives less sticky, viz. abruptly changing the value of λ from 40 to 0, results in a dramatic increase in crystallinity to 0.767 after annealing for a further 2.5×10^5 MC steps.

Thus, the formation of semicrystalline microstructure is a strong function of the crystallization conditions. Increasing the particle stickiness after crystallinity has developed, has only a limited influence on polymer melting for a deeply quenched polymer ($U_p = 0.5$), but decreasing constraints by decreasing stickiness, results in significant further crystallization.

5.3.2. Crystallite Structure

Polymers crystallize into 2-dimensional objects (viz. lamellae) in our simulations, viz. the crystallite thickness (average fold length in the chain direction) is smaller than the lateral dimensions in the plane of the crystallite. Figure 5.6 shows a part of a large crystallite at $U_p = 0.5$ from a simulation of unadditivated polymer crystallized by cooling from $U_p = 0$ to $U_p = 0.5$, in steps of 0.05. The geometry observed for the crystallite here is also typical of structures obtained in simulations of additivated systems. We can clearly identify chain folded sections, including a few crystalline stems that show adjacent reentry into the crystallite.

We now examine the influence of additive stickiness on the dimensions of the crystallites formed. We observe that the decrease in crystallinity for increasing values of λ (Figure 5.4), is associated with a decrease in the average size and thickness of the crystallites, as might be intuitive. In all our simulations, we observe a very wide distribution of crystallite

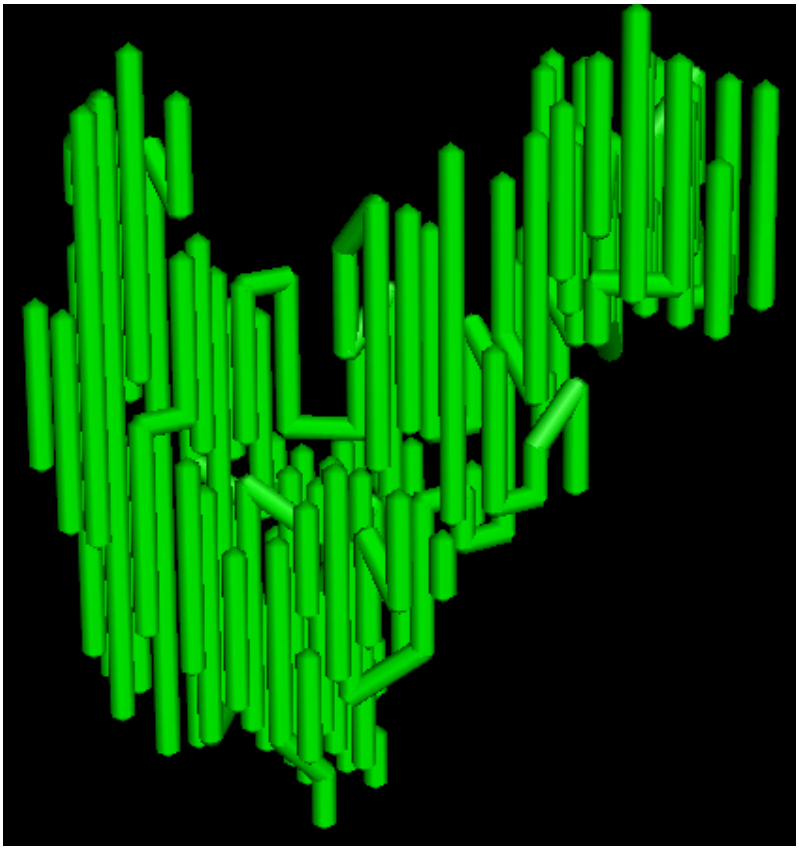

Figure 5.6: A snapshot of a typical crystallite from a simulation of an unadditivated polymer at U_p = 0.5. This crystallite contains around 650 crystalline monomers.

sizes – therefore, we note that a comparison of the values of $\langle S \rangle$, provides only a limited perspective of structure. The crystallite thickness, however, shows a relatively narrow distribution and the average thickness, $\langle L \rangle$, is close to the peak value of the distribution. $\langle L \rangle$ grows abruptly at the onset of crystallization, and then, rapidly approaches a λ-dependent plateau value for higher U_p (Figure 5.7), similar to the trend observed for crystallinity (see Figure 5.4). As the additives become stickier, (viz. as λ increases), the average thickness of the crystallites, decreases monotonically.

For unadditivated polymer, we have observed that for isothermal crystallization when quenched to various values, U_p^q, from the high temperature U_p = 0 state, the average crystallite thickness, $\langle L \rangle$ decreases with increased U_p^q (Figure 5.8) as expected. Higher undercoolings result in less-stable, thinner crystallites. Additivation with sticky additives, also results in the formation of thinner crystallites in our non-isothermal simulations.

The decrease in crystallinity and crystallite size with increase in λ, can be directly visualized in snapshots of our simulation box at U_p = 0.5 for the unadditivated polymer and for λ = 5, 20 and 40 (Figure 5.9). Near the edges of the box, it is also possible to observe parallel stacks of chains forming crystallites, similar to that for the unadditivated polymer shown in Figure 5.6. As can be observed, the additives remain well dispersed in the simulation box even after polymer crystallization, for all λ. This is quantitatively confirmed by calculating the value of the additive-additive (*a*-*a*) pair distribution function at the nearest neighbor position, g_{aa}.

To estimate the *local* polymer crystallinity in the vicinity of the additives, we calculate $g(1)_{ac}$, the pair distribution function for crystalline monomers in contact with additives at U_p = 0.5, and present these data, averaged over all additives and over 5000 MCS

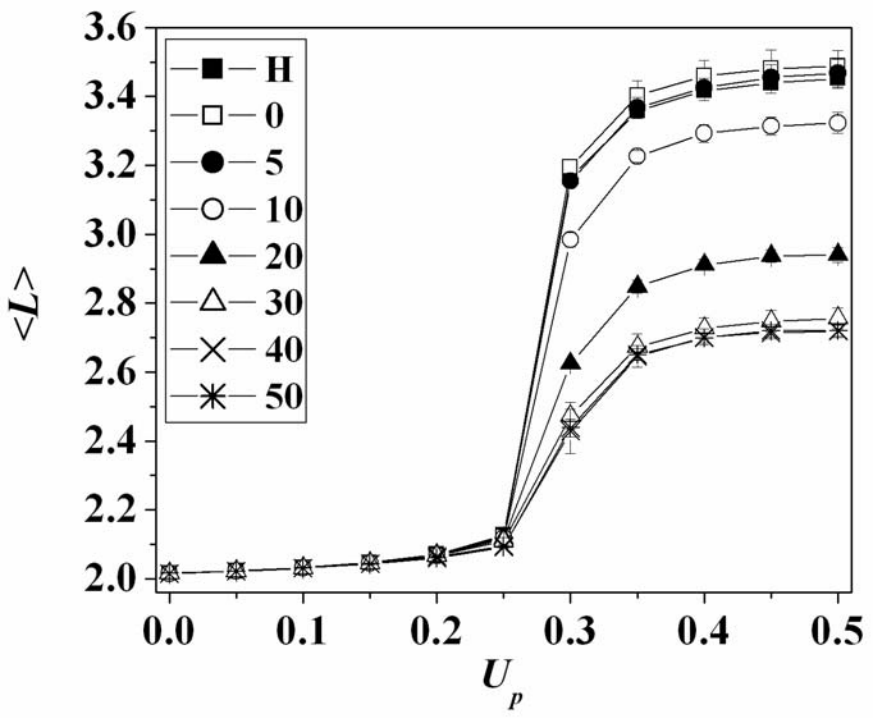

Figure 5.7: Change in average crystallite thickness with U_p for unadditivated (H) and additivated (λ = 0, 5, 10, 20, 30 and 40; additive concentration = 1.67%) polymers. The lines joining the points are meant only as a guide to the eye.

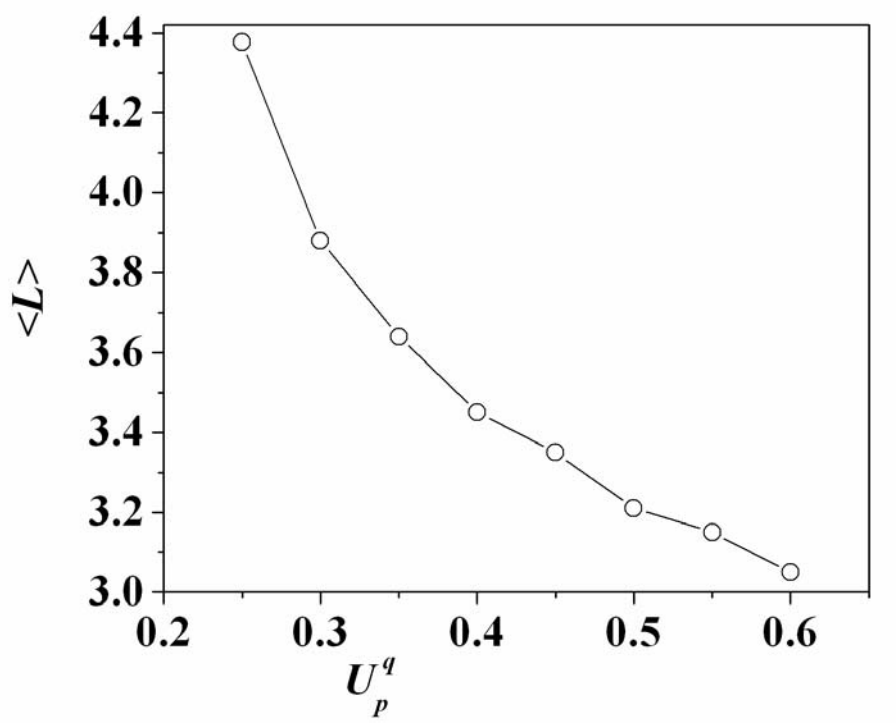

Figure 5.8: Change in average crystallite thickness, <L> with quench depth, U_p^q for an unadditivated polymer. The lines joining the points are meant only as a guide to the eye.

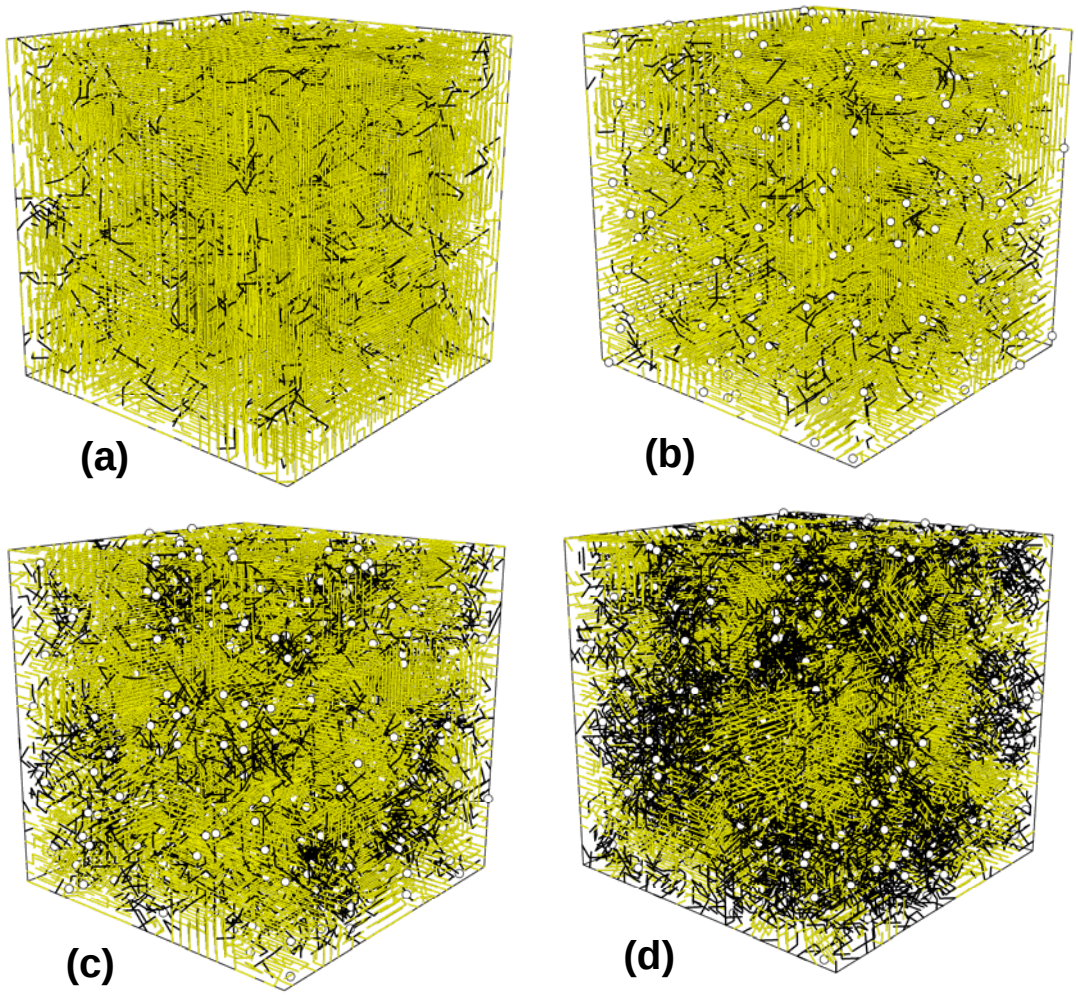

Figure 5.9: Snapshots at U_p = 0.5 from simulations for (a) unadditivated and additivated systems (b, c and d represent simulations at λ = 5, 20 and 40 respectively). The yellow lines represent crystalline bonds, black lines represent non-crystalline bonds and empty circles represent additives.

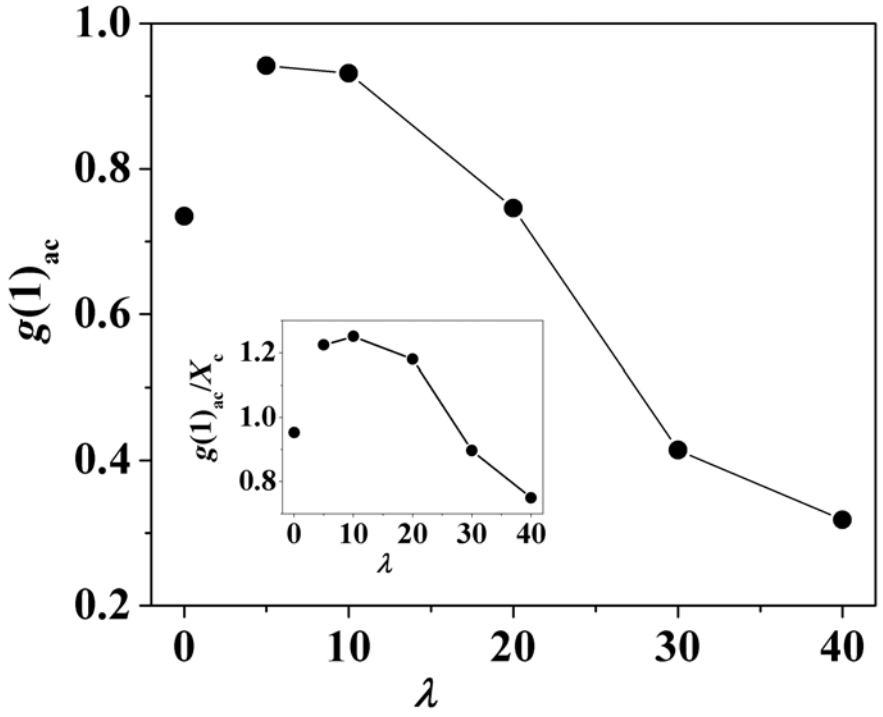

Figure 5.10: Change in average number of additive-crystalline monomer pair distribution function at r = 1, $g(1)_{ac}$ as a function of λ at U_p = 0.5 (additive concentration = 1.67%). Error bars for $g(1)_{ac}$ are comparable to the size of the symbol. The ratio of $g(1)_{ac}$ to X_c is shown in the inset. The lines joining the points are meant only as a guide to the eye.

(Figure 5.10). We observe that for λ = 0, voids are expelled preferentially to the vicinity of the additive as the polymer crystallizes, leading to a low value of $g(1)_{ac}$. For λ > 0, the additives attract monomers, and therefore, $g(1)_{ac} + g(1)_{anc} \approx 1$ for $U_p > 0$ ($g(1)_{anc}$ represents the fraction of nearest neighbor sites to the additive that are occupied by non-crystalline monomers), viz. all the nearest neighboring sites to the additives are occupied by monomers to increase additive-monomer contacts. For low λ (=5, 10), we observe that polymer crystallinity in the vicinity of the additives is very high at U_p = 0.5 ($g(1)_{ac} > 0.9$, Figure 5.10, compared with X_c^{sat} = 0.77 and 0.75, respectively for λ =5, 10, Figure 5.4). Further increase in λ results in a decrease in $g(1)_{ac}$. Interestingly, the ratio of $g(1)_{ac}$ to the bulk crystallinity is higher than 1 for λ = 5, 10 and 20 and lower than 1 for higher λ (Figure 5.10, inset).

Thus, the vicinity of the additives is more crystalline than the bulk for $\lambda \leq 20$, suggesting that localization of the monomer by the additive stickiness, enhances crystallinity in the vicinity of the additive for low to intermediate stickiness. For higher stickiness ($\lambda >$ 20), the local crystallinity in the vicinity of the additive, viz. $g(1)_{ac}$, is lower than the bulk crystallinity suggesting that, in this regime, crystallization in the vicinity of the additive is inhibited. At all U_p, $g(1)_{ac} / X_c$ shows a maximum at λ = 10. We will discuss the significance of this in Section 5.3.4.

5.3.3. Influence of Sticky Additives on Chain Mobility

Crystallization is governed by both, the driving force for phase change and polymer chain mobility. Having examined the structure of the crystallizing polymer/additive system, we now investigate the influence of the sticky additives on polymer chain mobility. We measure the mean square displacement of the center of mass (d_{cm}^2, a measure of chain diffusivity)

averaged over all chains as a function of U_p (Figure 5.11) without additive (H) and with additive (λ = 0, 5, 10, 20, 30 and 40). As we cool the system (viz. as U_p increases above 0), chain diffusivity decreases. In the melt state (U_p < 0.3), this decrease in chain diffusivity, is greater for increasing values of λ (Figure 5.11 and 5.12a). Thus, increased additive stickiness results in a decrease in polymer chain diffusivity in the melt state. At U_p = 0.3, the polymer crystallizes (see Figure 5.4) and there is an abrupt decrease in chain diffusivity for all systems. At $U_p \geq 0.3$, polymer chains in both additivated and unadditivated systems, have a low value of diffusivity. For $U_p \geq 0.3$, polymer chain diffusivity *increases* with increase in λ, probably due to the increase in amorphous content with increase in λ (Figure 5.12b). We have also calculated the mobility (viz. the mean square displacement) of monomers in the neighborhood of the additives, and observe that they show the same trends with U_p and λ as the chain diffusivity (Figures 5.12c and d).

The decrease in chain mobility with increasing λ in the melt state ($U_p \leq 0.3$) correlates with the observed decrease in crystallinity and in crystallite dimensions, as might be anticipated. It is worth noting here that in these simulations, we have 512 additive units and 472 chains, viz. around 1 additive unit per polymer chain. Therefore, the influence of additive particles on crystallization is readily apparent. These trends are, however, similar even at lower additive loadings, and we will present data on systems with different additive fractions later in this paper.

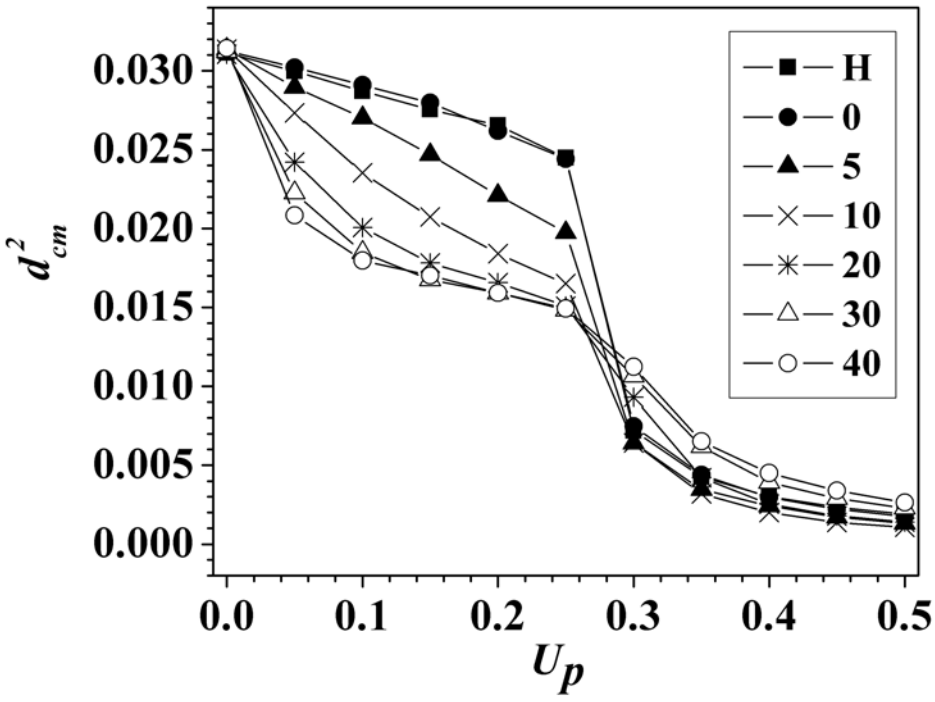

Figure 5.11: Change in mean square displacement of center of mass averaged over all polymer chains as a function of U_p for unadditivated (H) and additivated systems (λ = 0, 5, 10, 20, 30 and 40 ; additive concentration = 1.67%). The lines joining the points are meant only as a guide to the eye.

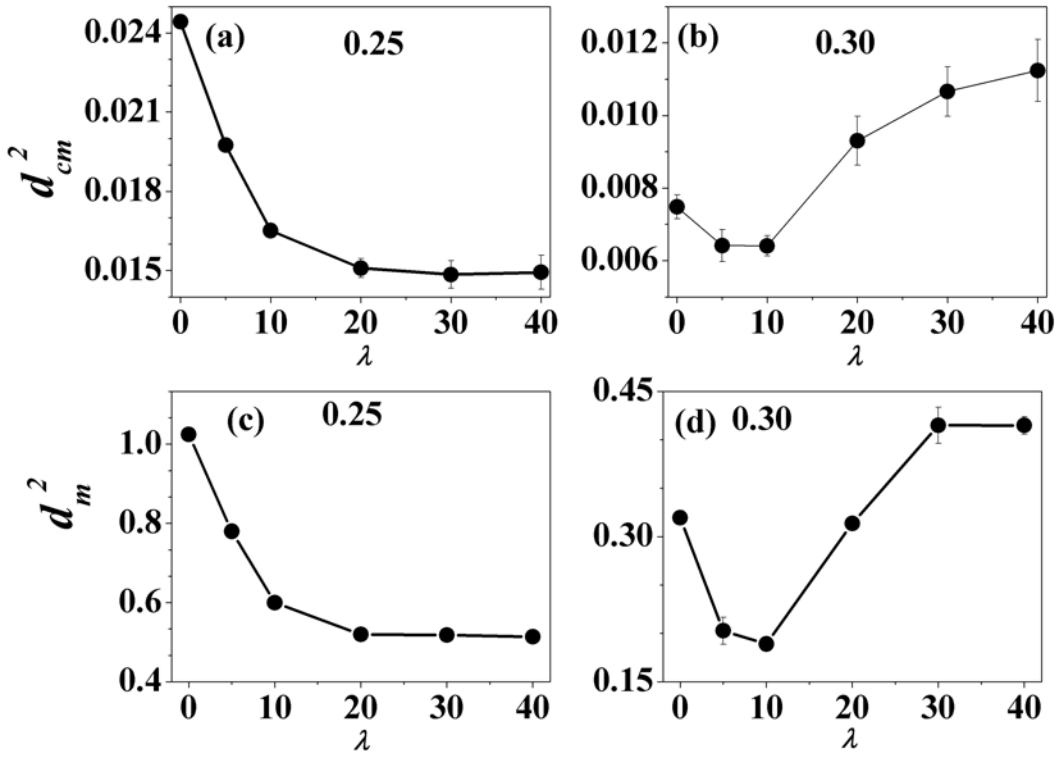

Figure 5.12: (a) and (b) Change in mean squared displacement of center of mass with stickiness parameter, λ, additive concentration = 1.67%) at U_p = 0.25 and 0.3 respectively. (c) and (d) Change in the mean squared displacement of monomers (which are next nearest neighbor to additive) at U_p = 0.25 and 0.3 respectively. The lines joining the points are meant only as a guide to the eye.

5.3.4. Unexpected Behavior at Intermediate λ

We measure the specific heat equivalent, C_v, from the mean square fluctuations in total energy as a function of U_p for unadditivated and additivated systems as they crystallize (Figure 5.13). The melt-crystal phase transition is indicated by a peak in C_v. We observe a peak in C_v at the same U_p (= 0.3) for all additivated and unadditivated systems (Figure 5.13), corresponding to the U_p at which X_c increases abruptly (Figure 5.4). Unexpectedly, the peak value of specific heat, C_v^*, exhibits a non-monotonic behavior with λ: C_v^* increases from $\lambda = 0$ to a maximum at $\lambda = 10$ and then decreases monotonically for higher λ (Figure 5.13, inset). The data presented in Figure 5.13 are averaged over five simulations and the error bars in the magnitude of C_v^* represent the variability over these independent simulations (Figure 5.13, inset). It is clear that the maximum observed for C_v^* at an intermediate value of λ, is not within the error of the simulations. The limited U_p resolution of our data make it difficult to unambiguously comment on the area of the C_v peak – however, it is reasonable to state that, to a first approximation, the peak area follows the same trend as for the peak value, C_v^*. Thus, one might expect that C_v^* would have the same (monotonically decreasing) λ-dependence as the X_c^{sat}. Therefore, the non-monotonicity observed for C_v^* is indeed surprising (see Figure 5.13, inset, compare with Figure 5.4). While the crystallinity decreases monotonically with increasing additive stickiness, as is intuitive, the magnitude of energy fluctuations at the phase transition is enhanced at intermediate values of λ. What is the reason for the observed maximum in C_v^* at intermediate λ? In our simulations, the change in energy of the system comes from changes in the number of parallel and collinear bonds, and from changes in additive-monomer contacts. We have calculated the magnitude of energy

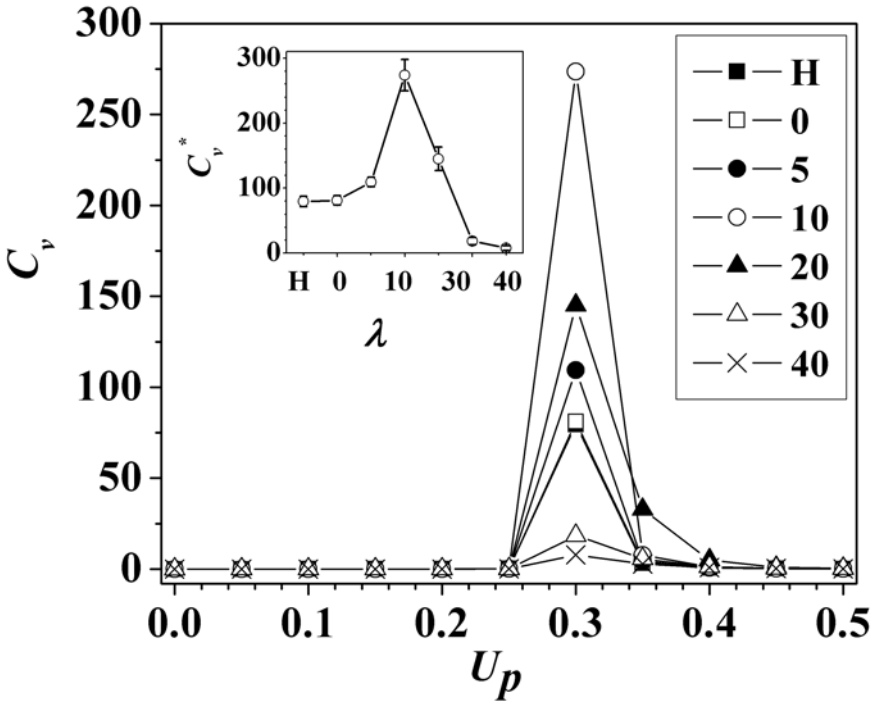

Figure 5.13: Change in specific heat, C_v with U_p for unadditivated (H) and additivated (λ = 0, 5, 10, 20, 30 and 40; additive concentration = 1.67%) systems. The inset shows the change in the peak value of C_v with λ. The lines joining the points are meant only as a guide to the eye.

fluctuations, based only on the changes in number of parallel and collinear bonds (viz. by ignoring energy fluctuations due to change in additive-monomer contacts), and have found that this dominates C_v. Thus, it is the fluctuations in the number of parallel and collinear bonds (rather than fluctuations in monomer-additive contacts) that determines C_v^* and they are, therefore, responsible for the maximum in C_v^* at intermediate λ. As crystallinity arises from the stacking of bonds parallel to each other, fluctuations in the number of parallel bonds, suggests fluctuations of monomers between crystal and amorphous states. Thus, the observed maximum in C_v^* at intermediate λ (= 10), appears to result from an enhancement in fluctuation of monomers between crystal and amorphous phases at that λ.

We do not have an unambiguous explanation for the unusual behavior of C_v^*. To gain insight into the behavior of C_v^*, we now examine structural attributes of the crystallizing bulk polymer at the phase transition. For sticky additives, viz. when $\lambda > 0$, the occupation density of monomers in the nearest neighboring positions to the additives is nearly 1 for $U_p > 0$. This is intuitive – when the additives are sticky, monomers occupy every lattice site in the vicinity of the additives, and exclude voids. Further, the mean square fluctuations in the occupation density around the additive, ($\mathrm{G}_t = \langle g(1)^2 \rangle - \langle g(1) \rangle^2$), are small and decrease with increasing λ (Figure 5.10). However, monomers in the vicinity of the additives, remain mobile (Figure 5.12d) and, monomer mobility increases with λ (since the crystallinity decreases with increased λ).

We now examine the fluctuations in the number of *crystalline* monomers in the vicinity of the additives. We calculate $\mathrm{G}_{ac} = \langle g(1)_{ac}^2 \rangle - \langle g(1)_{ac} \rangle^2$ as a function of U_p (Figure 5.14). G_{ac} is significantly larger than G_t (compare Figure 5.14 with Figure 5.15), and exhibits a peak (having a magnitude of G_{ac}^*) at the phase transition, for all values of λ

(Figure 5.14, inset). Similar to C_v, G_{ac} is small at all U_p, other than at the transition point (U_p=0.3), where it shows a maximum. Interestingly, at U_p= 0.3, the peak value is significant only at intermediate λ (= 10 and 20) and is small for all other λ.

To summarize, additive stickiness results in the following: (a) the vicinity (nearest neighbor position) of the additive has a monomer occupation density close to unity; (b) the monomers in the vicinity of the additive retain mobility at the phase transition, U_p= 0.3, and monomer mobility is largely dictated by the crystallinity, and (c) there is a large interchange between amorphous and crystalline monomers in the vicinity of the additive at the phase transition for intermediate values of λ, correlating with the maximum in C_v^*. Finally, we note that the maximum in C_v^* at λ = 10, also correlates with the maximum in $g(1)_{ac}/X_c$, both, at U_p=0.5 (Figure 5.10) and at the phase transition (U_p= 0.3, Figure 5.16). Thus, while the maximum in C_v^* correlates with several structural attributes at the phase transition, these do not unambiguously suggest the physical origin for its unusual trend. However, it is clear that the route to crystallization is modified at intermediate values of λ.

Our data suggest that crystallization kinetics, viz. the development of crystallinity, might occur differently at intermediate λ (= 10, 20), as compared with low or high λ. To investigate this further, we examine the isothermal crystallization of the additivated polymers as a function of MC steps on quenching from U_p = 0 to U_p = 0.5 (close to the phase transition temperature, shallow quench).

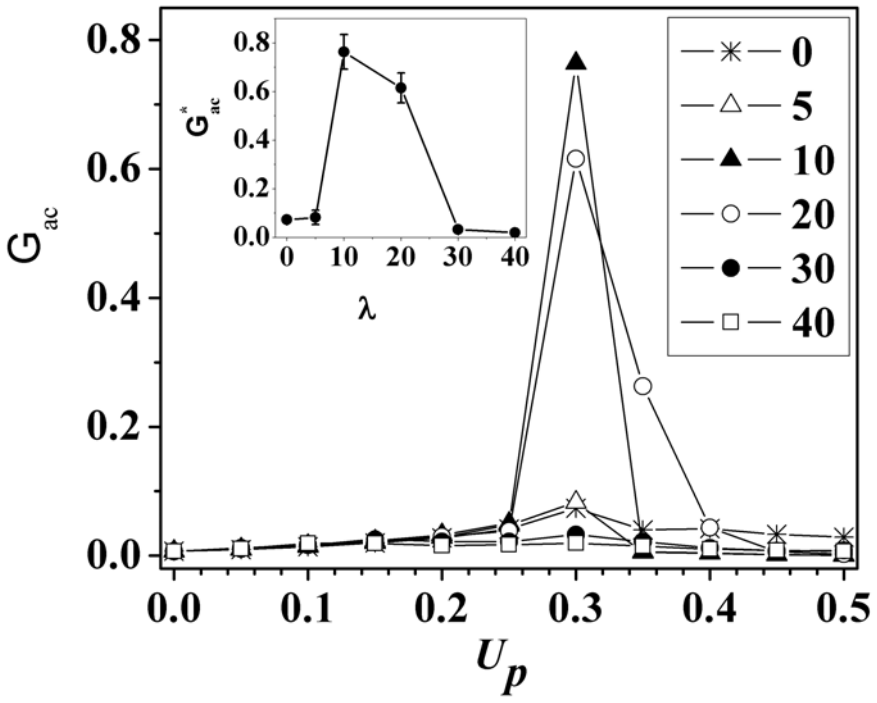

Figure 5.14: Fluctuations in additive-crystalline monomer pair distribution function at r = 1, as a function of U_p for additivated system (λ = 0, 5, 10, 20, 30 and 40 with additive concentration = 1.67%). The inset shows the change in the peak value of the fluctuations with λ. The lines joining the points are meant only as a guide to the eye.

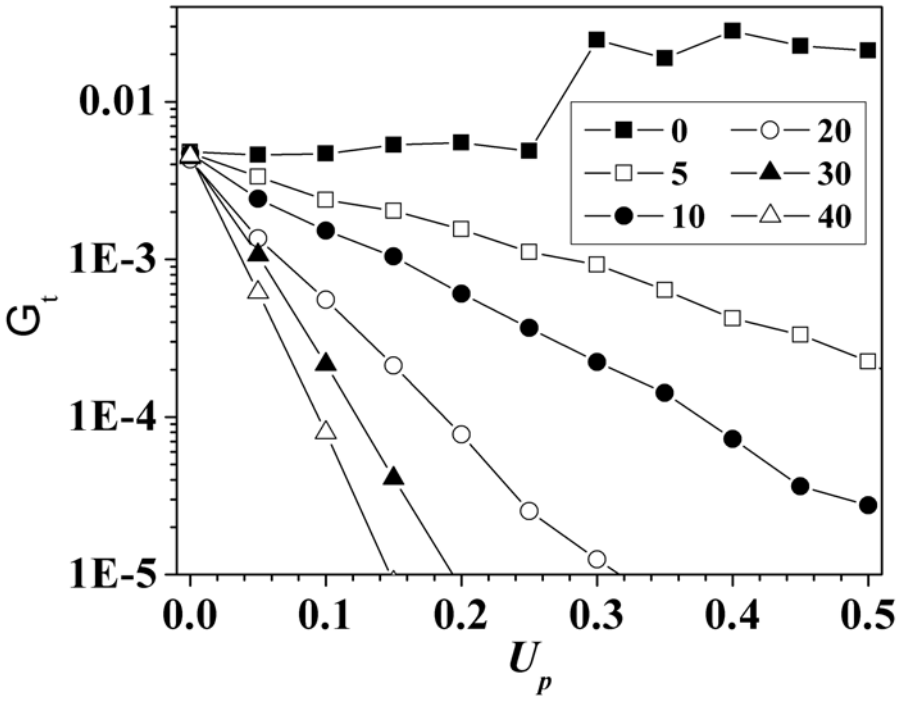

Figure 5.15: Mean square fluctuations in additive-monomer pair distribution function at r = 1, as a function of U_p for additivated (λ = 0, 5, 10, 20, 30 and 40; additive concentration = 1.67%) system. The lines joining the points are meant only as a guide to the eye.

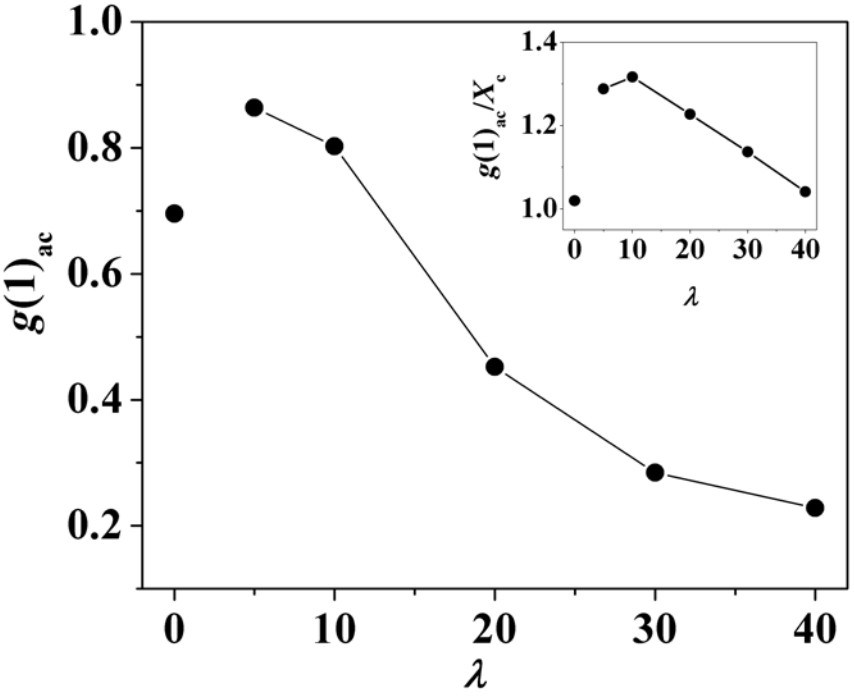

Figure 5.16: Change in average number of additive-crystalline monomer pair distribution function at r = 1, $g(1)_{ac}$ as a function of λ at U_p = 0.3, additive concentration = 1.67%. Error bars for $g(1)_{ac}$ are comparable to the size of the symbol. The ratio of $g(1)_{ac}$ to X_c is shown in the inset. The lines joining the points are meant only as a guide to the eye.

5.3.5. Isothermal Crystallization

On quenching the polymer from the athermal state ($U_p = 0$) to $U_p > 0.3$, its crystallinity builds up as a function of MCS. We observe the development of crystallinity for 2.5×10^5 MC steps for all values of λ and for H, on quenching to $U_p = 0.5$ (Figure 5.17a, b). We examine the crystallinity, X_c (Figure 5.17a) and the scaled crystallinity, $\frac{X_c - X_c^0}{X_c^\infty - X_c^0}$, that ranges from 0 to 1 (Figure 5.17b), to contrast the evolution of crystallinity at various λ. X_c^0 represents the crystallinity at the beginning of the annealing run while X_c^∞ is the crystallinity at the end of isothermal annealing (i.e., X_c at the end of 2.5×10^5 MC steps).

We observe that the scaled crystallinity evolves in the same manner for unadditivated polymer as well as for additivated polymer with low ($\lambda \leq 5$) and high ($\lambda \geq 30$) values of λ. For each of these systems, the evolution of the scaled crystallinity superposes, and follows the classical S-shaped Avrami-like increase with MCS. However, at intermediate λ (= 10, 20) wherein non-isothermal experiments showed anomalously large energy fluctuations, we observe an unusual two-stage increase in crystallinity. Thus, the evolution of crystallinity in an isothermal experiment is dramatically different for intermediate values of λ. This unusual behavior correlates with the anomalous increase in fluctuations at the phase transition for intermediate λ.

5.3.6. Influence of Additive Concentration

Finally, we describe the effect of additive concentration on crystallization. Results for simulations at different additive concentrations (viz. x = 0.42, 0.83, 3.125 and 6.25%), are presented in Figure 5.18. Here, the ratio of additive units to polymer chains varies from 0.27

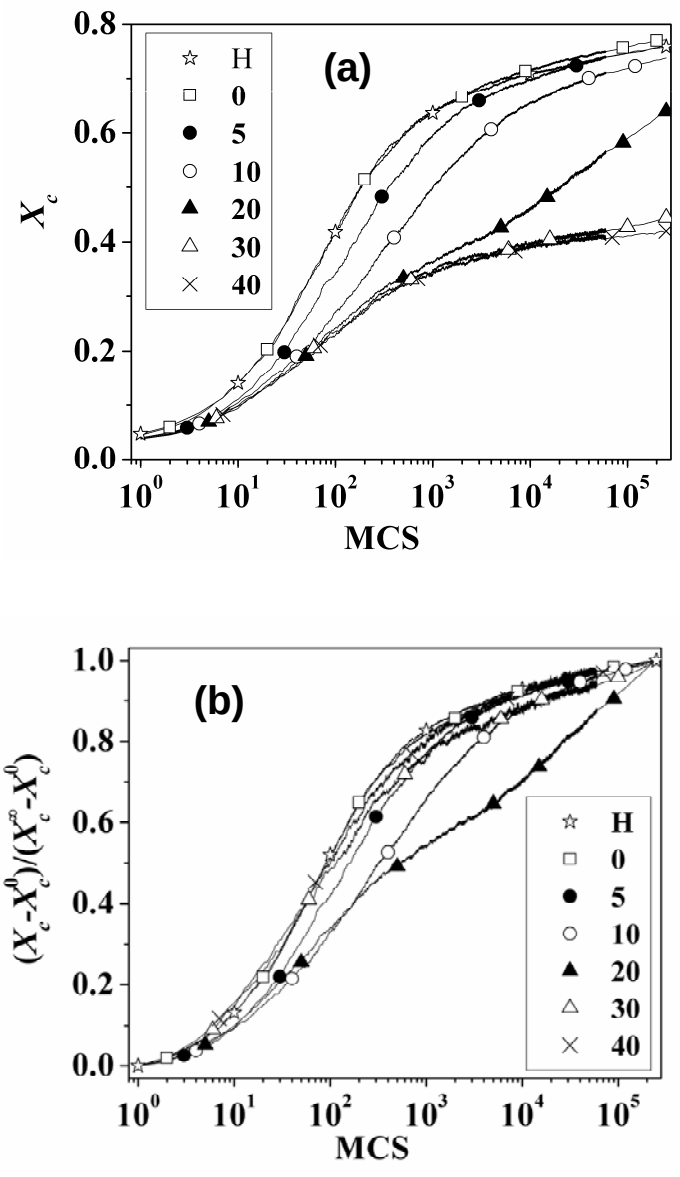

Figure 5.17: Change in the (a) crystallinity and (b) normalized crystallinity with number of MCS for unadditivated (H) and additivated polymer (with additive concentration = 1.67%) for a quench depth, U_p^q = 0.50. Limited number of data points shown by symbols in the trajectory, are meant as a guide to the eye.

(x = 0.42%) by over an order of magnitude to 4.27 (x = 6.25%). However, the evolution in crystallinity shows qualitatively similar trends for all values of x. At each x, there is a decrease in X_c^{sat} with increase in λ. This decrease is more pronounced at higher additive loadings (compare Figure 5.18 a, b, c and d at a fixed value of λ). At x = 0.42% and 0.83% (Figure 5.18a and 5.18b, respectively), appreciable change in crystallinity is observed only for $\lambda > 30$ and, even at $\lambda = 40$, X_c^{sat} decreases only to around 0.6 (compare with 0.77 for an unadditivated system). For increased additive fraction, x = 3.125% (Figure 5.18c), we observe a decrease in crystallinity even at λ = 10, and at x = 6.25% (Figure 5.18d) we observe that X_c^{sat} decreases even for $\lambda = 5$. The X_c^{sat} at $\lambda = 40$, decreases to around 0.23 for x = 3.125% and to around 0.1 for x = 6.25%.

Thus, as might be anticipated, crystallization in the presence of sticky additives is governed both by the loading (x) as well as the magnitude of stickiness, λ. This is clearly observed in a plot of X_c^{sat} as a function of additive loading, x for all λ (Figure 5.19). At low value of λ, X_c^{sat} is only weakly dependent on x (compare λ = 0, 5; Figure 5.19). Interestingly, for high λ (= 30, 40), X_c^{sat} depends only on x, and is almost independent of λ. Thus, the effect of the additive on crystallization, saturates beyond a threshold value of stickiness, and X_c becomes dependent only on x. Since the monomer-additive interaction is a short-range contact interaction, it is reasonable to expect that its effect saturates beyond a threshold value of λ, and any further increase in the value of λ produces no further change in the crystallization.

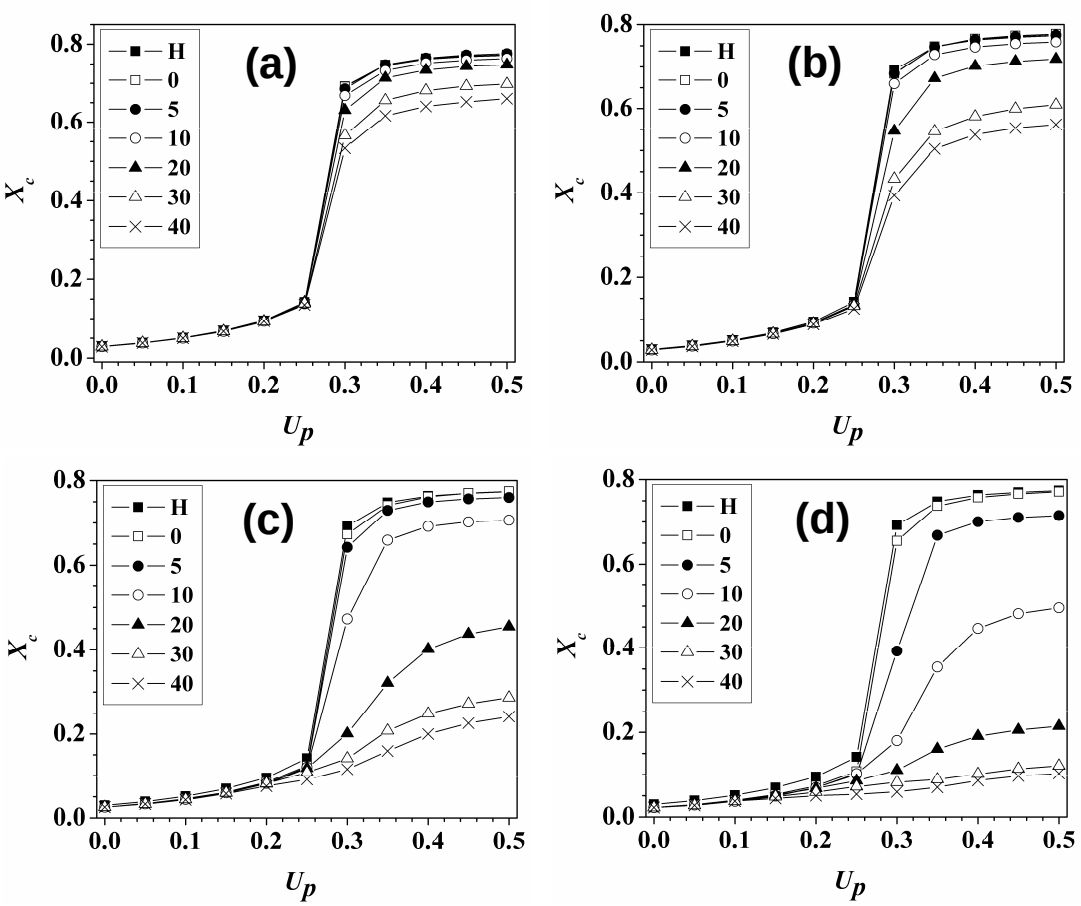

Figure 5.18: Change in crystallinity with U_p for unadditivated (H) and additivated (λ = 0, 5, 10, 20, 30 and 40;additive concentration = 1.67%) systems for varying additive loading, (a) 0.42, (b) 0.83, (c) 3.125 and (d) 6.25% respectively.

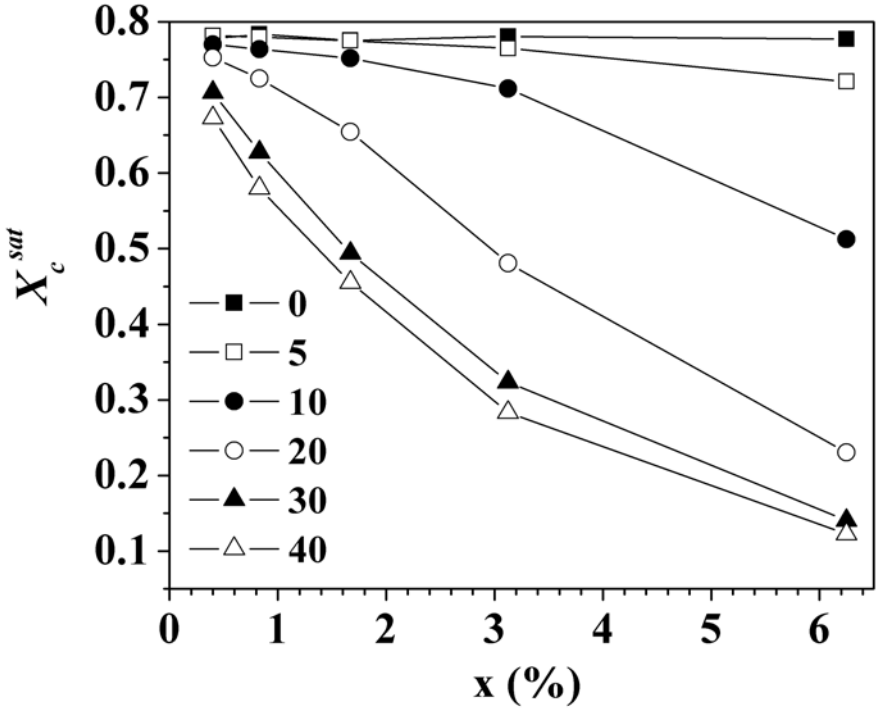

Figure 5.19: Change in saturated crystallinity, X_c^{sat} with additive loading, x for λ = 0, 5, 10, 20, 30 and, 40. The lines joining the points are meant only as a guide to the eye.

5.4. Summary

We describe the influence of "sticky" additives on the crystallization of a polymer melt. In our simulations, the attractive monomer-additive interaction results in dispersion of the additive in the polymer melt. An increase in additive loading, or in the stickiness at a given loading, results in a decrease in the crystallinity and in crystallite dimensions. We believe that the effect of the additives arises from a decrease in polymer melt diffusivity due to attractive monomer-additive interactions. At low additive loading of additives (~1 additive per 4 polymer chains) and at low additive stickiness, there is very little influence of the additive on crystallization. When the additives are very sticky, crystallization of monomers in the vicinity of the additives is highly inhibited. However, the effects of the additive, saturate above a threshold stickiness, and are then a function only of the loading.

The most interesting effect that we observe, is an anomalous increase in energy fluctuations at the phase transition for intermediate values of additive stickiness. These fluctuations correlate with monomers in the vicinity of the additive, undergoing a large interchange between crystal and amorphous states. This change in the route to crystallization dramatically influences the kinetics of crystal growth in isothermal crystallization experiments. At intermediate λ, the polymer no longer exhibits the classical Avrami-like S-shaped growth in crystallinity – rather, its approach to X_c^{∞} is slow, and appears to happen in two stages.

Our understanding of how "sticky" additives influence polymer crystallization might be used to design new "composite" materials with tailored crystallization kinetics, to optimize structure development during processing. For example, it might be interesting to systematically change the hydrogen bonding ability of additives (say, by comparing the influence of primary, secondary and tertiary amine surfactants) and to investigate the influence of these additives on the crystallization of polar polymers such as polyamides or

polyesters. There is little experimental literature on such systematic investigations, and our results suggest a potentially useful avenue for exploration. We believe that such studies might also be relevant in the case of more complex systems such as polymer nanocomposites, wherein attractive interactions are engineered between nanoparticulate additives and the matrix polymer.

References

(1) Mascia, L. *The role of additives in plastics*; Edward Arnold Publishers Ltd.: London, 1974.

(2) Anderson, S. L.; Grulke, E. A.; DeLassus, P. T.; Smith, P. B.; Kocher, C. W.; Landes, B. G. *Macromolecules* **1995**, *28*, 2944-2954.

(3) Maeda, Y.; Paul, D. R. *J. Polym. Sci. Part B: Polym. Phys.* **1987**, *25*, 1005-1016.

(4) Casalini, R.; Ngai, K. L.; Robertson, C. G.; Roland, C. M. *J. Polym. Sci. Part B: Polym. Phys.* **2000**, *38*, 1841-1847.

(5) Don, T.-M.; Bell, J. P.; Narkis, M. *Polym. Engg. Sci.* **1996**, *36*, 2601-2613.

(6) Perepechko, I. I.; Yakovenko, S. S. *Polymer Science U. S. S. R* **1981**, *23*, 1301-1306.

(7) Duda, J. L.; Rmdhane, I. H.; Danner, R. P. *J. Non-Cryst. Solids* **1994**, *172-174*, 715-720.

(8) Guerrero, S. J. *Macromolecules* **1989**, *22*, 3480-3485.

(9) Heux, L.; Lauprêtre, F.; Halary, J. L.; Monnerie, L. *Polymer* **1998**, *39*, 1269-1278.

(10) Lourdin, D.; Bizot, H.; Colonna, P. *J. Appl. Polym. Sci.* **1997**, *63*, 1047-1053.

(11) Ngai, K. L.; Rendell, R. W.; Yee, R. F.; Plazek, D. J. *Macromolecules* **1991**, *24*, 61-67.

(12) Rana, D.; Sauvant, V.; Halary, J. L. *J. Mater. Sci.* **2002**, *37*, 5267-5274.

(13) Soong, S. Y.; Cohen, R. E.; Boyce, M. C.; Chen, W. *Polymer* **2008**, *49*, 1440-1443.

(14) Steger, T. R.; Schaefer, J.; Stejskal, E. O.; McKay, R. A. *Macromolecules* **1980**, *13*, 1127-1132.

(15) Ueda, M. *Polym. Engg. Sci.* **2004**, *44*, 1877-1884.

(16) Riggleman, R. A.; Douglas, J. F.; de Pablo, J. J. *J. Chem. Phys.* **2007**, *126*, 234903-1-234903-10.

(17) Grassberger, P. *Phys. Rev. E* **1997**, *56*, 3682-3693.

(18) Siepmann, J. I.; Frenkel, D. *Molec. Phys.* **1992**, *75*, 59-70.

(19) Karaiskos, E.; deJoannis, J.; Anastasiadis, S. H.; Bitsanis, I. A. *Macromol. Theory Simul.* **2004**, *13*, 762-770.

(20) Houdayer, J. *J. Chem. Phys.* **2002**, *116*, 1783-1787.

(21) Pakula, T. *Macromolecules* **1987**, *20*, 679-682.

(22) Pakula, T.; Geyler, S. *Macromolecules* **1987**, *20*, 2909-2914.

(23) Binder, K.; Paul, W. *J. Polym. Sci. Part B: Polym. Phys.* **1997**, *35*, 1-35.

(24) Kremer, K.; Binder, K. *Comput. Phys. Rep.* **1988**, *7*, 259-310.

(25) Carmesin, I.; Kremer, K. *Macromolecules* **1988**, *21*, 2819-2823.

(26) Binder, K.; Paul, W. *Macromolecules* **2008**, *41*, 4537-4550.

(27) Hu, W. *J. Chem. Phys.* **2000**, *113*, 3901-3908.

(28) Hu, W. *J. Chem. Phys.* **1998**, *109*, 3686-3690.

(29) Hu, W.; Mathot, V. B. F.; Frenkel, D. *Macromolecules* **2003**, *36*, 2165-2175.

(30) Dasmahapatra, A. K.; Kumaraswamy, G.; Nanavati, H. *Macromolecules* **2006**, *39*, 9621-9629.

(31) Nishimura, Takuji; Matsumoto, Makoto *http://www. math. sci. hiroshima-u. ac. jp/~m-mat/MT/emt. html* **2002**.

(32) Shaffer, J. S. *J. Chem. Phys.* **1994**, *101*, 4205-4213.

(33) Shaffer, J. S. *J. Chem. Phys.* **1995**, *103*, 761-772.

(34) Madras, N.; Sokal, A. D. *J. Stat. Phys.* **1987**, *47*, 573-595.

(35) Metropolis, N.; Rosenbluth, A. W.; Rosenbluth, M. N.; Teller, A. H.; Teller, E. *J. Chem. Phys.* **1953**, *21*, 1087-1092.

(36) Cowie, J. M. G. *Polymers: Chemistry and Physics of Modern Materials*; Nelson Thornes: Cheltenham, Gloucestershire, U.K., 2001.

(37) Hu, W.; Frenkel, D. *Adv. Polym. Sci.* **2005**, *191*, 1-35.

(38) Auhl, R.; Everaers, R.; Grest, G. S.; Kremer, K.; Plimpton, S. J. *J. Chem. Phys.* **2003**, *119*, 12718-12728.

(39) Goodstein, D. L. *States of Matter*; Dover Publications, Inc.: New York, 1985.

(40) Hu, W. *J. Chem. Phys.* **2001**, *115*, 4395-4401.

(41) Hu, W.; Frenkel, D.; Mathot, V. B. F. *Macromolecules* **2003**, *36*, 549-552.

(42) Alizadeh, A.; Richardson, L.; Xu, J.; McCartney, S.; Marand, H.; Cheung, Y. W.; Chum, S. *Macromolecules* **1999**, *32*, 6221-6235.

Chapter 6

Understanding Polymer Nucleation by Weighted Histogram Analysis Method

6.1. Introduction

Nucleation is a process by which a new phase appears in a matrix of the old, through the formation of small "nuclei". The difference in the bulk free energy between the new phase and the old, drives the transformation into the new phase (this contribution to the free energy is proportional to the volume of the nucleus); however, the creation of an interface between the old and new phases, destabilizes the nucleus (this contribution to the free energy scales with the surface area of the nucleus). Thus, the free energy for the formation of a spherical nucleus, is given by: $\Delta G = \frac{4}{3}\pi R^3 \rho \Delta\mu + 4\pi R^2 \gamma$, where, ρ is the molar density of the liquid phase, $\Delta\mu$ is the difference in chemical potential between two phases (liquid and solid), γ is the surface free energy, and R is the radius of the nucleus. For transitions to a more stable phase, the first term in the equation, is negative (lowering of free energy) while the second term is positive. Thus, the net free energy, passes through a maximum, as a function of size of the nucleus. The size at which the free energy shows a maximum,

corresponds to the critical nucleus. Entities smaller than the critical nucleus size are unstable, and dissolve into the matrix, while only nuclei that are larger than the critical nucleus grow. The size of the critical nucleus is given by $R^* = \frac{2\gamma}{\rho\Delta\mu}$, and the corresponding critical free energy, $\Delta G^* = \frac{16\gamma^3}{3(\rho\Delta\mu)^2}$. The size and the rate of formation of critical nuclei, depend on the degree of supercooling (liquid-solid phase transition) or superheating (liquid-vapor phase transition). The rate of the nucleation also depends on the position of the liquid-liquid phase boundary, which can be achieved by adding suitable a additive (cf. precipitator). Galkin et al.[1] have shown that although the rate of protein crystal nucleation, can be suppressed with the addition of glycerol, it can be enhanced by adding poly(ethylene glycol). Accordingly, the free energy barrier for the nucleation varies. As reported in the literature[2,3] the typical energy barrier associated in the nucleation, in an experiment[4] (nucleation of liquid mercury), is in the range of 75 kT and the probability of finding a nucleus at the top of the energy barrier[2], is of the order of 10^{-12} per cm^3. Once the system is at the top of the barrier, it can rapidly proceed either to the new phase, or return to the old phase. Typically, the time spent at the top of the barrier is of the order of microseconds[5]or less[2]. Therefore, nucleation is a rapid event, and nuclei are transient species, difficult to observe.

Nucleation is not only an important research topic of academic interest, but also equally important to several applications. Understanding of nucleation, is useful in various important fields, such as atmospheric science[6,7], materials science[8] and biological sciences[1]. Formation of water droplets and ice crystals in the atmosphere, is governed by nucleation, and they have a pronounced effect on weather and climate[6,7]. In materials processing, material morphology can be tailored by varying the degree of super cooling. For example, when gallium melt is cooled to around -75ºC, a stable α phase is nucleated, but on further supercooling, four different metastable phases (β, γ, δ and ε), can be formed[8]. Nucleation is

also important in the crystallization of biomolecules, such as proteins[1], to understand the possible ways to enhance or suppress the rate of protein nucleation, which is important in protein separation and diseases related to protein aggreagate formation.

Investigating nucleation, either experimentally or via computer simulation is very difficult. In experiments, in most cases, nucleation is heterogeneous, i.e., it is assisted by the presence of small amount of impurities, while, in computer simulation, one usually studies homogeneous nucleation. The influence of impurities on the nucleation of a colloidal system is relatively small and the nucleation can be considered to be homogeneous. Recent progress in experimental techniques, such as real space imaging with laser scanning confocal microscopy on model colloidal systems[9], has resulted in significant advances in our ability to study nucleation. There are several methods being used in computer simulation to study nucleation. These are Umbrella Sampling (US), Forward Flux Sampling (FFS), Transition Path Sampling (TPS) and Weighted Histogram Analysis Method (WHAM). While the first three methods improve the sampling of the rare conformations in the simulation ensemble, WHAM works on data obtained from NVT equilibrium simulation with Metropolis sampling. In WHAM, free energy for nucleation is estimated from the density of states (DOS) for the parameter range under consideration.

WHAM was originally developed by Ferrenberg and Swendsen[10,11] and is based on the use of multiple histograms generated from NVT simulation. A histogram is essentially a probability distribution of the total energy of the system. In the multiple histogram technique, many single histograms at different parameters are combined to form a single histogram. It has been employed in various investigations to determine the free energy across a range of parameters. For example, Kumar and co-workers[12] have applied WHAM to estimate the potential of mean force of the pseudo-rotation phase angle of the sugar ring in deoxyadenosine. It has also been implemented in many other investigations such as,

estimating the energy landscape for ligand-protein binding energy[13], to generate free energy profiles for the conformational transition of protein molecules[14], to estimate surface tension by calculating surface free energy[15], to calculate the chain elasticity and free energy profile for polyethylene chain[16], etc. WHAM has also been used in combination with other simulation tools to extend the applicability of the tools to a wider parameter space. For example, Gallicchio and co-workers[17] combined replica exchange MD simulation with WHAM to estimate the potential of mean force for a peptide molecule. Chodera and Dill[18]have combined parallel tempering and simulated annealing with WHAM, to estimate the potential of mean force for alanine dipeptide in both, implicit and explicit solvent condition. Chen et al.[19] combined WHAM with aggregation-volume-biased Monte Carlo and adaptive umbrella sampling, to study the vapor-liquid water nucleation over the temperature range, 200K to 300K.

Most of the simulation methods discussed earlier have been applied to non-polymeric system, such as crystallization in colloidal systems.[3,20] Study of the nucleation in polymer crystallization is itself challenging, since crystallization in polymers typically happens far from equilibrium, due to constraints imposed by the covalent connectivity between monomers. Here, we report the first attempt to study nucleation in polymer melt crystallization using WHAM. Since WHAM has primarily been implemented on data from NVT simulations, and since our simulation system is based on an NVT ensemble, we expect our system to be well-suited for application of WHAM, rather than applying other methods that require a change in simulation methodology (such as TPS, FFS etc.). The objective here is to determine whether the WHAM can be successfully applied to study nucleation in polymer crystallization.

We organize this chapter as follows: in the section 6.2, we describe the principle of WHAM; subsequently, we describe the results we have obtained for our system in the section

6.3, and finally, we summarize and describe the applicability limitation of this method, with respect to polymer crystallization, in section 6.4.

6.2. Model and Simulation Technique

We use a dynamic Monte Carlo (DMC) algorithm to simulate polymer melt crystallization. Our simulation system contains 480 chains, each comprising 64 monomeric repeat units, placed in a cubic lattice of size 32^3, with periodic boundary conditions. We employ a micro-relaxation algorithm, viz. a combination of single site bond fluctuation and slithering diffusion to move the chain units along the lattice sites with.[21,22] The success of the attempted moves is governed by the Metropolis[23] scheme with a probability, $p = \exp(-\beta\Delta E)$, where ΔE is the change of energy for the transition from the old to new conformation, $\beta = 1/kT$, k is the Boltzmann constant and T is the absolute temperature. The change in energy, ΔE, for a move in our simulation is calculated as: $\Delta E/kT = \Delta N_p U_p + \Delta N_c U_c$, where, ΔN_p, and ΔN_c are the net changes in the numbers of contacts of non-bonded parallel bonds and collinear bonds, respectively; U_p and U_c, are the energies (normalized by kT) for a pair of non-bonded parallel bonds and collinear bonds, respectively and we assume $U_c/U_p = 1$.

We generate the initial structure as follows: chains are placed on the lattice in a regular fashion and the simulation is run at U_p = 0, to generate an athermal melt. Subsequently, we cool the melt down to U_p = 0.15 by increasing U_p in steps of 0.01. The melt state at U_p = 0.15, forms the starting point for our study. In the present study, we present simulation data for U_p between 0.15 to 0.245, and cool the melt in steps of ΔU_p = 0.001. This is done to ensure that the histogram describing the energy distribution at any U_p, has an appreciable overlap with those at higher and lower U_p values. Significant overlap

with neighboring histograms, is a necessary condition for successful implementation of WHAM, since this ensures that all energy states spanned in our simulations, are sampled adequately to generate the accurate density of states. Ideally, the combined histogram obtaining by combining histograms from all the simulations, should be flat. This flat energy histogram, ensures that all the energy states within the temperature range, are sampled with equal probability. At each U_p, we equilibrate the sample for 6×10^4 MCS, and data are obtained by running for another 4×10^4 MCS.

We describe here the construction of a histogram over U_p value range from 0.15 to 0.245. First, we provide the rationale behind the selection of the U_p range. To estimate the free energy during nucleation, the temperature range should span from the melt to the crystalline state. This is possible by estimating the equilibrium melting temperature. Ideally, a polymer melt will crystallize at any temperature below the equilibrium melting temperature, on annealing for a long enough time. Therefore, the knowledge of equilibrium melting point is essential. We have estimated the possible value of U_p, corresponding to the equilibrium melting point, U_{pm}^{∞}, by simulating in the presence of an existing crystal. We artificially put a large crystal of dimension 16×8×16, in the simulation box. We equilibrate the sample at U_p = 0, keeping the chains of this crystal intact (viz., no MC move is attempted for these chains). After equilibration, we quench the sample to different values of U_p^q, and this time, all the chains are subjected to moves. At U_p^q, we estimate the crystallinity, after annealing the sample for 2.5×10^5 MCS. We observe that the existing crystal begins growing at U_p = 0.18, but melts at 0.17. Hence, the equilibrium melting point lies within the range of U_p = 0.17 to 0.18. The temperature range we have covered for the WHAM study, therefore spans over the melt and the crystalline phases.

We now describe the implementation details of WHAM to study nucleation. Specifically, we are interested in estimating the free energy barrier for the nucleation and the critical nucleus size. We now describe the principle of WHAM and explore the possibility of using WHAM to study crystal nucleation in a polymer melt. As already mentioned in the introduction, the sampling probability for energy states at the top of the nucleation barrier is very low and thus, reweighting by combining multiple histograms, improves the sampling probability of those conformations at the top of the barrier. From the combined histogram, we estimate the density of states (DOS), as described later in this section. Once we have the DOS, we can calculate any thermodynamic property of the system for a wide range of parameters. From the free energy profile spanning from melt to crystal state, we can predict the states of the system corresponding to the critical nucleus, the incipient of crystallization.

The implementation of WHAM for our homopolymer melt system, is as follows. At each U_p, we generate a histogram based on 4×10^4 conformations, as mentioned earlier. We construct a histogram, $H(E)$, based on the scaled total energy (E) of the system, where the energy (scaled by U_p) is defined as $E = N_p + N_c$, where N_p and N_c represent the total number of parallel and collinear bond contacts, respectively. The combined histogram includes 96 histograms, one at each U_p from 0.15 to 0.245 in steps of 0.001. The method of estimation of DOS is described as follows[11,12]:

From the energy histograms, $H(E)$, the probability of finding a system at β, at the energy state E, is given by[11,12]:

$$P(E,\beta) = \frac{\sum_{n=1}^{R} g_n^{-1} H_n(E) \exp[\beta E]}{\sum_{m=1}^{R} N_m g_m^{-1} \exp[\beta_m E - f_m]}, \quad \text{.....(1)}$$

where N_m is the number of conformations sampled at the *m*-th simulation; g_m represents the statistical inefficiency, and is related to the correlation time*, τ_m, for the *m*-th simulation. If all the successive conformations sampled for the histogram, are independent, $g_m = 1$, otherwise, $g_m = 1 + 2\tau_m$; f_m is the parameter equal to the free energy at β_m, for the *m*-th simulation; *R* is total number of NVT simulations performed. The probability, $P(E, \beta)$, and free energy, f_m, are related by the following relation:

$$\exp[f_m] = \sum_E P(E, \beta_m) \quad \text{.....(2)}$$

Thus, equations 1 and 2 need to be solved self-consistently, to obtain the free energy values, f_m. The density of states is then calculated from the following expression:

$$\Omega(E) = \frac{\sum_{n=1}^{R} g_n^{-1} H_n(E)}{\sum_{m=1}^{R} N_m g_m^{-1}(E) \exp[\beta_m E - f_m]} \quad \text{.....(3)}$$

and the average quantity of an observable, *A*, is then calculated as

$$\langle A \rangle_\beta = \frac{\int A(E)\Omega(E)\exp[-\beta E]dE}{\int \Omega(E)\exp[-\beta E]dE} \quad \text{.....(4)}$$

* Correlation time, τ, is the time integral of correlation function, $C(\tau)$. The correlation function describes how an observable parameter, *A*, at time *t*, *A*(*t*), is related to its value at time $(t + \tau)$. Mathematically, $C(\tau)$ is expressed as: $C(\tau) = \left\langle \left(A(t+\tau) - A(t)\right)^2 \right\rangle$. $C(\tau)$ approaches 0, for uncorrelated values of *A*.

From the DOS, we obtain the partition function, *Z*, as:

$$Z = \sum_{\{E\}} \Omega(E) \exp(-\beta E) \quad \text{.....(5)}$$

Using the partition function, we can calculate the Helmholtz free energy as a function of U_p

$$F(\beta) = -kT \ln(Z) \quad \text{.....(6)}$$

Thus, we obtain the free energy as a function of the energy state as:

$$F(E) = -kT \ln[\Omega(E)] \exp(-\beta E) \quad \text{.....(7)}$$

For studying nucleation, we need to estimate the critical nucleus size and the energy barrier for the nucleation, viz. we require the dependence of the free energy on the nucleus size. In our simulations, we have noted that the total energy of the system, increases proportionally with the average crystallite size (*S*). Thus, from the obtained relationship, *F*(*E*) vs. *E*, we can relate the average energy of the system to the average nucleus size, *S*, and thus, are able to transform our data to *F*(*S*) vs. *S*.

To monitor the phase transition from a disordered molten state to an ordered crystalline state, we calculate the fractional crystallinity, X_c, as a function of U_p for the U_p range 0.15 to 0.245. We arbitrarily define a bond as crystalline, if it is surrounded by more than five nearest non-bonded parallel bonds, in a manner similar to the work reported by Hu

and Frenkel[24]. Crystallinity is defined as the ratio of the number of crystalline bonds, to the total number of bonds in the system.

6.3. Results and Discussions

Our simulations as the polymer is cooled from U_p from 0.15 to 0.245, in steps of ΔU_p = 0.001, are used to generate 96 energy histograms. We have determined that these histograms have significant overlap in energies, and, are therefore, suitable for combination to generate the DOS using WHAM. Since it is difficult to present all 96 histograms in one figure, we group the data and present combined histograms for U_p = 0.15 to 0.157; 0.158 to 0.165 and so on, until U_p = 0.238 to 0.245 in Figure 6.1. We observe that the combined histogram for the U_p range from 0.15 to 0.245 shows a monotonic decrease with lower frequency of higher energy states – thus, the combined histogram is not flat (Figure 6.2).

After having the combined histogram, we use equations 1 and 2 self consistently, taking g_m = 1[*], to obtain the values of free energies for each U_p value, and then, using these free energies, we calculate the DOS and average properties (in this case average *E*). Direct implementation of WHAM, poses numerical problems - we were unable to calculate the free energies since the large values of E in our simulations led to numerical overflow. However, we were able to implement WHAM on smaller U_p ranges, such as 0.15 to 0.159, where, the energies span a relatively smaller range. Thus, we have directly implemented WHAM on small sub-ranges of U_p, have successfully solved the WHAM equations, and have demonstrated that the average values of *E* from our calculations, match the values directly obtained from simulation.

[*] We sample the conformation at the end of each MCS. One MCS involves 480×64 numbers of MC moves. Each MC move represents one conformation. Thus, conformation sampled at intervals of 480×64 moves, can be treated as statistically independent, and we can use g_m =1.

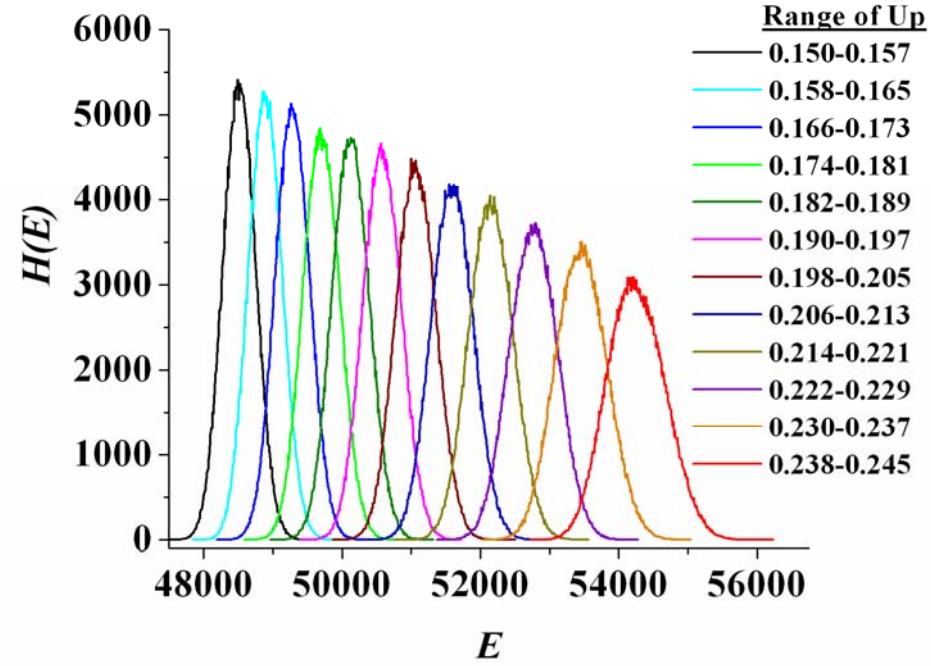

Figure 6.1: Energy histogram *H*(*E*), for U_p ranges from 0.15 to 0.245. Each histogram represents a combined histogram for the U_p range specified in the graph.

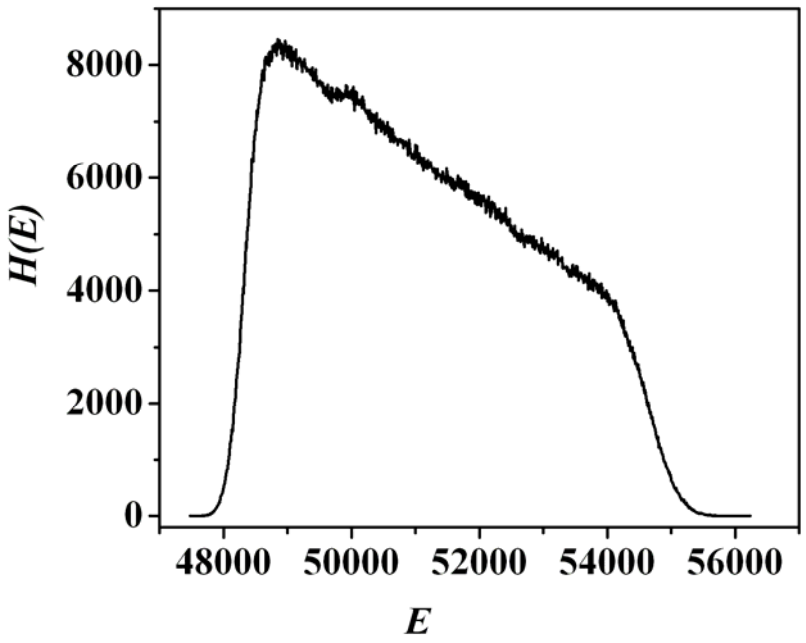

Figure 6.2: Combined histogram for the U_p ranges from 0.15 to 0.245.

In a similar fashion to that described earlier, we have applied the WHAM equations in small subranges of U_p, and have split the entire U_p range into smaller subranges (0.15 – 0.159; 0.155 – 0.164; 0.16 – 0.169, etc.), such that there is appreciable overlap in energy histograms. We have estimated the free energies for each U_p value. In Figure 6.3, we observe that the free energy decreases monotonically with increase in U_p, without appreciable change in slope. This indicates that our simulations from 0.15 to 0.245, only span the melt state and a transition to the crystalline state, is not observed in our simulations.

In our canonical simulations where the melt is cooled in steps of 0.01, we observe a gradual increase in crystallinity until U_p = 0.3, followed by an abrupt increase, indicating the onset of rapid crystallization. The gradual increase in crystallinity observed at U_p less than 0.3, is suggestive of ordering in the melt, driven by the tendency of the bonds to orient collinearly and to pack parallel to each other. Our definition of crystallinity is arbitrary –we define a crystalline bond as one with more than 5 parallel nearest neighbors. We observe that the crystallinity smoothly increases from ~ 0.07 at U_p = 0.15 to ~ 0.14 at 0.245 (Figure 6.4). Therefore, the increase in "crystallinity" that we observe in our simulations might be indicative of conformational transitions in the melt, rather than of true crystal formation. There are experimental reports that describe the formation of helical organization in iPP[25,26] or an increase in the number of all-trans regions in PE, in the melt state, prior to crystallization[27,28].

Thus, the energy terms that drive bonds to arrange collinearly or parallel in our simulations reflect coarse-graining of the physically realistic interactions, that drive the organization observed experimentally. Accordingly, the gradual increase in crystallinity that we report in the simulations used for the WHAM calculations, might indicate the pre-

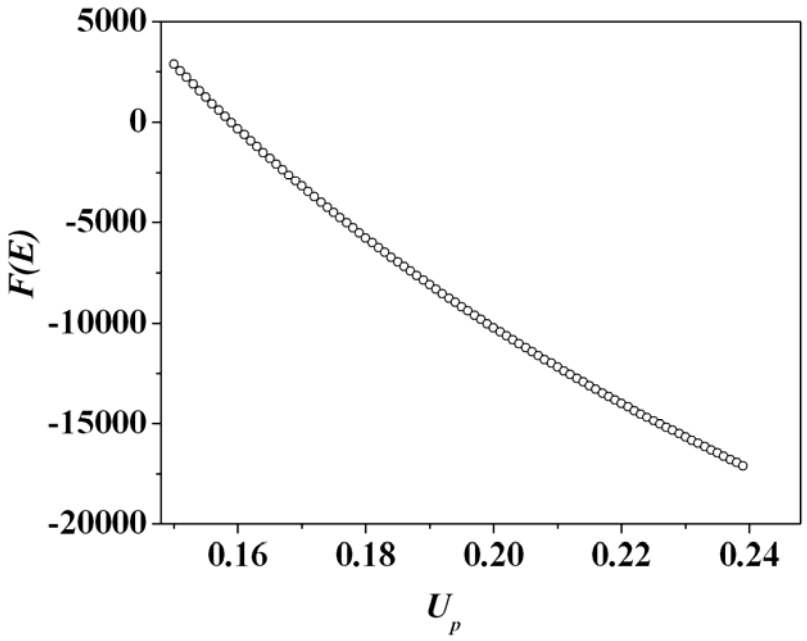

Figure 6.3: Change of free energy as a function of U_p.

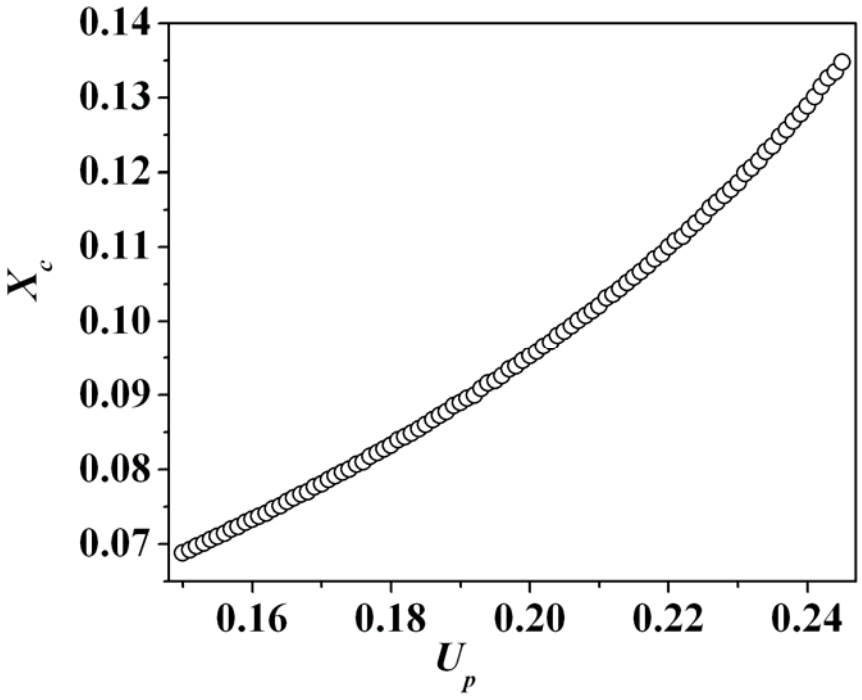

Figure 6.4: Change of crystallinity (X_c) with as a function of U_p

ordering in the melt state, and therefore, we do not observe a change in the slope of the free energy, as would be expected had the system transitioned to a crystalline state. This would also account for the shape of the combined histogram (Figure 6.1). The gradual decrease observed in the frequency of higher energy states might result from the ordering processes in the melt that precede crystallization.

It is commonly believed that equilibrium states are never achieved during polymer crystallization (for a recent, controversial equilibrium view of polymer crystallization, see the paper by Muthukumar[29]). In our simulations, we observe that the system evolves continuously as the polymer crystallizes, until a frozen non-equilibrium steady state is achieved. While, like in experiments, we obtain reproducible values of crystallinity on repeating simulations under similar conditions, it is clear that the final steady state obtained is a non-equilibrium state. While the Metropolis-DMC technique is strictly only applicable to equilibrium systems, the extension to investigate phenomena such as polymer crystallization has been reported earlier, and has been shown to accurately reproduce experimentally observed phenomena. Similarly, while WHAM is strictly valid only for systems at equilibrium, we believe that its extension to examine the initial stages of crystallization is appropriate.

As we have tried to span the region from the melt to the initial stages of crystallization in this work, we work at U_p values where the crystallinity values are modest. However, U_p = 0.245 is well above the U_{pm}^{∞} (viz. temperature is below T_m^{∞}) – therefore, when we run multiple simulations at this U_p, we observe that occasionally, a higher degree of crystallinity can form – viz. in some simulations, large crystalline domains form and we observe a wide range of system energies. We have carried out more than 20 independent simulations, and in some cases, the simulations yield crystallinity more than 0.5, which abruptly increases with MCS, while for others, the crystallinity is limited to ~ 0.15. However, in simulations where

we obtain high crystallinity, the system rapidly grows from the critical nuclei, and we are unable to obtain good statistics in sampling the energy states that represent the critical nuclei. Thus, as soon as the system reaches the transition point, it immediately crystallizes and spends very little time in the transition zone. Thus, very few conformations are sampled in the transition zone, and we are unable to construct a DOS distribution that adequately represents these states. The large difference in the energies between melt and crystal states, leads to a combined histogram with reasonably well sampled energy states in the melt and crystal regions, and poor sampling in between, in the transition zone (see, for example, Figure 6.5). The combined histogram taking into account the higher energy states at U_p = 0.245, is shown in Figure 6.5.

WHAM requires that conformations be sampled efficiently in the transition zone (where X_c ~ 0.2-0.25), viz. at crystallinities beyond the melt state. We have performed the simulation at U_p = 0 with the initial regularly folded arrangement, and have cooled the system until we achiev crystallinity ~ 0.14.

The system has now some existing crystalline domains which can initiate further crystallization, on application of sufficient degree of supercooling (viz. temperature below equilibrium melting point). We have examined the development of crystallinity at different supercoolings. At U_p < 0.18, we have observed that the crystallinity decreases continuously as the preformed crystal melts; while for $U_p \geq 18$, the crystal grows rapidly, and the crystallinity rapidly increases to 0.5. Thus, we are unable to achieve simulation conditions, where the system is maintained at a low, relatively constant value of crystallinity, so that the energy states are well sampled in the transition zone. Thus, the sampling of energy states near the transition zone, has been inadequate in our implementation.

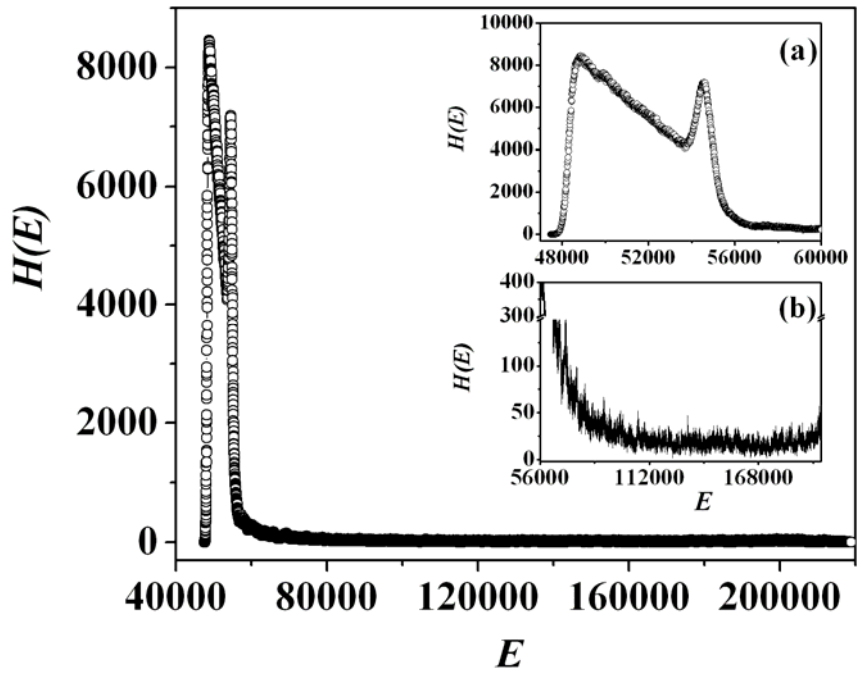

Figure 6.5: Combined histogram for the U_p ranges from 0.15 to 0.245 with higher energy states. Inset (a): histogram for the energy range from 48000 to 60000 and (b): histogram for the energy range from 56000 to 200000.

6.4. Summary

We have explored the applicability of WHAM to understand the nucleation in polymer crystallization. We have constructed energy histograms for U_p ranging from 0.15 to 0.245, with a step of 0.001. Thus, the combined histogram (Figure 6.2) is based the histograms from 96 NVT simulations. The energy values are too large to apply WHAM equations on the combined histogram. We have implemented WHAM by splitting the range of U_p into subzones, and have estimated the free energy as a function of U_p; and we observe a decrease in free energy as U_p increases. However, we have not observed the transition to the crystalline state in the U_p range investigated (see Figure 6.3). The abrupt transition from melt to crystal, makes it difficult to sample the conformations in the transition zone. On the other hand, there is pre-ordering in the melt state as temperature is reduced. Consequently, we do not obtain a flat histogram, even in the melt.

We infer that at this time, one cannot effectively implement WHAM, to address the problem of polymer nucleation, simultaneously keeping track of the large numbers occurring at the transition region. If we can overcome the difficulties in obtaining a flat histogram, then applying WHAM to the area of polymer nucleation will become feasible. A possible way to overcome this problem is to introduce a restraining potential, which will make the transition less abrupt and will allow sampling in the transition zone.

Additionally, in energy calculations, we have considered only parallel and collinear pair potentials and we observe an abrupt transition from the melt to the crystal state. A restraining potential could retain the system to evolve in the transition zone for a longer duration. For example, instead of U_c/U_p = 1 (see Modeling and Simulation Technique section), we can use a higher value. At higher values of U_c/U_p, the system will be reluctant to crystallize, because of the enhanced stiffness of the chain. Thus, by varying the value of

U_c/U_p, we can control the development of crystallinity and enhance sampling conformations in the transition zone.

An alternative way is to add small molecular "sticky" additives (described in detail in chapter 5) into the polymer melt. We have observed that the presence of "sticky" additives, makes the chain relatively less mobile, and gives rise to decreasing crystallinity as the value of stickiness parameter increases. Again, by varying the stickiness parameter, we can make the system spend more time in the energy states corresponding to the transition zone. Thus, we might obtain a flat histogram, enabling implementation of WHAM. Besides WHAM, in our future studies, we will also employ other techniques such as umbrella sampling, transition path sampling, Wang-Landau sampling and forward flux sampling, to study nucleation in polymer crystallization.

References

(1) Galkin, O.; Vekilov, P. G. *Proc. Natl. Acad. Sci. USA* **2000**, *97*, 6277-6281.

(2) ten Wolde, Pieter Rein *PhD Thesis* **1998,** University of Amsterdam, Amsterdam, The Netherlands,

(3) ten Wolde, P. R.; Ruiz-Montero, M. J.; Frenkel Daan. *Faraday Discuss.* **1996**, *104*, 93-110.

(4) Kelton, K. F., "Crystal Nucleation in Liquids and Glasses" in *Solid State Physics*, Ehrenreich, H. and Turnbull, D. (Eds.) Academic Press, Boston, **1991**, 45, 75-177

(5) Meldrum, F. C.; Sear, R. P. *Science* **2008**, *322*, 1802-1803.

(6) Kulmala, M.; Riipinen, I.; Sipilä, M.; Manninen, H. E.; Petäjä, T.; Junninen, H.; Maso, M. D.; Mordas, G.; Mirme, A.; Vana, M.; Hirsikko, A.; Laakso, L.; Harrison, R. M.; Hanson, I.; Leung, C.; Lehtinen, K. E. J.; Kerminen, V.-M. *Science* **2007**, *318*, 89-92.

(7) Sear, R. P. *Euro. Phys. Lett.* **2008**, *83*, 66002-1-66002-6.

(8) Teske, D.; Drumheller, J. E. *J. Phys. : Condens. Matter* **1999**, *11*, 4935-4940.

(9) Gasser, U.; Weeks, E. R.; Schofield, A.; Pusey, P. N.; Weitz, D. A. *Science* **2001**, *292*, 258-262.

(10) Ferrenberg, A. M.; Swendsen, R. H. *Phys. Rev. Lett.* **1988**, *61*, 2635-2638.

(11) Ferrenberg, A. M.; Swendsen, R. H. *Phys. Rev. Lett.* **1989**, *63*, 1195-1198.

(12) Kumar, S.; Bouzida, D.; Swendsen, R. H.; Kol lman, P. A.; Rosenberg, J. M. *J. Comp. Chem.* **1992**, *13*, 1011-1021.

(13) Bouzida, D.; Rejto, P. A.; Verkhivker, G. M. *Int J Quantum Chem* **1999**, *73*, 113-121.

(14) Castells, V.; Tassel, P. R. V. *J. Chem. Phys.* **2005**, *122*, 084707-1-084707-9.

(15) Ghoufi, A.; Goujon, F.; Lachet, V.; Malfreyt, P. *J. Chem. Phys.* **2008**, *128*, 154718-1-154718-12.

(16) Inda, M. A.; Frenkel, D. *Macromol. Theory Simul.* **2004**, *13*, 36-43.

(17) Gallicchio, E.; Andrec, M.; Felts, A. K.; Levy, R. M. *J. Phys. Chem. B* **2005**, *109*, 6722-6731.

(18) Chodera, J. D.; Swope, W. C.; Pitera, J. W.; Seok, C.; Dill, K. A. *J. Chem. Theory Comput.* **2007**, *3*, 26-41.

(19) Chen, B.; Siepmann, J. I.; Klein, M. L. *J. Phys. Chem. A* **2005**, *109*, 1137-1145.

(20) ten Wolde, P. R.; Ruiz-Montero, M. J.; Frenkel, D. *Phys. Rev. Lett.* **1995**, *75*, 2714-2717.

(21) Dasmahapatra, A. K.; Kumaraswamy, G.; Nanavati, H. *Macromolecules* **2006**, *39*, 9621-9629.

(22) Hu, W. *J. Chem. Phys.* **1998**, *109*, 3686-3690.

(23) Metropolis, N.; Rosenbluth, A. W.; Rosenbluth, M. N.; Teller, A. H.; Teller, E. *J. Chem. Phys.* **1953**, *21*, 1087-1092.

(24) Hu, W.; Mathot, V. B. F.; Frenkel, D. *Macromolecules* **2003**, *36*, 2165-2175.

(25) Chen, X.; Kumar, S. K.; Ozisik, R. *J. Polym. Sci. Part B: Polym. Phys.* **2006**, *44*, 3453-3460.

(26) Chen, X.; Ozisik, R.; Kumar, S. K.; Choi, P. *J. Polym. Sci. Part B: Polym. Phys.* **2007**, *45*, 3349-3360.

(27) Kavassalis, T. A.; Sundararajan, P. R. *Macromolecules* **1993**, *26*, 4144-4150.

(28) Zhang, X.; Li, Z.; Lu, Z.; Sun, C.-C. *Polymer* **2002**, *43*, 3223-3227.

(29) Muthukumar, M. *Phil. Trans. R. Soc. Lond. A* **2003**, *361*, 539-556.

Chapter 7

Conclusions and Future Scope

7.1. Summary and Conclusions

In this thesis, we have examined some aspects of phase transitions in polymeric system in the presence of heterospecies. These can be broadly divided (with respect to our investigation) into (a) coil-globule transition in dilute solution of copolymers containing solvophobic comonomers, and (b) crystallization in the presence of sticky additives. In addition, we have also explored nucleation in homopolymer crystallization.

The method that we have employed is dynamic Monte Carlo (DMC) simulations of chain molecules on a lattice. The DMC algorithm has been coupled with the bond fluctuation method (BFM) algorithm, which allows the bond to fluctuate within a certain range. We have applied the DMC simulation algorithm to investigate the single chain coil to globule collapse transition of random copolymer, and subsequently, we have compared the collapse behavior of random with uniform distribution. We have also successfully applied the DMC to study melt crystallization in the presence of sticky additives. Finally, we have employed the data generated from NVT simulation and applied Weighted Histogram Analysis Method (WHAM), to understand nucleation in polymer crystallization.

7.1.1 Collapse Transition of Copolymer Chains in Dilute Solution

We have modeled the collapse of copolymers containing solvophobic comonomer, *c*-units (e.g., polar *c*-units in nonpolar solvent) along with less solvophobic *m*-units, in a Flory-like approach. There is a net attraction between *c*-units as a result of the repulsive interaction between *m*-*s*, *c*-*s* and *m*-*c* pairs (*s* stands for solvent molecules). The strong *c*-*c* attraction increases the overall solvophobicity of the chain, relative to a homopolymer, and therefore, copolymers collapse more abruptly and at a higher effective temperature, relative to homopolymers. To compare the collapse behavior of copolymers with homopolymer, we have renormalized the collapsed data to the same theta value, to account for the overall solvophobicity. This comparison reveals that at the expanded coil state, the enthalpic interaction is unimportant and behavior of copolymers is identical to that of homopolymer. Beyond theta state, copolymers with *c* content $\leq$ 50%, collapse more abruptly (viz. collapse happens over a narrower temperature range) than the corresponding homopolymer, even after accounting for the difference in overall solvophobicity. Collapse of copolymers containing higher *c* content, is dominated entirely by the *c*-*c* attractions, and these chains behave qualitatively like homopolymers, with a higher effective solvophobicity.

Analysis of the chain structure during collapse provides a structural reason for the qualitative difference in collapse of copolymers with low *c* content. For these copolymers, strong mutual attraction between *c*-units, facilitates aggregate formation, to form a dense isotropic core, surrounded by an anisotropic *m*-shell, as the chain is cooled below theta, thus exhibiting distinct *c*-core – *m*-shell morphology. The shell densifies as the copolymer is further cooled, but remains anisotropic for the finite chain sizes investigated. Our data suggest that the aggregation of the comonomers to form a core-shell structure in copolymers containing < 50% *c*-units, persists as the chain length is increased. The effect of solvophobicity-normalized copolymer microstructure is limited to the *path* or *mechanism* of

the collapse, as the solvent quality becomes poorer. However, the final shape of the collapsed globule is independent of this microstructure.

The copolymer chain microstructure (viz. the distribution of comonomer units along a copolymer chain), plays an important role in determining the path towards the collapsed state. Our simulation results show that the uniform copolymer collapses at a lower temperature, relative to random copolymer. The collapse of the uniform copolymer is more abrupt (viz. collapse happens over a narrow range of temperature) and "cooperative", compared to random copolymer. Both random and uniform copolymers, collapse via an intermediate core-shell structure. The intermediate is more compact in uniform copolymer compared to that in a random copolymer. The formation of this intermediate structure, can be explained as arising from an interplay of the enthalpy of *c*-*c* interactions with the entropic penalty for the formation of loops, when *c*-units aggregate. Our work suggests that the regular chain microstructure of a uniform copolymer leads to the abrupt, formation of a compact, nearly-collapsed intermediate core-shell state; the random copolymer microstructure leads to the formation of intermediates with "fluffy" monomer shells, over a wider temperature range. This difference between the collapse pathways for random and uniform copolymers, consistently persists to high chain lengths (N = 512), except that for $N \geq 512$, uniform copolymers tend to form multiple comonomer cores.

7.1.2. Melt Crystallization in the Presence of Sticky Additive

The DMC algorithm has also been implemented to examine polymer melt crystallization in a cubic lattice with an occupation density of 0.9375. Trends of crystallinity and "specific heat" with temperature, indicate that the transition is first order in nature. Crystallization and melting exhibit hysteresis, which is a characteristic feature of a first order transition in bulk polymeric system. Structural analysis indicates the formation of lamellar

type crystals. We have employed DMC to investigate the effect of "sticky" additives (viz. those that have attractive interactions with the polymer) on polymer crystallization. The attractive monomer-additive interaction, results in dispersion of the additive in the polymer melt and a slowing down of the polymer chain diffusivity in the melt state. This decrease in chain mobility with increase in additive loading or the stickiness, correlates to the decrease in the crystallinity and crystal thickness. The "specific heat" peak shows unusual non-monotonic behavior with the additive stickiness, and exhibits a maximum for intermediate values of additive stickiness. We have demonstrated that the unusual behavior of the specific heat peak, correlates with the large interchange between crystalline and amorphous states of the monomers in the vicinity of the additives. At this intermediate additive stickiness, we also observe that crystallization follows a qualitatively different route, and the time (no. of MC steps) evolution of crystallinity, shows a non-Avrami-like behavior, in contrast to cases at low or high additive stickiness.

7.1.3. Polymer Nucleation Studies via WHAM

Crystallization consists of nucleation followed by the growth. We have observed the effect of additive on the crystallization. It is interesting to know the effect of such additive on the nucleation in polymer crystallization. As a first step towards this goal, we have explored the applicability of WHAM to study polymer nucleation without additives. We have constructed 96 histograms from U_p = 0.15 to 0.245 at an interval of 0.001. The abrupt transition from melt to crystal, makes it difficult to sample conformations in the transition zone. On the other hand, there is pre-ordering in the melt state as temperature is reduced. Consequently, we do not obtain a flat combined histogram, even in the melt, which is a pre-requisite condition for the applicability of WHAM. Thus, we have not been able to apply

WHAM to study nucleation due to two reasons: (a) the range of energies is too high to use WHAM equations; (b) not enough conformations are sampled in the transition zone.

To overcome (a), we applied WHAM equation by dividing the entire temperature ranges into a number of smaller zones. We estimated DOS for each zone and combined them to get a combined DOS. To overcome (b), we propose the introduction of a restraining potential, which will make the transition less abrupt, and will allow sampling in the transition zone. This can be achieved by varying the value of U_c/U_p, instead of keeping it constant at unity. At higher values of U_c/U_p, the polymer will exhibit a enhanced tendency for interchain stiffening rather than crystallization via parallel stacking. An alternative is to add "sticky" additive into the polymer melt before crystallization. The stickiness of the additives, makes the chains less mobile, and the transition from melt to crystal will be less abrupt. By varying the stickiness parameter, we can make the system spend more time in the energy states corresponding to the transition zone. Thus, we might obtain a flat histogram, enabling implementation of WHAM.

7.2. Scope for Future Work

In this work, we have implemented dynamic Monte Carlo simulations, to examine single chain collapse transition and bulk melt crystallization. There are ample opportunities to extend the current understanding further. Some of them are described below:

a. We have reported here the collapse transition of linear flexible chains. The current methodology can be extended to the study the collapse transition of polymers with complex architecture such as star and ring polymers. Reptation moves are not possible in case of these polymers. Special attention needs to be given for the movement of the branch point. In case of ring polymers, only single site bond fluctuation and partial slithering diffusion (cf. kink diffusion) are possible. The

understanding of the solution behavior of star polymers can be extended to higher levels of branching, corresponding to industrially important highly branched polymers such as LDPE or LLDPE.

b. The two letter HP model has been successfully used to study the protein folding problem. A protein folds to its native state in a unique way, which depends on its primary structure. Not all the protein molecules can attain this native state. The folding nature of the protein and the feasibility to achieve the native state, depends on the microstructure of the protein molecule –the type of amino acids and their relative position (viz. sequence distribution of amino acids), along the chain. For example, for two active groups to form hydrogen bonding, they should present at (1, 4) positions to yield the alpha-helix conformation, in the native state. Similarly, to attain beta-sheets, the positions of the amino acids should be in such that they can organize themselves in the form of a stack of parallel bond segments, stabilized by intramolecular hydrogen bonding. Designing a protein molecule to yield a specific native state with useful functional properties is a challenging problem. Khokhlov and co-workers[1] have used a labeling technique to design the primary sequence of the protein molecule (protein-like copolymer). The outer layer of a globule of a homopolymer chain, corresponds to hydrophilic groups and remaining groups are hydrophobic. This generic model needs to be refined for real globular proteins, which comprise unique core as well as overall three dimensional structures.

c. Our model polymer in collapse transition is a copolymer with sticky (viz. having strong self-aggregation tendency) comonomer. This can be considered as a model for an ionomer. Ionomers are copolymers with less than 15 mole% ionic co-units. In the absence of dissociation, the ionic co-units form multiplets and clusters. The interaction between co-units is primarily electrostatic in nature. However, in our

model we cannot model long range ionic interaction. Instead, we use a lumped parameter to represent the attractive interaction, between co-units. Presence of ionic aggregates makes the chain less mobile and hinders crystallization. How the formation of ionic aggregate influences the formation of crystalline domain, is an interesting problem to investigate.

d. We have set up a model system for polymer-additive "composite" system. Our understanding of how "sticky" additives influence polymer crystallization might motivate design of new "composite" materials with tailored crystallization kinetics, to optimize structure development during processing. Crystallization of polar polymers such as polyamides or polyesters are influenced by the intra- and inter-molecular hydrogen bonding. Amine surfactants (primary, secondary or tertiary) are potential additives for these types of polymers. It might be interesting to systematically change the hydrogen bonding ability of additives (amine surfactants) and to investigate the influence of these additives on the crystallization of polar polymers. There is little experimental literature on such systematic investigations and our results suggest a potentially useful avenue for exploration.

We believe that such studies might also be relevant in the case of more complex systems such as polymer nanocomposites (PNC), wherein attractive interactions are engineered between nanoparticulate additives and the matrix polymer. The difference between PNCs and the current system, is in the length scale of the additive – in PNC, nanoparticles are of the order of the radius of gyration of the chain, whereas our current model deals with small molecule, monomeric additives. The interaction between nanoparticles and the polymer matrix is not well understood. The size and shape of the nanoparticles also play a great role in determining the properties of the composite[2-4]. To scale up and include the size of the nanoparticles, off-lattice

simulation would be a superior choice to lattice simulation. The interaction between nanoparticle and polymer matrix is tuned by applying suitable surface modifying agent. The interaction between nanoparticles and polymer is essentially the interaction between the surface coating molecules and polymer.

e. We have explored the applicability of WHAM in polymer nucleation studies, but our methodology has been limited by the non-flat nature of the resulting combined histogram. By improving the sampling in the transition zone, we believe that it should be possible to generate a flat histogram applicable to polymer nucleation. To address this, one can introduce a restraining potential into the system, so that the system does not exhibit an abrupt transition; rather it would pass through a smooth transition. Via NVT simulation systems, one can then apply umbrella sampling and combine with WHAM, to study nucleation. There are several simulation algorithms in use to study nucleation in non-polymeric systems. For polymeric system, however, there is a need to develop a suitable algorithm for nucleation. Polymer crystallization is not an equilibrium transition, and several methods have failed to address this problem. Therefore, it is an open challenge to develop a simulation algorithm for polymer nucleation.

f. We know that a block copolymer generates a numbers of different phases through self-assembly. A vast majority of the block copolymers investigated are amorphous. By making one or both the block crystallizable and investigating the crystallization of such polymer, we will be able to understand the effect of one block on the phase behavior of the other. The most interesting and challenging problem to investigate is the crystallization of a diblock copolymer wherein both blocks are crystallizable[5-9]. If the melting temperatures of the blocks are different, then different scenarios can be observed depending on the relative compositions of the two blocks. The block which

can crystallize earlier, will create a confinement for the crystallization of the other block. Phase transition under a confinement is itself is very important topic for investigation. Thus, in examining crystallization of such a diblock copolymer, we will be able to investigate the confinement effect on the crystallization, as well as be able to understand the mechanisms of homogeneous and heterogeneous nucleation. It may also be possible that the block which crystallizes first, may behave as a nucleating agent for the second. Thus, we will have an option to obtain additional insight for heterogeneous nucleation. Another motivation for the study of the crystallization of crystallizable diblock copolymers is its application in the biomedical field. Poly(L-lactic acid) (PLLA) has been used in biomedical applications for a long time. PLLA is also a crystallizable polymer, whose property can be tailored by incorporating another crystallizable polymer such as PEO (polyethylene oxide), and by varying the compositions of the two blocks.

References

(1) Khokhlov, A. R.; Khalatur, P. G. *Phys. Rev. Lett* **1999**, *82*, 3456-3459.

(2) Balazs, A. C.; Emrick, T.; Russell, T. P. *Science* **2006**, *314*, 1107-1110.

(3) Chervanyov, A. I.; Balazs, A. C. *J. Chem. Phys.* **2003**, *119*, 3529-3534.

(4) Lee, J. Y.; Thompson, R. B.; Jasnow, D.; Balazs, A. C. *Macromolecules* **2002**, *35*, 4855-4858.

(5) Ikeda, H.; Ohguma, Y.; Nojima, S. *Polymer Journal* **2008**, *40*, 241-248.

(6) Müller, A.; Albuerne, J.; Esteves, L. M.; Marquez, L.; Raquez, J.-M.; Degée, P.; Dubois, P.; Collins, S.; Hamley, I. W. *Macromol. Symp.* **2004**, *215*, 369-382.

(7) Myers, S. B.; Register, R. A. *Macromolecules* **2008**, *41*, 6773-6779.

(8) Nojima, S.; Akutsu, Y.; Washino, A.; Tanimoto, S. *Polymer* **2004**, *45*, 7317-7324.

(9) Nojima, S.; Akutsu, Y.; Akaba, M.; Tanimoto, S. *Polymer* **2005**, *46*, 4060-4067.

Contributions: Publications/Conference

Publications:

1. A. K. Dasmahapatra, K. Guruswamy and H. Nanavati, "**Polymer Crystallization in the Presence of "Sticky" Additives**", Accepted in *J. Chem. Phys.*, 2009
2. A. K. Dasmahapatra, H. Nanavati, and K. Guruswamy "**Pathway to Copolymer Collapse in Dilute Solution: Uniform versus Random Distribution of Comonomers**", *J. Chem. Phys., 127*, 234901 (2007).
3. A. K. Dasmahapatra, K. Guruswamy and H. Nanavati, "**Collapse transition in random copolymer solutions**", *Macromolecules*, 39, 9621 (2006).

Conferences:

International

1. Paper entitled "**Effect of sticky additive on homopolymer crystallization"** presented on Macro 2008 (International conference on Polymers at Frontiers of Science and Technology) at Taipei, Taiwan during June 29 – July 04, 2008.
2. Paper entitled "**Effect of Copolymer Microstructure on Single Chain Collapse"** presented on STATPHYS23 (International conference on Statistical Physics) at Genova, Italy during July 09 – 13, 2007.
3. Presented a paper titled "**Dynamic Monte Carlo Simulation in Polymer Crystallization**" in MACRO 2004, the International Conference on polymers for advanced Technology at Thiruvananthapuram, India during December 14 – 17, 2004.

National

1. Poster entitled "**Effect of "sticky" additives on homopolymer crystallization**" presented in National Science Day, February 26, 2008, at NCL, Pune.
2. Poster entitled **"Dynamic Monte Carlo Simulations of Heteropolymer Collapse"** presented in National Science Day, February 28, 2007, at NCL, Pune

3. Paper entitled "**Dynamic Monte Carlo Simulation of Random Heteropolymer Collapse**" presented in MACRO-2006 (Polymer for advanced technologies), during December 17 – 20, 2006, at NCL Pune.
4. Poster entitled **"Coil-Globule Transitions in Copolymers with Highly Attractive Comonomers"**, presented in National Science Day, February 28, 2006, at NCL, Pune
5. Paper presented on "**Monte Carlo Simulation of a Single Flexible Chain**" in CHEMCON-2004, December 27-31, 2004 at Mumbai

Awards and Honors:

1. Awarded best poster presentation award in National Science day 2006, NCL.
2. Awarded best poster presentation award in Research Scholars' Symposium 2007 at IIT Bombay
3. Awarded best poster presentation award in National Science day 2007, NCL.
4. Awarded best poster presentation award in National Science day 2008, NCL.
5. Nominated for the best research scholars' award in the Engineering Science category at the National Chemical Laboratory, Pune, 2007
6. Awarded travel fellowship from DST, New Delhi to present a research paper at STATPHYS 23, at Genova, Italy during July 09 – 13, 2007
7. Awarded travel fellowship from CSIR, New Delhi to present a research paper at Macro2008, at Taipei, Taiwan during July 09 – 13, 2007
8. Awarded CSIR –Junior Research Fellowship to peruse graduate studies (direct Ph. D.), 2003.
9. Presented an invited lecture on "Effect of Copolymer Microstructure on Single Chain Collapse" at the Indian Association for the Cultivation of Science, November, 2008.

Acknowledgements

It is a great pleasure for me to express the sincere gratitude to my advisor, **Prof. Hemant Nanavati** and **Dr. Guruswamy Kumaraswamy (NCL, Pune)** for their constant support, encouragements and constructive criticisms throughout my research work. I would also like to thank my RPC members, Prof. A. K. Suresh, Prof. V. A. Juvekar and Prof. D. V. Khakhar for their valuable comments and suggestions. I thank all the faculty members and academic and non-academic staff for their help whenever it was required. I would also thank Prof. Sanat Kumar and his student Mr. Sumit Sharma (Department of Chemical Engineering, Columbia University, USA) for helping me in understanding WHAM. I sincerely thank to the thesis examiners, Prof. P. B. Sunill Kumar, Department of Physics, IITM and Prof. R. P. Chhabra, Department of Chemical Engineering, IITK, for their valuable comments.

My special thanks to my lab mates and friends especially, Vimal and Ganpat for their constant support through out my research work both personally and professionally.

I sincerely acknowledge the financial support from CSIR, India through GATE-JRF scheme and computational support from CDAC, Pune. I would also thank Dr. R P Thangavelu for providing computing resources at CMMACS, Bangalore.

Finally, I would like thank my family members for their self-less support, love, care and co-operation throughout my research work.

Ashok Kumar Das Mahapatra

(July 13, 2009)